

# Density Model for Pilot Whales (*Globicephala spp.*) for the U.S. East Coast: Supplementary Report

Model Version 7.1

Duke University Marine Geospatial Ecology Laboratory\*

2023-05-27


## Citation

When citing our methodology or results generally, please cite Roberts et al. (2016, 2023). The complete references appear at the end of this document. We are preparing a new article for a peer-reviewed journal that will eventually replace those. Until that is published, those are the best general citations.

When citing this model specifically, please use this reference:

Roberts JJ, Yack TM, Cañadas A, Fujioka E, Halpin PN, Barco SG, Boisseau O, Chavez-Rosales S, Cole TVN, Cotter MP, Cummings EW, Davis GE, DiGiovanni Jr. RA, Garrison LP, Gowan TA, Jackson KA, Kenney RD, Khan CB, Lockhart GG, Lomac-MacNair KS, McAlarney RJ, McLellan WA, Mullin KD, Nowacek DP, O'Brien O, Pabst DA, Palka DL, Quintana-Rizzo E, Redfern JV, Rickard ME, White M, Whitt AD, Zoidis AM (2022) Density Model for Pilot Whales (*Globicephala spp.*) for the U.S. East Coast, Version 7.1, 2023-05-27, and Supplementary Report. Marine Geospatial Ecology Laboratory, Duke University, Durham, North Carolina.

## Copyright and License

 This document and the accompanying results are © 2023 by the Duke University Marine Geospatial Ecology Laboratory and are licensed under a [Creative Commons Attribution 4.0 International License](https://creativecommons.org/licenses/by/4.0/).

## Model Version History

Version	Date	Description
1	2014-09-01	Initial version.
2	2014-10-23	Added Palka (2006) survey-specific $g(0)$ estimates. Updated distance to eddy predictors using Chelton et al.'s 2014 database. Removed distance to eddy predictors from shelf model; added distance to canyon predictor. Removed wind speed predictor from all models. Fixed missing pixels in several climatological predictors, which led to not all segments being utilized. Eliminated Cape Cod Bay subregion (combined it with Shelf).
3	2014-11-19	Reconfigured detection hierarchy and adjusted NARWSS detection functions based on additional information from Tim Cole. Removed CumVGPM180 predictor. Updated documentation.
4	2014-12-04	Fixed bug that applied the wrong detection function to segments NE_narwss_1999_widgeon_hapo dataset. Refitted model. Updated documentation.
4.1	2015-03-06	Updated the documentation. No changes to the model.

\*For questions or to offer feedback please contact Jason Roberts ([jason.roberts@duke.edu](mailto:jason.roberts@duke.edu)) and Tina Yack ([tina.yack@duke.edu](mailto:tina.yack@duke.edu))

*(continued)*

---

Version	Date	Description
4.2	2015-05-14	Updated calculation of CVs. Switched density rasters to logarithmic breaks. No changes to the model.
4.3	2015-09-30	Updated the documentation. No changes to the model. Model files released as supplementary information to Roberts et al. (2016).
5	2017-06-01	Began update to Roberts et al. (2015) model. Introduced new surveys from AMAPPS, NARWSS, UNCW, VAMSC, and the SEUS NARW teams. Updated modeling methodology. Refitted detection functions and spatial models from scratch using new and reprocessed covariates.
6	2017-08-08	Combined "Shelf" and "Slope and Abyss" subregions into single "Surveyed Area" subregion, to try to eliminate extreme extrapolations in very cold water. Model released as part of a scheduled update to the U.S. Navy Marine Species Density Database (NMSDD).
7	2022-06-20	This model is a major update over the prior version, with substantial additional data, improved statistical methods, and an increased spatial resolution. It was released as part of the final delivery of the U.S. Navy Marine Species Density Database (NMSDD) for the Atlantic Fleet Testing and Training (AFTT) Phase IV Environmental Impact Statement. Several new collaborators joined and contributed survey data: New York State Department of Environmental Conservation, TetraTech, HDR, and Marine Conservation Research. We incorporated additional surveys from all continuing and new collaborators through the end of 2020. (Because some environmental covariates were only available through 2019, certain models only extend through 2019.) We increased the spatial resolution to 5 km and, at NOAA's request, we extended the model further inshore from New York through Maine. We reformulated and refitted all detection functions and spatial models. We updated all environmental covariates to newer products, when available, and added several covariates to the set of candidates. For models that incorporated dynamic covariates, we estimated model uncertainty using a new method that accounts for both model parameter error and temporal variability.
7.1	2023-05-27	Completed the supplementary report documenting the details of this model. The model itself was not changed.

---



# 1 Survey Data

We built this model from data collected between 1998-2019 (Table 1, Figure 1). We also excluded surveys that did not include pilot whales within their list of target species, as well as aerial surveys flown at 750 ft altitude and those flown by NYS-DEC, as we lacked the sightings to confidently model detectability for those surveys. In keeping with our primary strategy for the 2022 modeling cycle, we excluded data prior to 1998 in order to utilize biological covariates derived from satellite ocean color observations, which were only available for a few months before 1998. We excluded data after 2019 in order to utilize zooplankton and micronekton biomass estimates from SEAPODYM (Lehodey et al. 2008), which preliminary modeling indicated were effective spatial covariates but were only available through 2019. We restricted the model to aerial survey transects with sea states of Beaufort 4 or less. For shipboard surveys the model was restricted to survey transects of Beaufort 5 or less, except for MCR which was Beaufort 4 or less. We also excluded transects with poor weather or visibility for surveys that reported those conditions.

Table 1: Survey effort and observations considered for this model. Effort is tallied as the cumulative length of on-effort transects. Observations are the number of groups and individuals encountered while on effort. Off effort observations and those lacking an estimate of group size or distance to the group were excluded.

Institution	Program	Period	Effort		Observations	
			1000s km	Groups	Individuals	Mean Group Size
<b>Aerial Surveys</b>						
HDR	Navy Norfolk Canyon	2018-2019	11	64	894	14.0
NEAq	CNM	2017-2019	2	4	81	20.2
NEAq	MMS-WEA	2017-2019	31	2	9	4.5
NEAq	NLPSC	2011-2015	43	9	54	6.0
NEFSC	AMAPPS	2010-2019	83	76	393	5.2
NEFSC	NARWSS	2003-2016	380	378	3,723	9.8
NEFSC	Pre-AMAPPS	1999-2008	45	148	1,120	7.6
SEFSC	AMAPPS	2010-2019	110	66	1,320	20.0
UNCW	Navy Cape Hatteras	2011-2017	34	151	3,005	19.9
UNCW	Navy Jacksonville	2009-2017	92	20	264	13.2
UNCW	Navy Norfolk Canyon	2015-2017	14	45	687	15.3
UNCW	Navy Onslow Bay	2007-2011	49	7	149	21.3
VAMSC	MD DNR WEA	2013-2015	16	0	0	
VAMSC	Navy VACAPES	2016-2017	19	0	0	
VAMSC	VA CZM WEA	2012-2015	21	0	0	
		<b>Total</b>	<b>949</b>	<b>970</b>	<b>11,699</b>	<b>12.1</b>
<b>Shipboard Surveys</b>						
MCR	SOTW Visual	2012-2019	8	18	176	9.8
NEFSC	AMAPPS	2011-2016	15	230	2,121	9.2
NEFSC	Pre-AMAPPS	1998-2007	11	90	1,109	12.3
SEFSC	AMAPPS	2011-2016	16	77	1,734	22.5
SEFSC	Pre-AMAPPS	1998-2006	30	132	2,282	17.3
		<b>Total</b>	<b>80</b>	<b>547</b>	<b>7,422</b>	<b>13.6</b>
		<b>Grand Total</b>	<b>1,030</b>	<b>1,517</b>	<b>19,121</b>	<b>12.6</b>

Table 2: Institutions that contributed surveys used in this model.

Institution	Full Name
HDR	HDR, Inc.
MCR	Marine Conservation Research
NEAq	New England Aquarium
NEFSC	NOAA Northeast Fisheries Science Center
SEFSC	NOAA Southeast Fisheries Science Center
UNCW	University of North Carolina Wilmington
VAMSC	Virginia Aquarium & Marine Science Center

Table 3: Descriptions and references for survey programs used in this model.

Program	Description	References
AMAPPS	Atlantic Marine Assessment Program for Protected Species	Palka et al. (2017), Palka et al. (2021)
CNM	Northeast Canyons Marine National Monument Aerial Surveys	Redfern et al. (2021)
MD DNR WEA	Aerial Surveys of the Maryland Wind Energy Area	Barco et al. (2015)
MMS-WEA	Marine Mammal Surveys of the MA and RI Wind Energy Areas	Quintana-Rizzo et al. (2021), O'Brien et al. (2022)
NARWSS	North Atlantic Right Whale Sighting Surveys	Cole et al. (2007)
Navy Cape Hatteras	Aerial Surveys of the Navy's Cape Hatteras Study Area	McLellan et al. (2018)
Navy Jacksonville	Aerial Surveys of the Navy's Jacksonville Study Area	Foley et al. (2019)
Navy Norfolk Canyon	Aerial Surveys of the Navy's Norfolk Canyon Study Area	Cotter (2019), McAlarney et al. (2018)
Navy Onslow Bay	Aerial Surveys of the Navy's Onslow Bay Study Area	Read et al. (2014)
Navy VACAPES	Aerial Survey Baseline Monitoring in the Continental Shelf Region of the VACAPES OPAREA	Malette et al. (2017)
NLPSC	Northeast Large Pelagic Survey Collaborative Aerial Surveys	Leiter et al. (2017), Stone et al. (2017)
Pre-AMAPPS	Pre-AMAPPS Marine Mammal Abundance Surveys	Mullin and Fulling (2003), Garrison et al. (2010), Palka (2006)
SOTW Visual	R/V Song of the Whale Visual Surveys	Ryan et al. (2013)
VA CZM WEA	Virginia CZM Wind Energy Area Surveys	Malette et al. (2014), Malette et al. (2015)

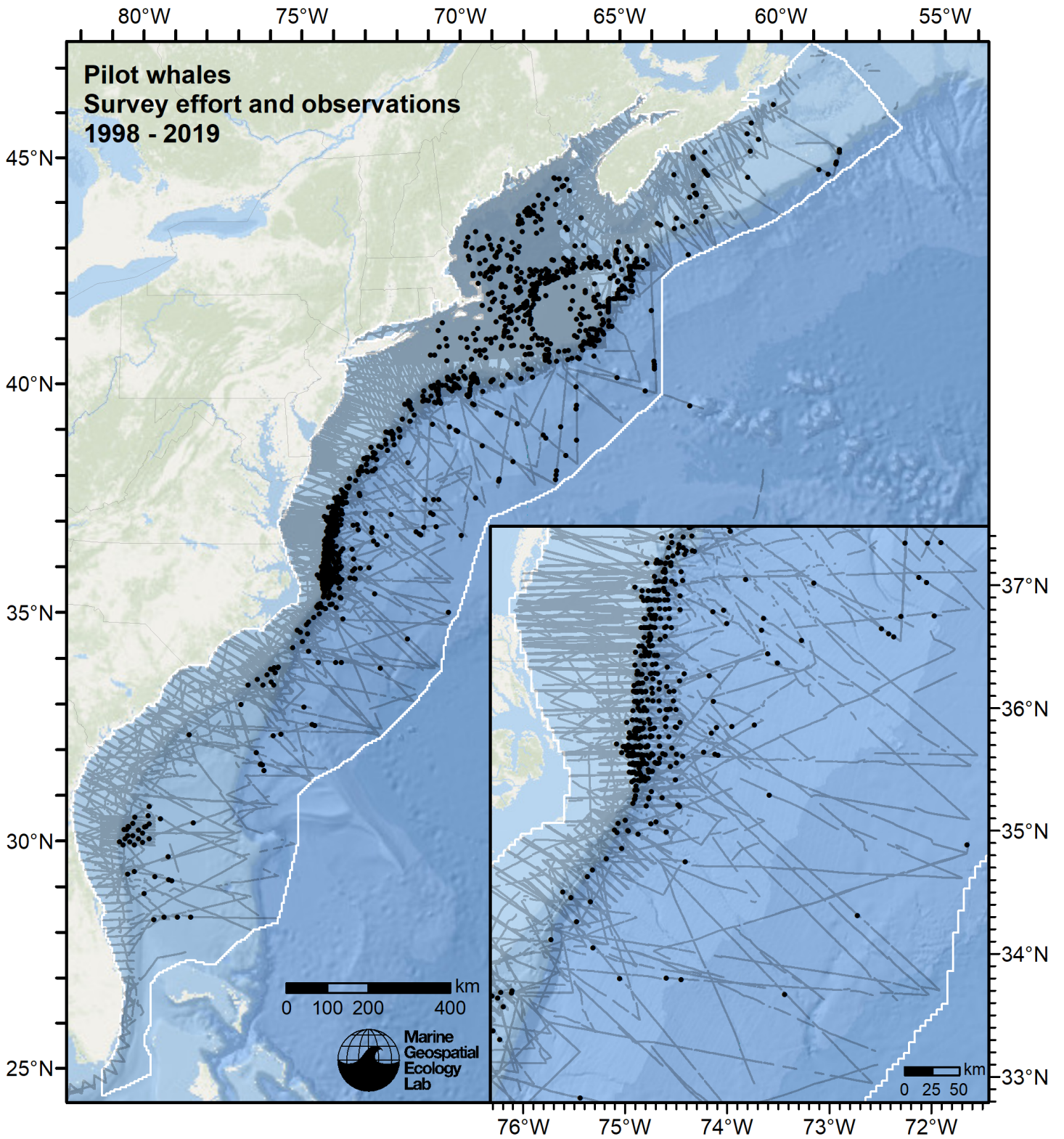


Figure 1: Survey effort and pilot whales observations available for density modeling, after detection functions were applied, and excluded segments and truncated observations were removed.

## 2 Detection Functions

### 2.1 Taxon Specific

We fitted the detection functions in this section to pilot whales observations exclusively, without pooling in other species. We usually adopted this approach when we had enough sightings of this taxon to fit a detection function without pooling and we judged that this taxon's detectability differed in important respects from others that pooling should be avoided if possible. We also occasionally used this approach for certain taxa that had similar detectability to others but for which we had so many sightings that pooling in other species provided little benefit.

## 2.1.1 Aerial Surveys

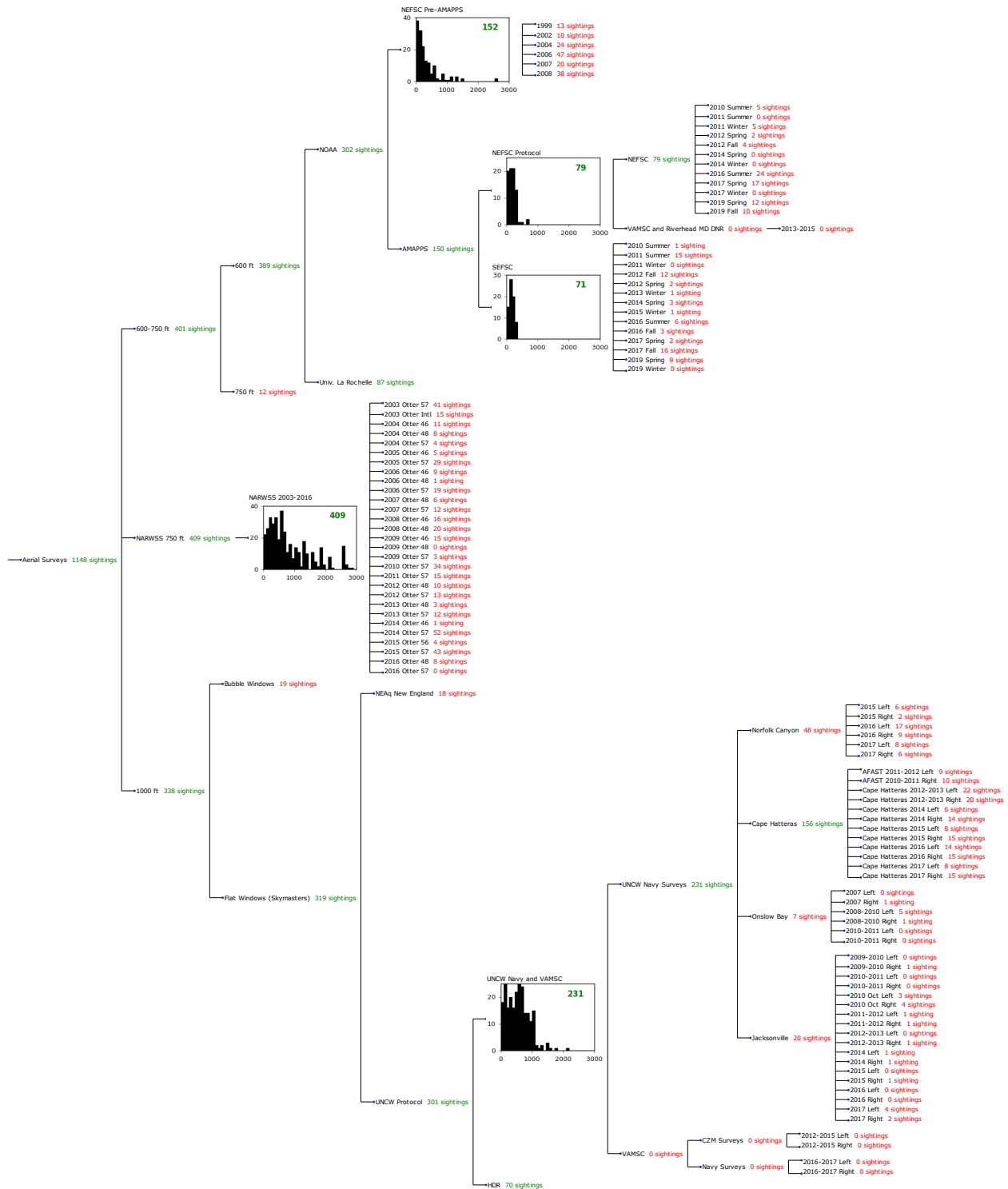


Figure 2: Detection hierarchy for aerial surveys, showing how they were pooled during detectability modeling, for taxon-specific detection functions. Each histogram represents a detection function and summarizes the perpendicular distances of observations that were pooled to fit it, prior to truncation. Observation counts, also prior to truncation, are shown in green when they met the recommendation of Buckland et al. (2001) that detection functions utilize at least 60 sightings, and red otherwise. For rare taxa, it was not always possible to meet this recommendation, yielding higher statistical uncertainty. During the spatial modeling stage of the analysis, effective strip widths were computed for each survey using the closest detection function above it in the hierarchy (i.e. moving from right to left in the figure). Surveys that do not have a detection function above them in this figure were either addressed by a detection function presented in a different section of this report, or were omitted from the analysis.

### 2.1.1.1 NEFSC Pre-AMAPPS

After right-truncating observations greater than 1300 m, we fitted the detection function to the 148 observations that remained. The selected detection function (Figure 3) used a hazard rate key function with no covariates.

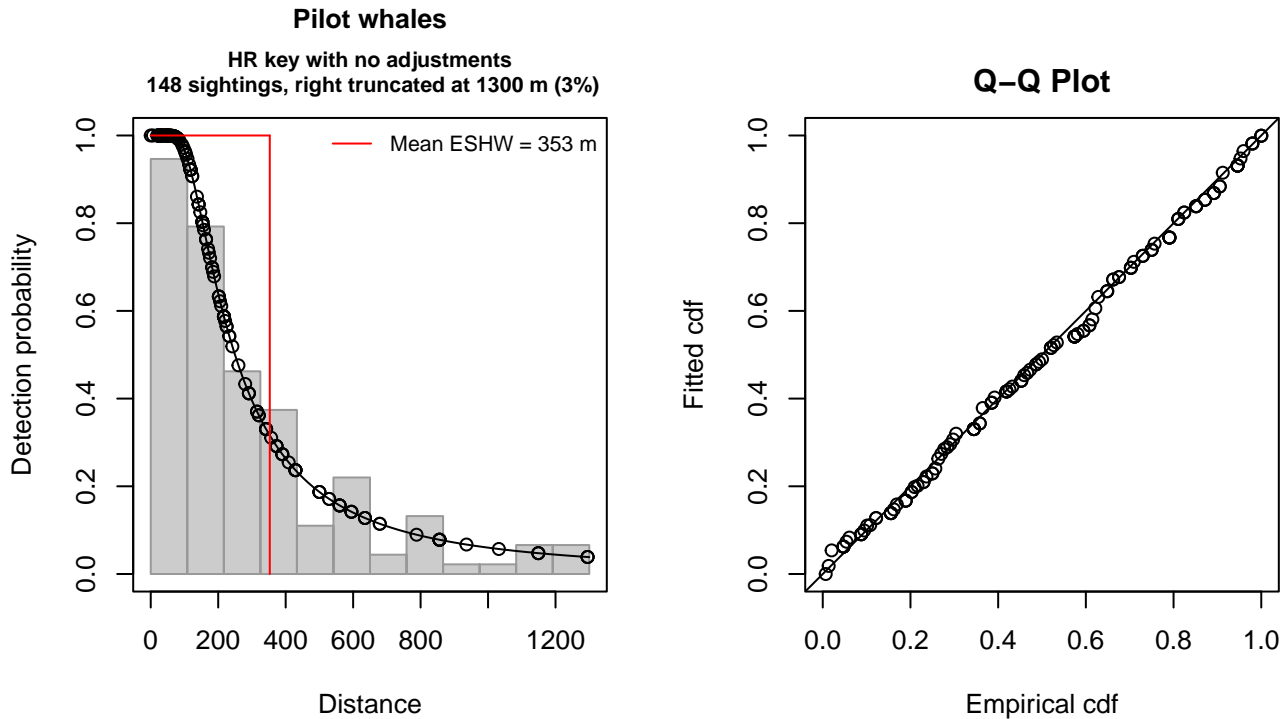


Figure 3: NEFSC Pre-AMAPPS detection function and Q-Q plot showing its goodness of fit.

Statistical output for this detection function:

Summary for ds object

Number of observations : 148  
 Distance range : 0 - 1300  
 AIC : 1975.46

Detection function:

Hazard-rate key function

Detection function parameters

Scale coefficient(s):  
 estimate se  
 (Intercept) 5.309563 0.201217

Shape coefficient(s):  
 estimate se  
 (Intercept) 0.553678 0.1391051

	Estimate	SE	CV
Average p	0.2714724	0.03352391	0.1234892
N in covered region	545.1751832	77.43036241	0.1420284

Distance sampling Cramer-von Mises test (unweighted)

Test statistic = 0.030044 p = 0.976024

### 2.1.1.2 NEFSC AMAPPS Protocol

After right-truncating observations greater than 400 m, we fitted the detection function to the 76 observations that remained. The selected detection function (Figure 4) used a hazard rate key function with no covariates.

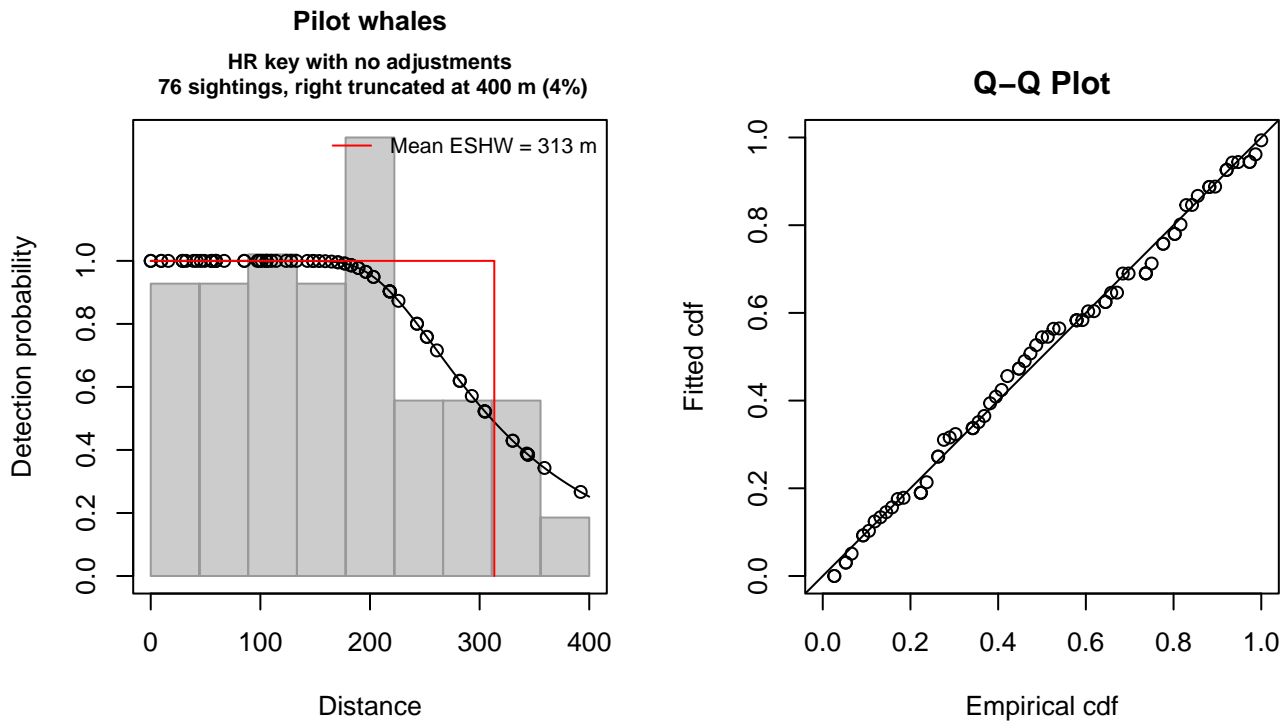


Figure 4: NEFSC AMAPPS Protocol detection function and Q-Q plot showing its goodness of fit.

Statistical output for this detection function:

Summary for ds object

Number of observations : 76  
 Distance range : 0 - 400  
 AIC : 904.8838

Detection function:

Hazard-rate key function

Detection function parameters

Scale coefficient(s):  
 estimate se  
 (Intercept) 5.631383 0.1576848

Shape coefficient(s):  
 estimate se  
 (Intercept) 1.23501 0.6793866

	Estimate	SE	CV
Average p	0.7834181	0.07558225	0.09647754
N in covered region	97.0107823	10.69658944	0.11026186

Distance sampling Cramer-von Mises test (unweighted)

Test statistic = 0.038402 p = 0.941209



### 2.1.1.3 SEFSC AMAPPS

After right-truncating observations greater than 400 m and left-truncating observations less than 50 m (Figure 6), we fitted the detection function to the 66 observations that remained. The selected detection function (Figure 5) used a hazard rate key function with Season (Figure 7) as a covariate.

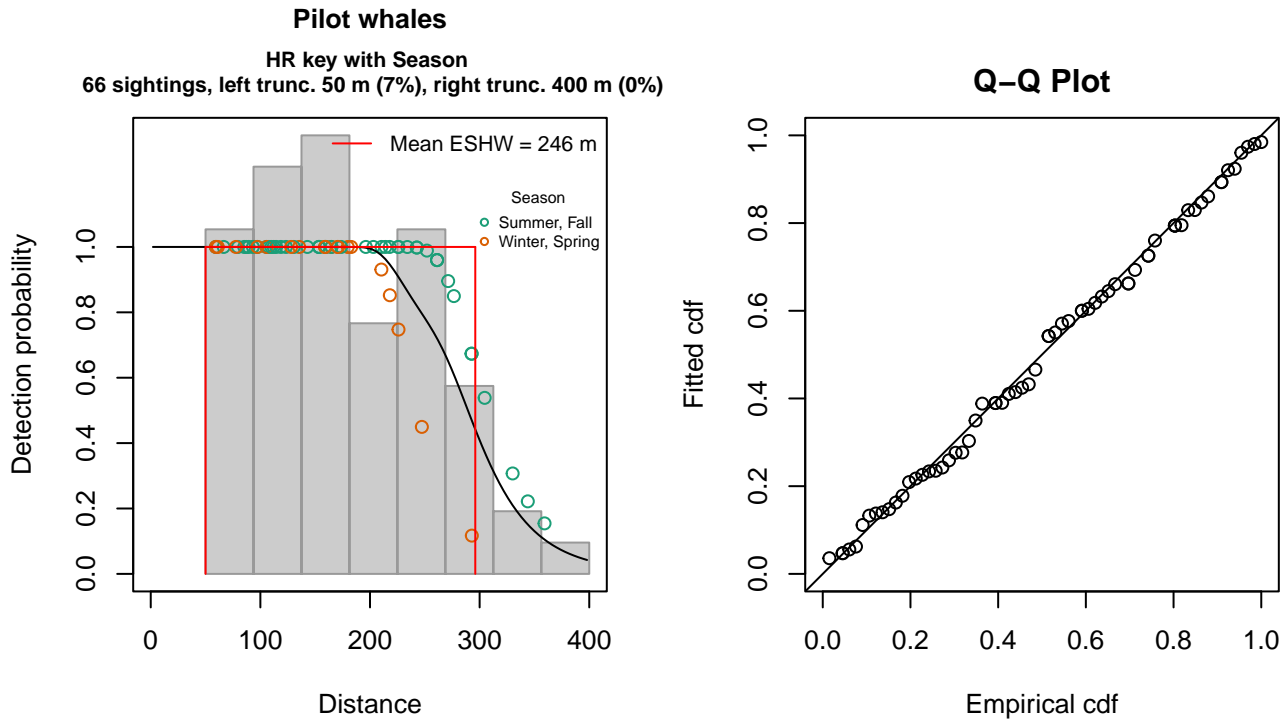


Figure 5: SEFSC AMAPPS detection function and Q-Q plot showing its goodness of fit.

Statistical output for this detection function:

Summary for ds object

Number of observations : 66  
 Distance range : 50 - 400  
 AIC : 751.372

Detection function:

Hazard-rate key function

Detection function parameters

Scale coefficient(s):

	estimate	se
(Intercept)	5.6912232	0.08088691
SeasonWinter, Spring	-0.2362593	0.11111187

Shape coefficient(s):

	estimate	se
(Intercept)	2.226235	0.4916471

	Estimate	SE	CV
Average p	0.6916246	0.04665417	0.06745591
N in covered region	95.4274847	9.24933528	0.09692528

Distance sampling Cramer-von Mises test (unweighted)

Test statistic = 0.023690 p = 0.992090



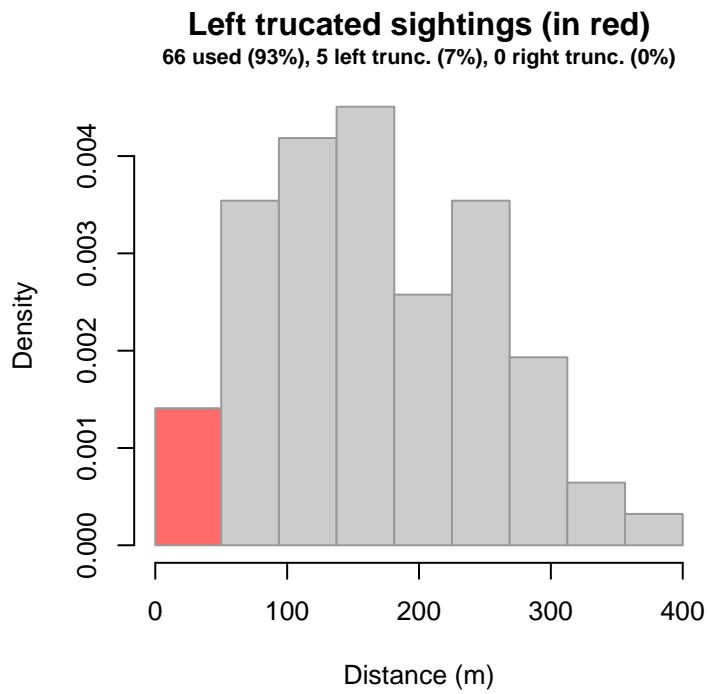


Figure 6: Density histogram of observations used to fit the SEFSC AMAPPS detection function, with the left-most bar showing observations at distances less than 50 m, which were left-truncated and excluded from the analysis [Buckland et al. (2001)]. (This bar may be very short if there were very few left-truncated sightings, or very narrow if the left truncation distance was very small; in either case it may not appear red.)

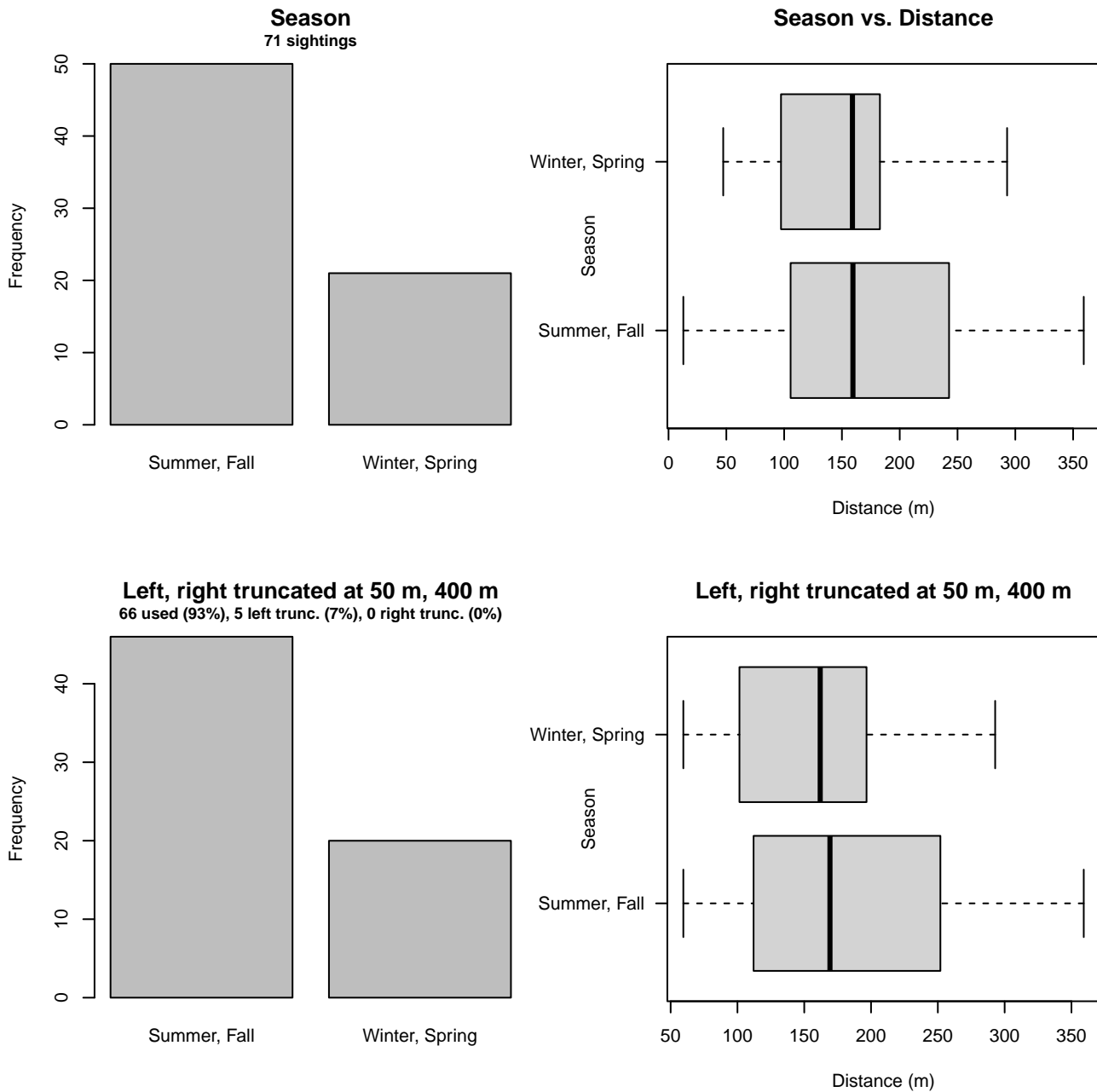


Figure 7: Distribution of the Season covariate before (top row) and after (bottom row) observations were truncated to fit the SEFSC AMAPPS detection function.

#### 2.1.1.4 NARWSS 2003-2016

After right-truncating observations greater than 2905 m, we fitted the detection function to the 378 observations that remained. The selected detection function (Figure 8) used a hazard rate key function with no covariates.

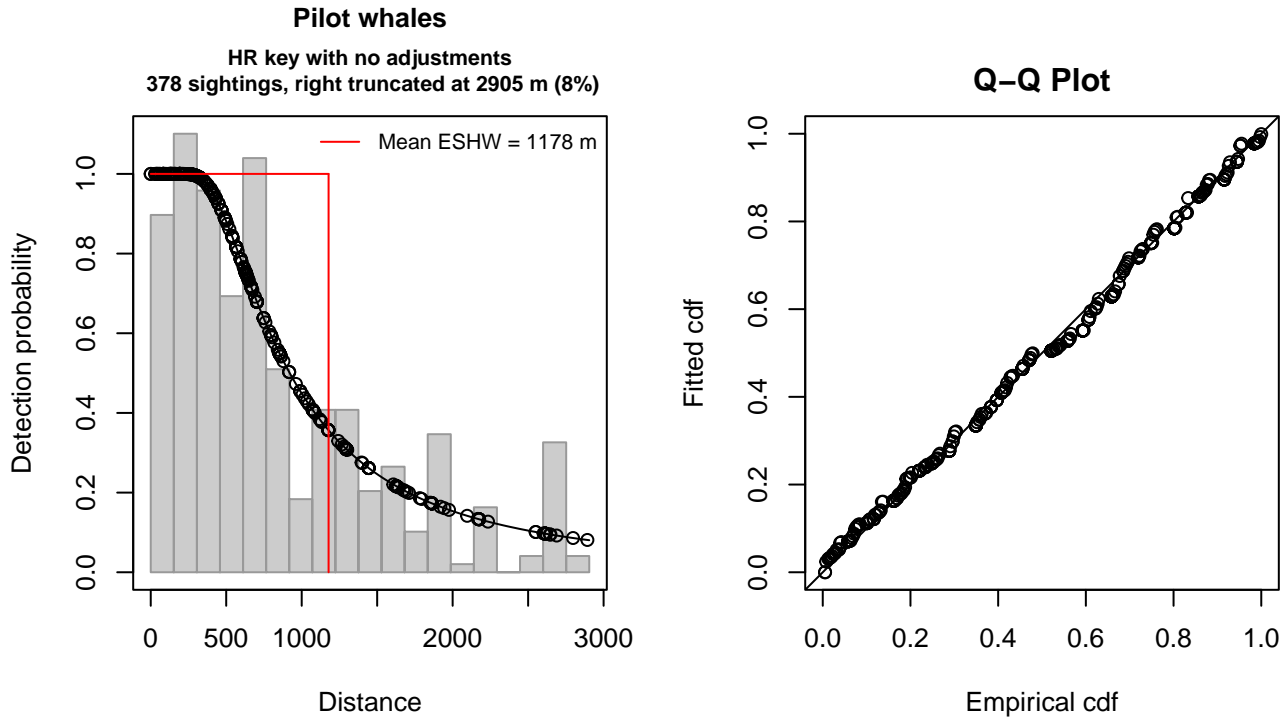


Figure 8: NARWSS 2003-2016 detection function and Q-Q plot showing its goodness of fit.

Statistical output for this detection function:

Summary for ds object

Number of observations : 378  
 Distance range : 0 - 2905  
 AIC : 5801.896

Detection function:

Hazard-rate key function

Detection function parameters

Scale coefficient(s):  
 estimate se  
 (Intercept) 6.625804 0.1236403

Shape coefficient(s):  
 estimate se  
 (Intercept) 0.6086148 0.1167705

	Estimate	SE	CV
Average p	0.4055758	0.02923159	0.07207430
N in covered region	932.0082800	76.67010343	0.08226333

Distance sampling Cramer-von Mises test (unweighted)  
 Test statistic = 0.089244 p = 0.640205

### 2.1.1.5 UNCW Navy and VAMSC

After right-truncating observations greater than 1300 m, we fitted the detection function to the 223 observations that remained. The selected detection function (Figure 9) used a hazard rate key function with no covariates.

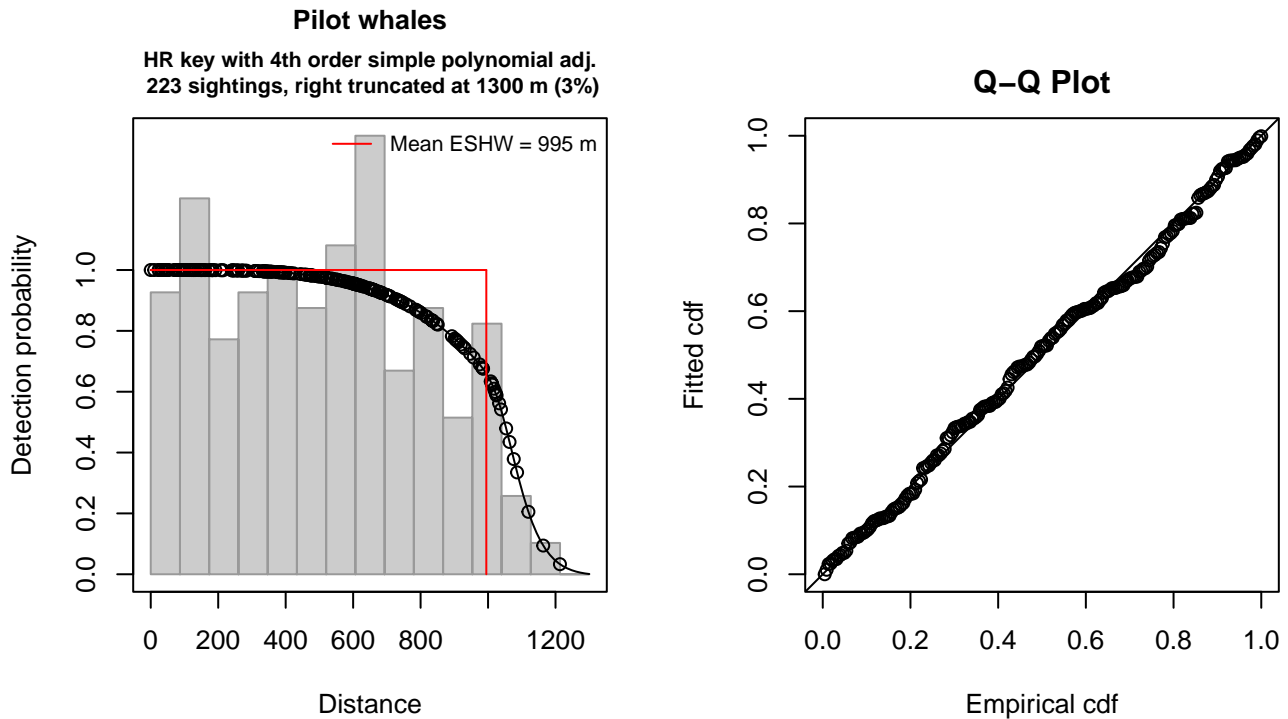


Figure 9: UNCW Navy and VAMSC detection function and Q-Q plot showing its goodness of fit.

Statistical output for this detection function:

Summary for ds object

Number of observations : 223  
 Distance range : 0 - 1300  
 AIC : 3141.583

Detection function:

Hazard-rate key function with simple polynomial adjustment term of order 4

Detection function parameters

Scale coefficient(s):  

	estimate	se
(Intercept)	6.991458	0.0679075

Shape coefficient(s):  

	estimate	se
(Intercept)	2.89807	0.5770609

Adjustment term coefficient(s):  

	estimate	se
poly, order 4	-0.9784486	0.508104

Monotonicity constraints were enforced.

	Estimate	SE	CV
Average p	0.7652709	0.03280955	0.04287312
N in covered region	291.4000633	15.66719507	0.05376524

Monotonicity constraints were enforced.

Distance sampling Cramer-von Mises test (unweighted)  
 Test statistic = 0.059526 p = 0.816969

## 2.1.2 Shipboard Surveys

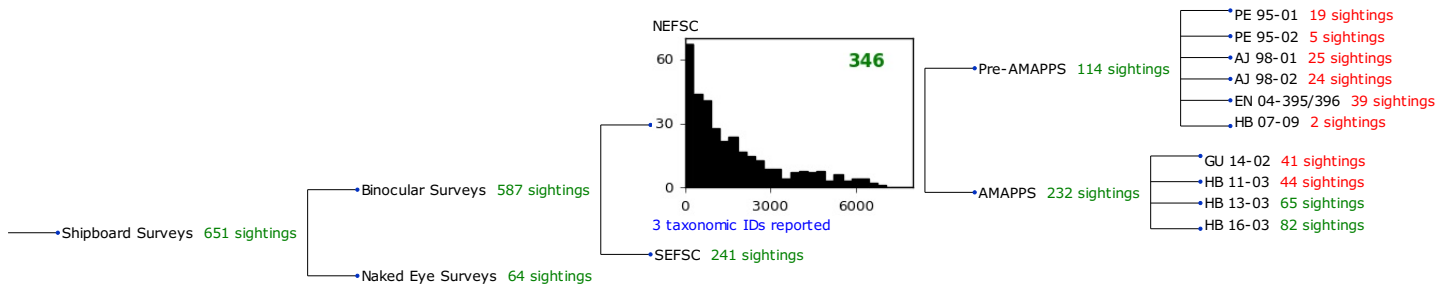


Figure 10: Detection hierarchy for shipboard surveys, showing how they were pooled during detectability modeling, for taxon-specific detection functions. Each histogram represents a detection function and summarizes the perpendicular distances of observations that were pooled to fit it, prior to truncation. Observation counts, also prior to truncation, are shown in green when they met the recommendation of Buckland et al. (2001) that detection functions utilize at least 60 sightings, and red otherwise. For rare taxa, it was not always possible to meet this recommendation, yielding higher statistical uncertainty. During the spatial modeling stage of the analysis, effective strip widths were computed for each survey using the closest detection function above it in the hierarchy (i.e. moving from right to left in the figure). Surveys that do not have a detection function above them in this figure were either addressed by a detection function presented in a different section of this report, or were omitted from the analysis.

### 2.1.2.1 NEFSC

After right-truncating observations greater than 6500 m, we fitted the detection function to the 344 observations that remained. The selected detection function (Figure 11) used a hazard rate key function with Beaufort (Figure 12) and VesselName (Figure 13) as covariates.

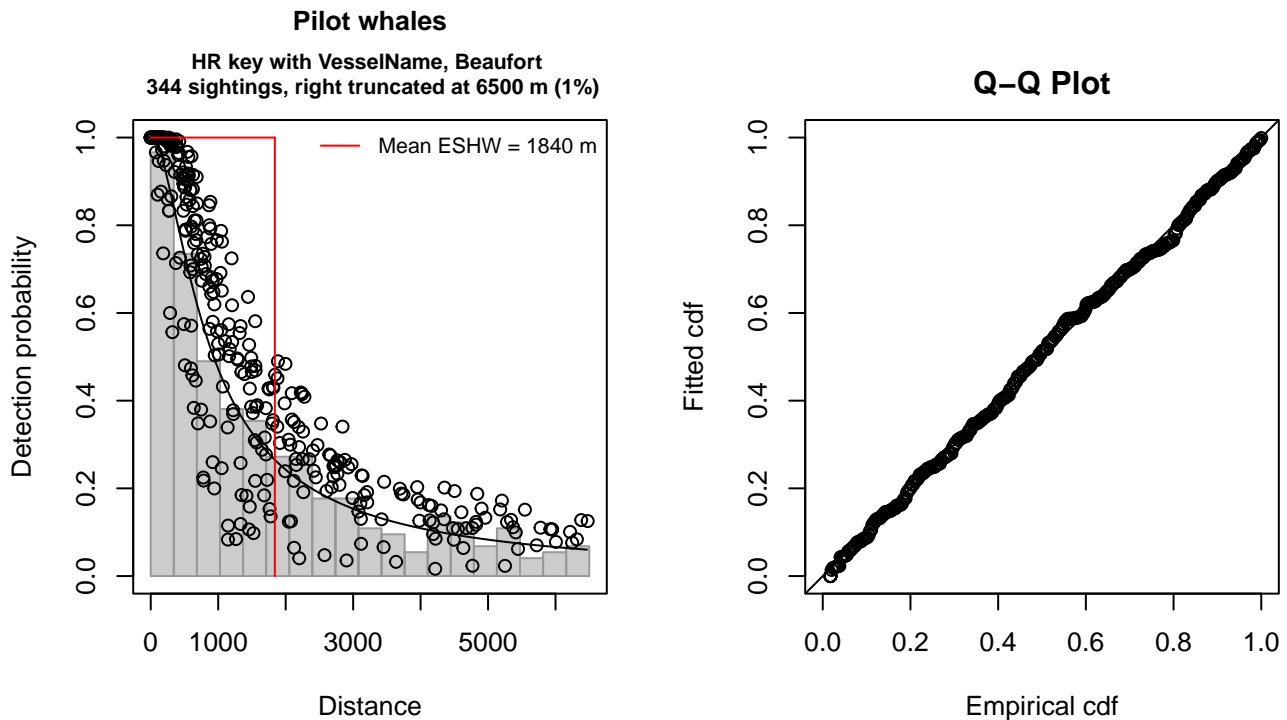


Figure 11: NEFSC detection function and Q-Q plot showing its goodness of fit.

Statistical output for this detection function:

Summary for ds object

Number of observations : 344  
Distance range : 0 - 6500  
AIC : 5777.37

Detection function:  
Hazard-rate key function

Detection function parameters  
Scale coefficient(s):

	estimate	se
(Intercept)	7.4581029	0.3592647
VesselNameGunter	-1.1888116	0.3946265
VesselNamePelican	-0.7668908	0.4617480
Beaufort	-0.2187465	0.1211862

Shape coefficient(s):

	estimate	se
(Intercept)	0.2683997	0.1051816

	Estimate	SE	CV
Average p	0.2463876	0.03095675	0.1256425
N in covered region	1396.1742676	187.74961003	0.1344743

Distance sampling Cramer-von Mises test (unweighted)  
Test statistic = 0.034671 p = 0.958426

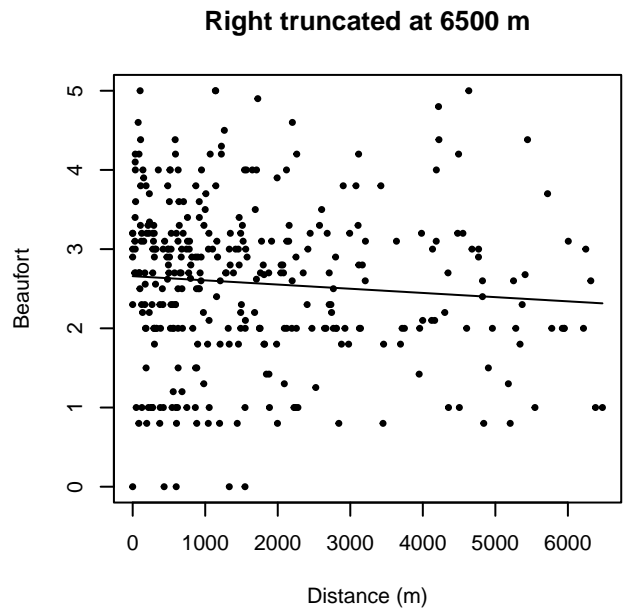
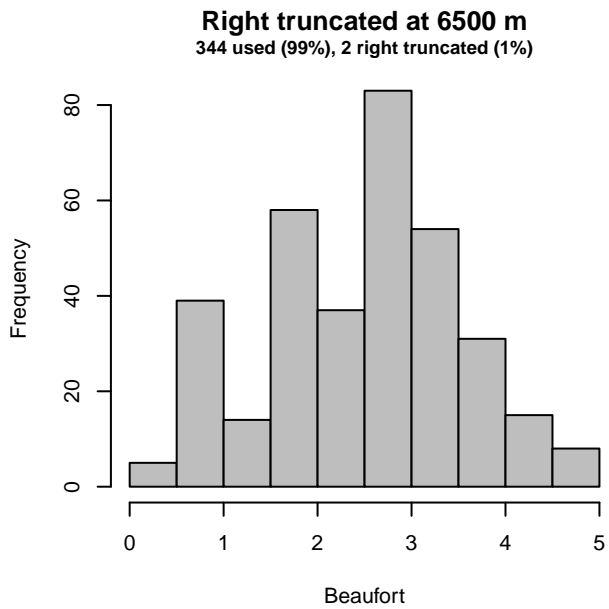
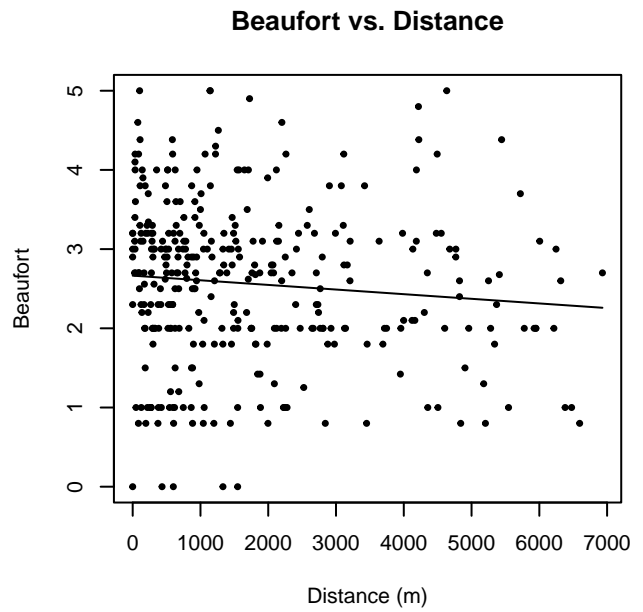
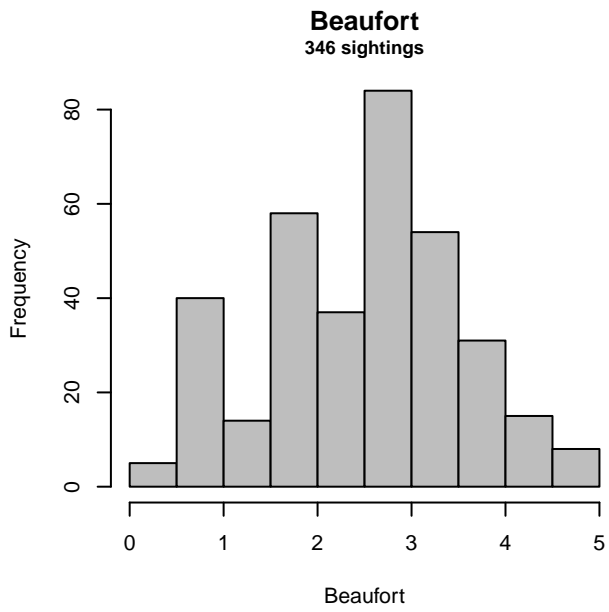


Figure 12: Distribution of the Beaufort covariate before (top row) and after (bottom row) observations were truncated to fit the NEFSC detection function.

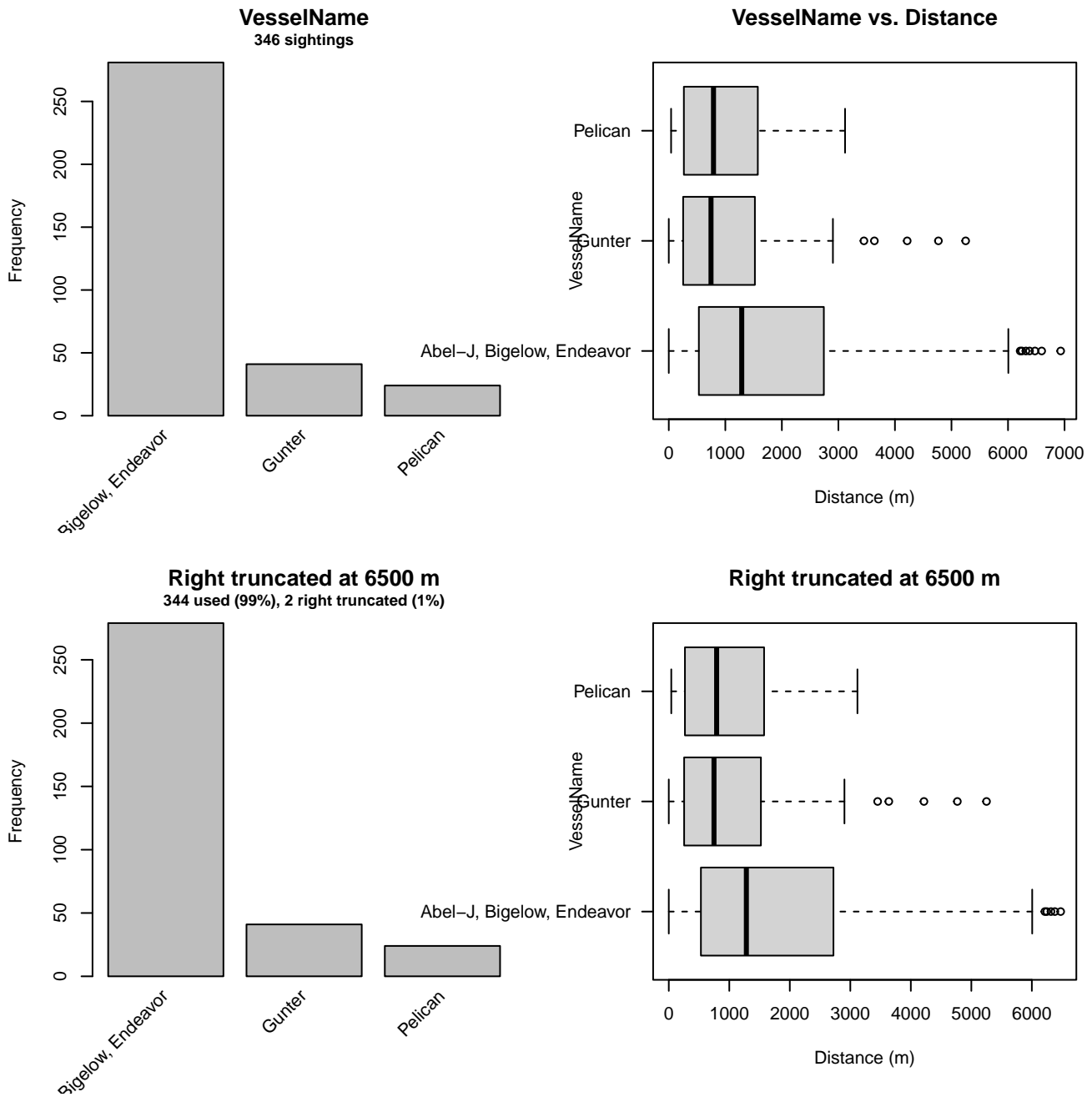


Figure 13: Distribution of the VesselName covariate before (top row) and after (bottom row) observations were truncated to fit the NEFSC detection function.

## 2.2 Without a Taxonomic Covariate

We fitted the detection functions in this section to pools of species with similar detectability characteristics but could not use a taxonomic identification as a covariate to account for differences between them. We usually took this approach after trying the taxonomic covariate and finding it had insufficient statistical power to be retained. We also resorted to it when the focal taxon being modeled had too few observations to be allocated its own taxonomic covariate level and was too poorly known for us to confidently determine which other taxa we could group it with.



## 2.2.1 Blackfish

### 2.2.1.1 Shipboard Surveys

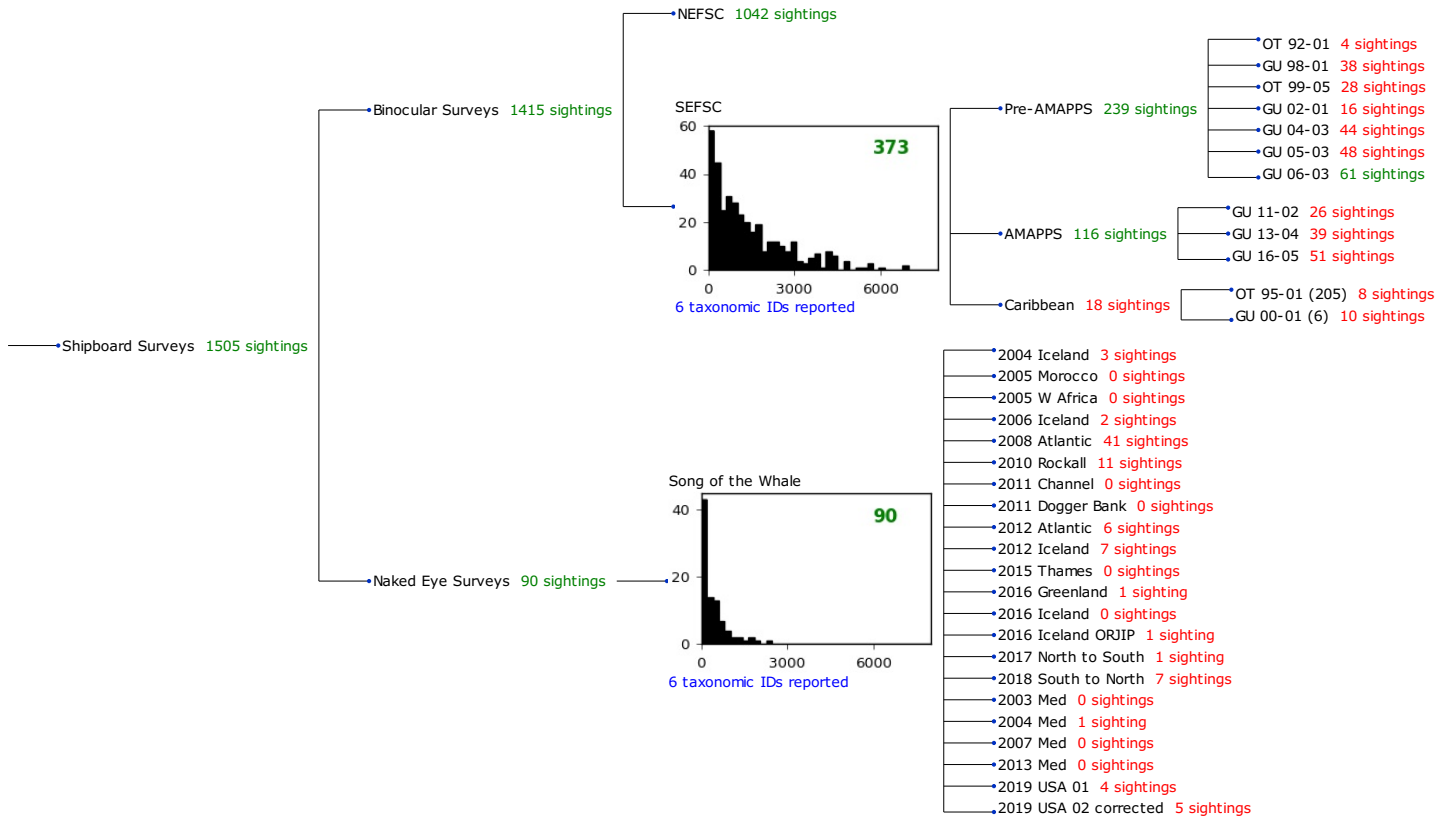


Figure 14: Detection hierarchy for shipboard surveys, showing how they were pooled during detectability modeling, for detection functions that pooled multiple taxa but could not use a taxonomic covariate to account for differences between them. Each histogram represents a detection function and summarizes the perpendicular distances of observations that were pooled to fit it, prior to truncation. Observation counts, also prior to truncation, are shown in green when they met the recommendation of Buckland et al. (2001) that detection functions utilize at least 60 sightings, and red otherwise. For rare taxa, it was not always possible to meet this recommendation, yielding higher statistical uncertainty. During the spatial modeling stage of the analysis, effective strip widths were computed for each survey using the closest detection function above it in the hierarchy (i.e. moving from right to left in the figure). Surveys that do not have a detection function above them in this figure were either addressed by a detection function presented in a different section of this report, or were omitted from the analysis.

#### 2.2.1.1.1 SEFSC

After right-truncating observations greater than 4500 m, we fitted the detection function to the 361 observations that remained (Table 4). The selected detection function (Figure 15) used a hazard rate key function with Beaufort (Figure 16) and VesselName (Figure 17) as covariates.

Table 4: Observations used to fit the SEFSC detection function.

ScientificName	n
Feresa attenuata/Peponocephala electra	7
Globicephala	227
Grampus griseus	121
Orcinus orca	1
Peponocephala electra	3
Pseudorca crassidens	2
<b>Total</b>	<b>361</b>

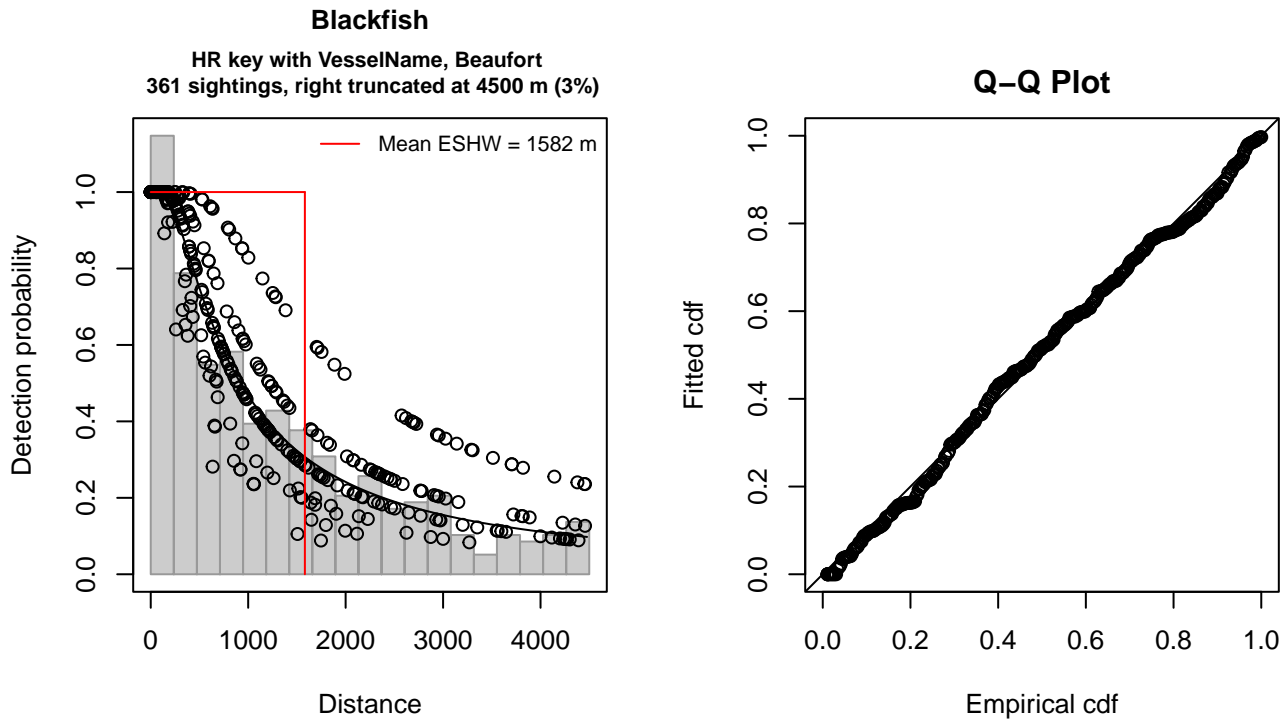


Figure 15: SEFSC detection function and Q-Q plot showing its goodness of fit.

Statistical output for this detection function:

Summary for ds object

Number of observations : 361  
 Distance range : 0 - 4500  
 AIC : 5876.279

Detection function:

Hazard-rate key function

Detection function parameters

Scale coefficient(s):

	estimate	se
(Intercept)	7.3597538	0.3426685
VesselNameOregon II	-0.5805409	0.4158932
Beaufort2	-0.5439643	0.4011114
Beaufort3-4	-0.8577400	0.3820711
Beaufort5	-1.2038982	0.5170081

Shape coefficient(s):

	estimate	se
(Intercept)	0.2309157	0.1254747

	Estimate	SE	CV
Average p	0.3253837	0.03477386	0.1068703
N in covered region	1109.4594048	128.24893603	0.1155959

Distance sampling Cramer-von Mises test (unweighted)

Test statistic = 0.112666 p = 0.526278

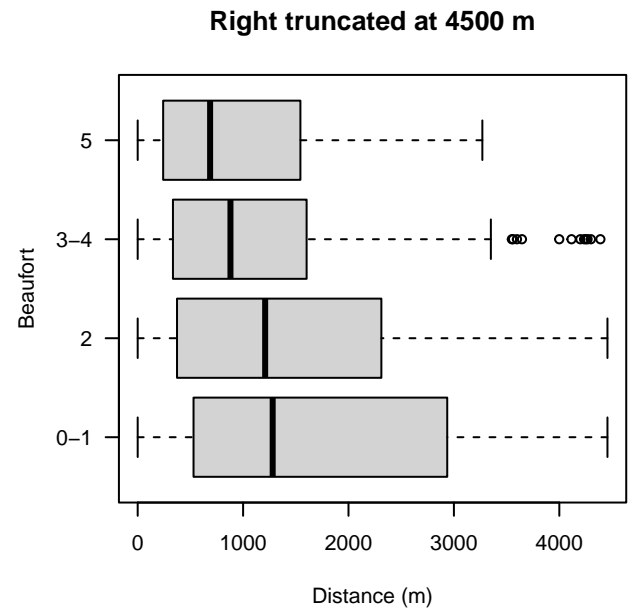
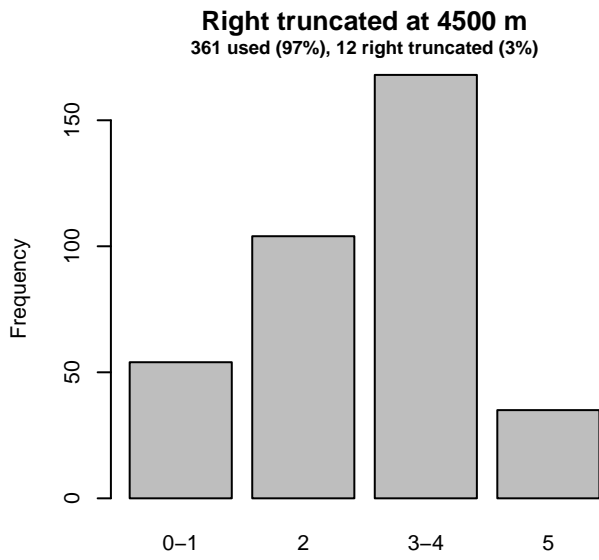
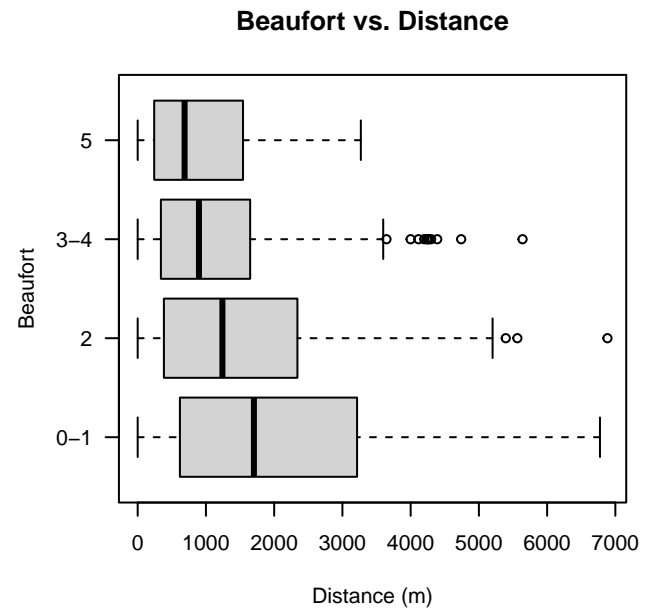
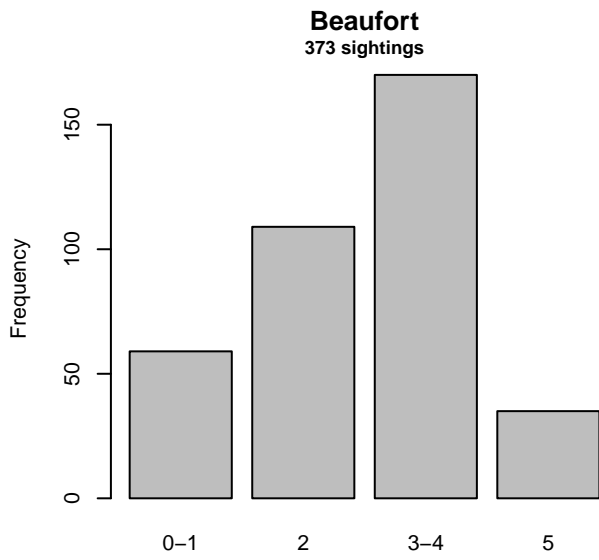


Figure 16: Distribution of the Beaufort covariate before (top row) and after (bottom row) observations were truncated to fit the SEFSC detection function.

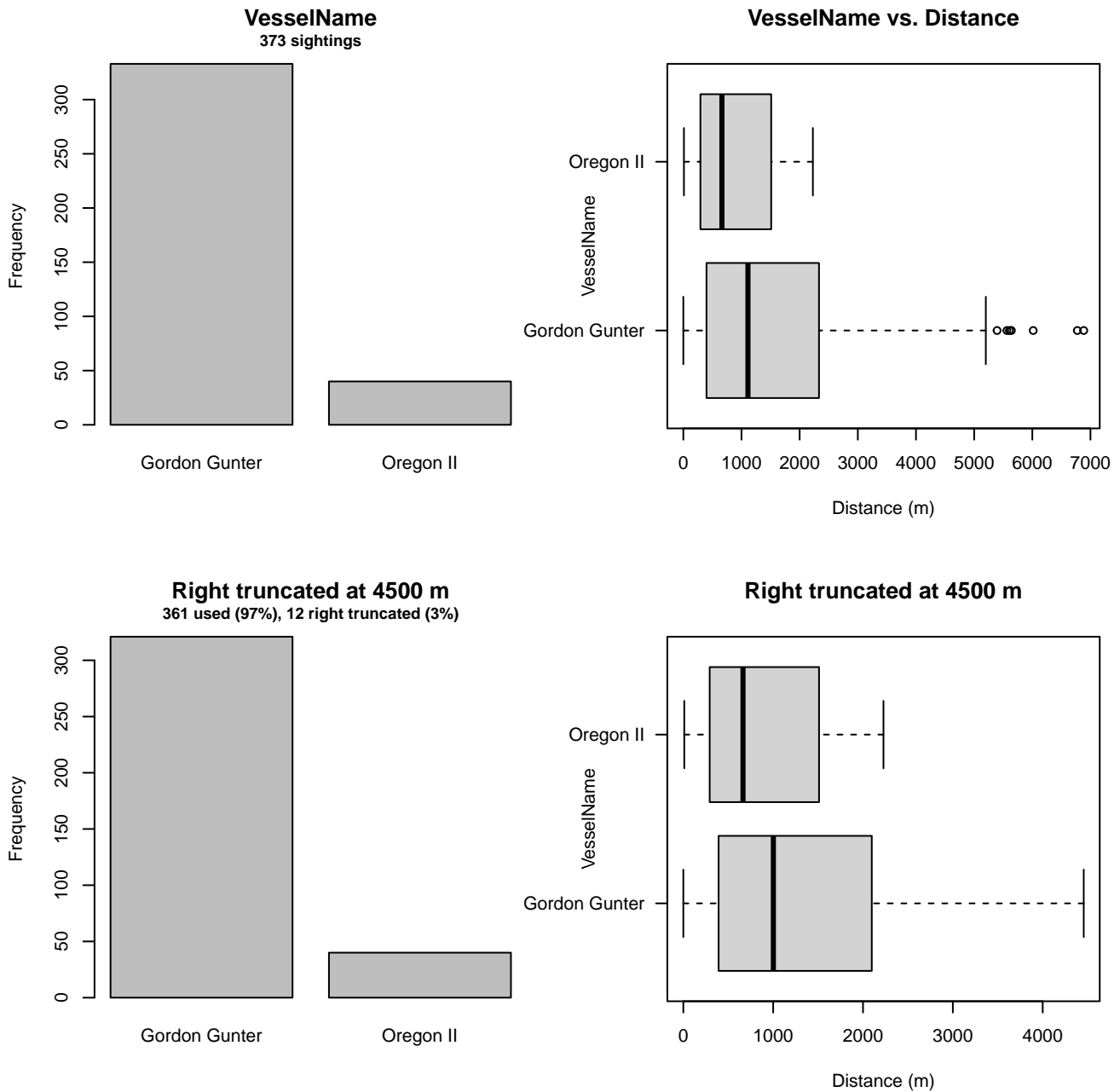


Figure 17: Distribution of the VesselName covariate before (top row) and after (bottom row) observations were truncated to fit the SEFSC detection function.

### 2.2.1.1.2 Song of the Whale

After right-truncating observations greater than 1500 m, we fitted the detection function to the 86 observations that remained (Table 5). The selected detection function (Figure 18) used a hazard rate key function with Beaufort (Figure 19) and Clouds (Figure 20) as covariates.

Table 5: Observations used to fit the Song of the Whale detection function.

ScientificName	n
Globicephala	48
Globicephala macrorhynchus	10
Globicephala melas	3
Grampus griseus	15
Orcinus orca	6
Pseudorca crassidens	4
<b>Total</b>	<b>86</b>

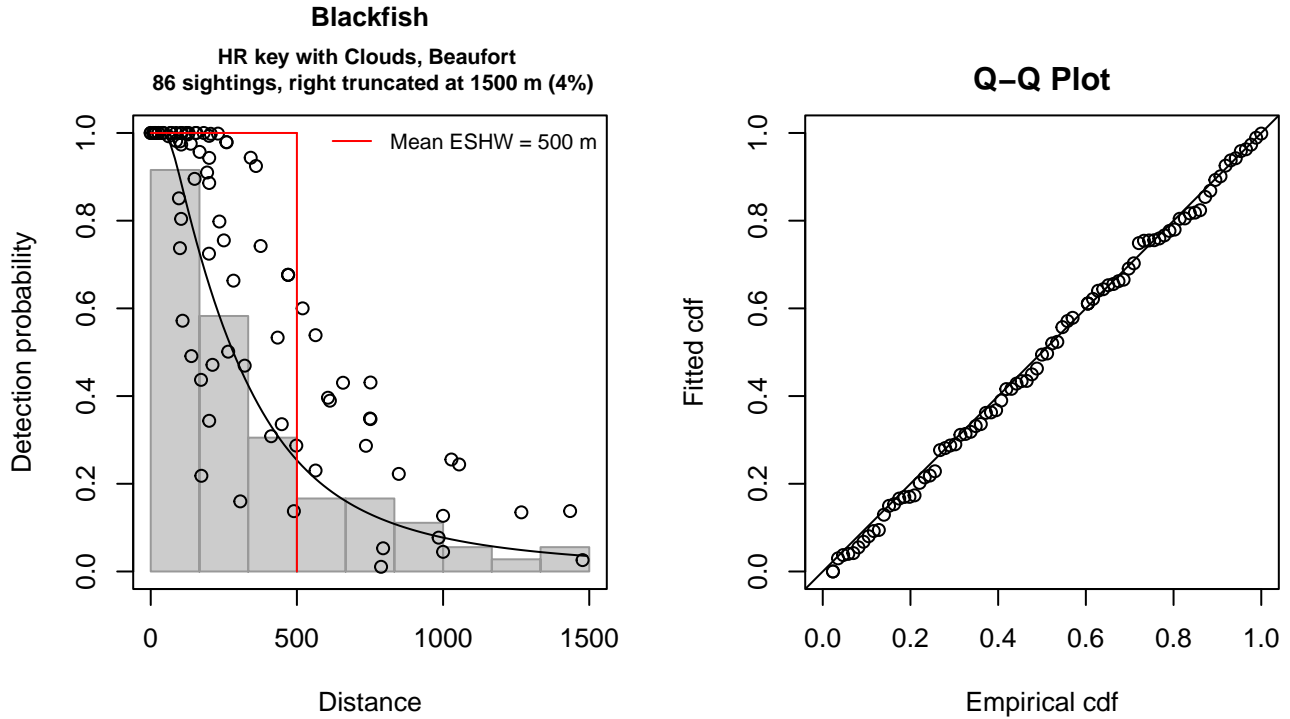


Figure 18: Song of the Whale detection function and Q-Q plot showing its goodness of fit.

Statistical output for this detection function:

Summary for ds object

Number of observations : 86  
 Distance range : 0 - 1500  
 AIC : 1170.598

Detection function:

Hazard-rate key function

Detection function parameters

Scale coefficient(s):

	estimate	se
(Intercept)	6.4796997	0.26905817
Clouds	-0.1344265	0.04822789
Beaufort3-4	-0.6588095	0.31406041

Shape coefficient(s):

	estimate	se
(Intercept)	0.7265327	0.1798353

	Estimate	SE	CV
Average p	0.265116	0.04508089	0.1700421
N in covered region	324.386340	63.44454836	0.1955833

Distance sampling Cramer-von Mises test (unweighted)  
 Test statistic = 0.019751 p = 0.997226

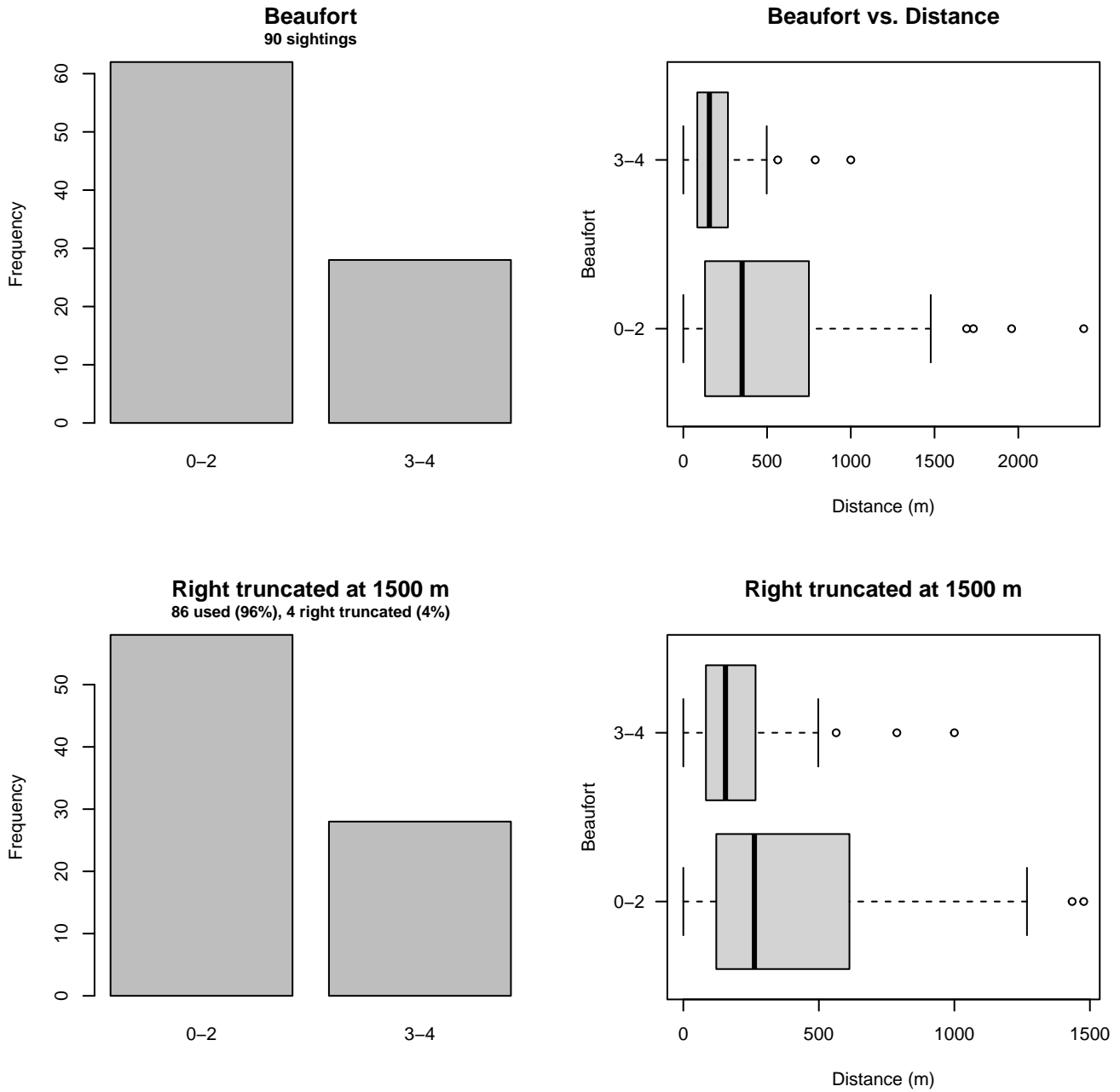


Figure 19: Distribution of the Beaufort covariate before (top row) and after (bottom row) observations were truncated to fit the Song of the Whale detection function.

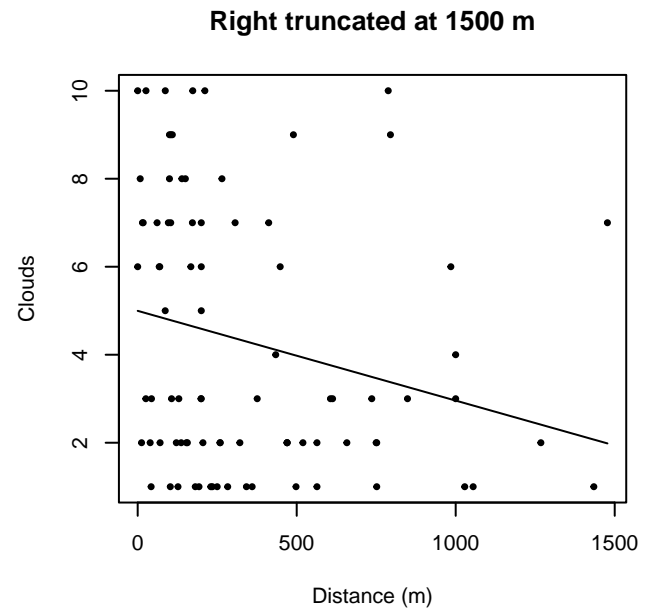
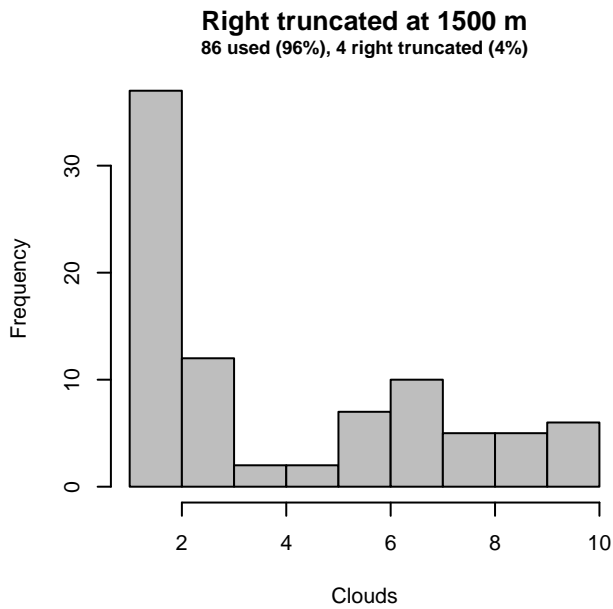
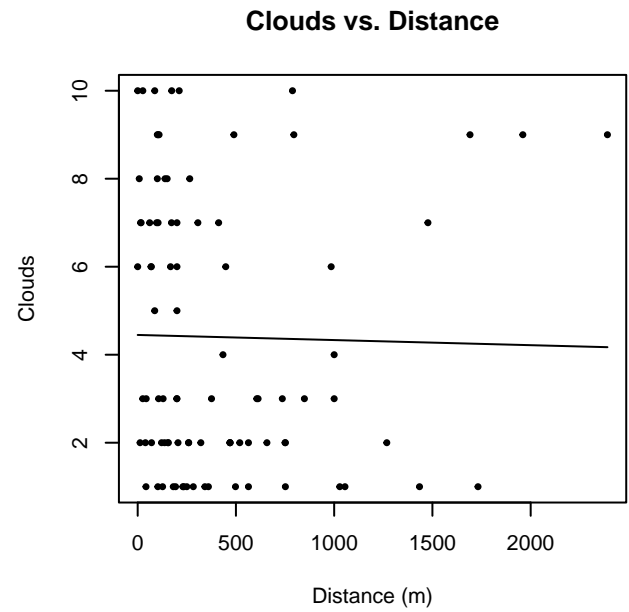
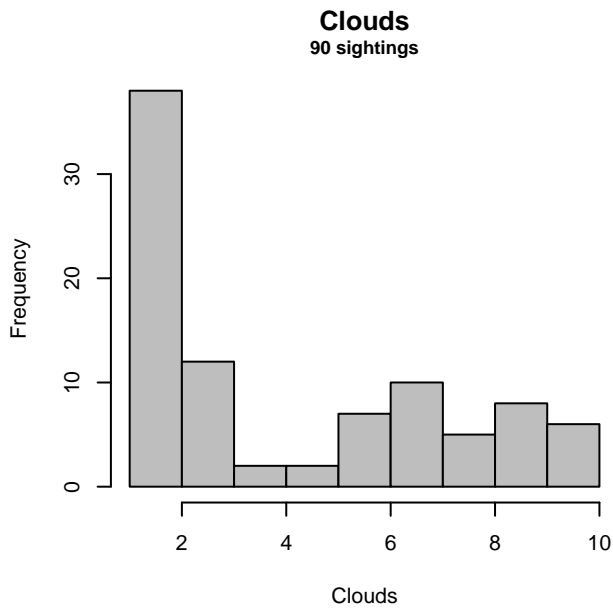


Figure 20: Distribution of the Clouds covariate before (top row) and after (bottom row) observations were truncated to fit the Song of the Whale detection function.

## 2.2.2 Pilot Whales and Risso’s Dolphin

### 2.2.2.1 Aerial Surveys

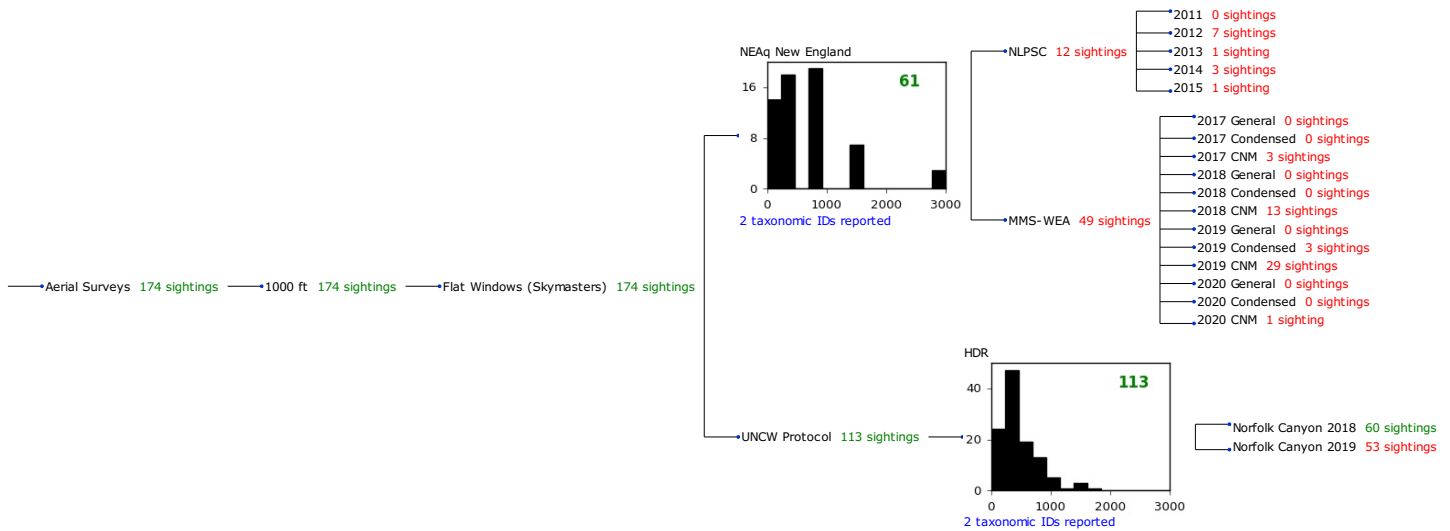


Figure 21: Detection hierarchy for aerial surveys, showing how they were pooled during detectability modeling, for detection functions that pooled multiple taxa but could not use a taxonomic covariate to account for differences between them. Each histogram represents a detection function and summarizes the perpendicular distances of observations that were pooled to fit it, prior to truncation. Observation counts, also prior to truncation, are shown in green when they met the recommendation of Buckland et al. (2001) that detection functions utilize at least 60 sightings, and red otherwise. For rare taxa, it was not always possible to meet this recommendation, yielding higher statistical uncertainty. During the spatial modeling stage of the analysis, effective strip widths were computed for each survey using the closest detection function above it in the hierarchy (i.e. moving from right to left in the figure). Surveys that do not have a detection function above them in this figure were either addressed by a detection function presented in a different section of this report, or were omitted from the analysis.

#### 2.2.2.1.1 NEAq New England

After right-truncating observations greater than 1852 m and left-truncating observations less than 71 m (Figure 23), we fitted the detection function to the 58 observations that remained (Table 6). The selected detection function (Figure 22) used a half normal key function with no covariates.

Table 6: Observations used to fit the NEAq New England detection function.

ScientificName	n
Globicephala	16
Grampus griseus	42
<b>Total</b>	<b>58</b>



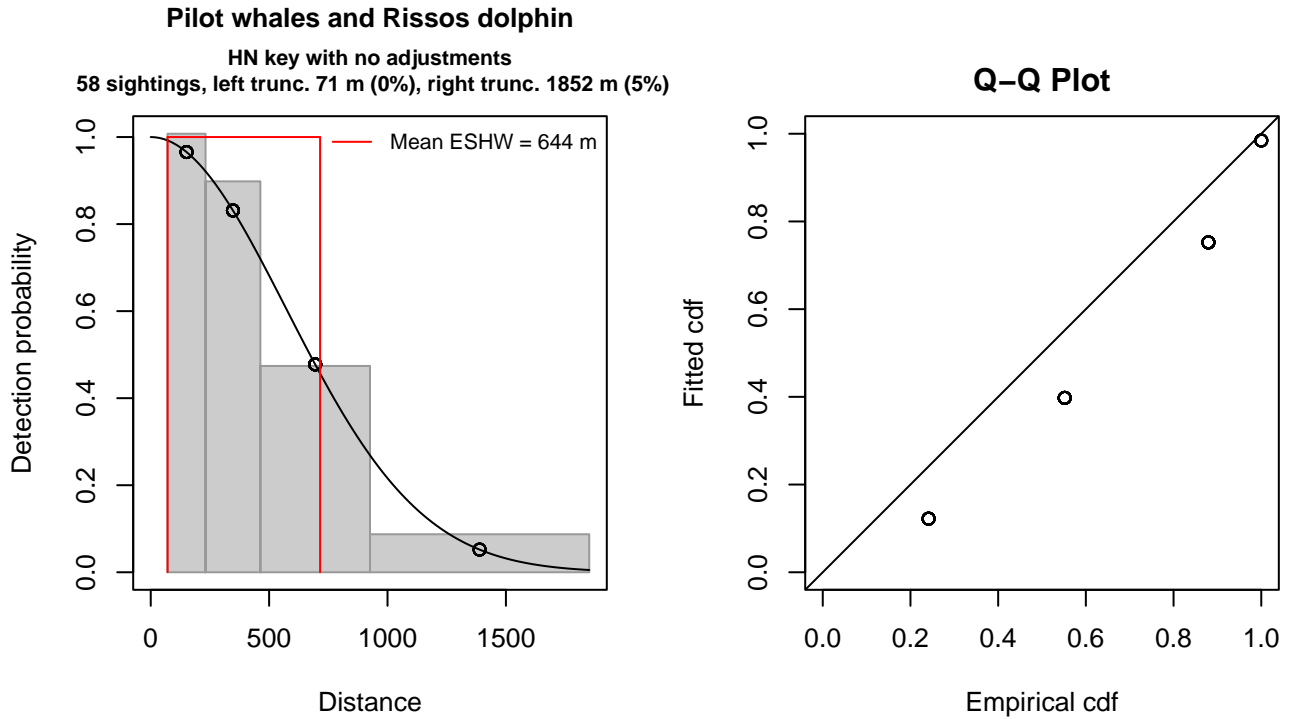


Figure 22: NEAq New England detection function and Q-Q plot showing its goodness of fit.

Statistical output for this detection function:

Summary for ds object

Number of observations : 58  
 Distance range : 71 - 1852  
 AIC : 156.0466

Detection function:

Half-normal key function

Detection function parameters

Scale coefficient(s):

	estimate	se
(Intercept)	6.347853	0.1032999

	Estimate	SE	CV
Average p	0.3617668	0.04089634	0.1130461
N in covered region	160.3242530	24.72501947	0.1542188

Distance sampling Cramer-von Mises test (unweighted)

Test statistic = 0.430759 p = 0.060002

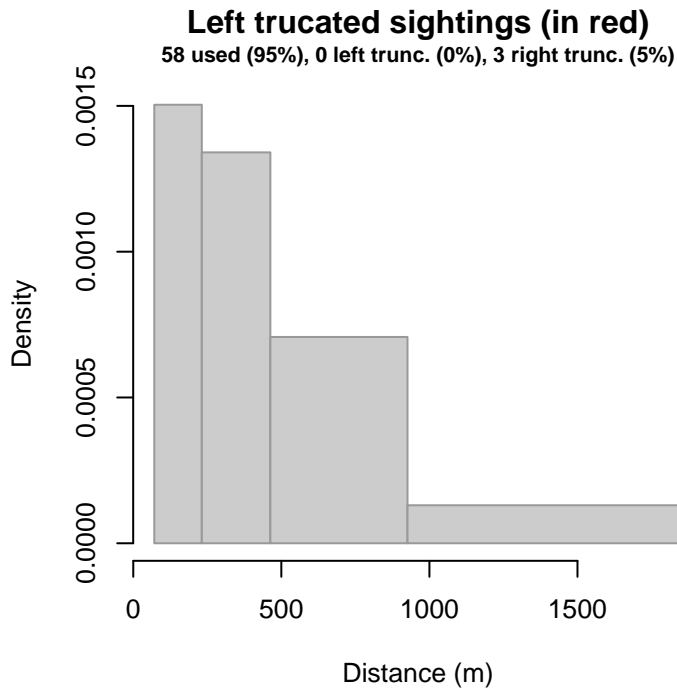


Figure 23: Density histogram of observations used to fit the NEAq New England detection function, with the left-most bar showing observations at distances less than 71 m, which were left-truncated and excluded from the analysis [Buckland et al. (2001)]. (This bar may be very short if there were very few left-truncated sightings, or very narrow if the left truncation distance was very small; in either case it may not appear red.)

#### 2.2.2.1.2 HDR

After right-truncating observations greater than 1500 m and left-truncating observations less than 111 m (Figure 25), we fitted the detection function to the 108 observations that remained (Table 7). The selected detection function (Figure 24) used a hazard rate key function with Swell (Figure 26) as a covariate.

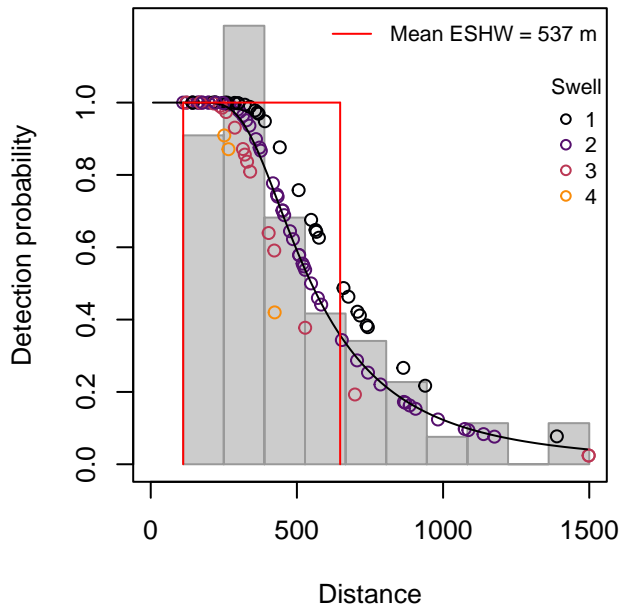
Table 7: Observations used to fit the HDR detection function.

ScientificName	n
Globicephala	66
Grampus griseus	42
<b>Total</b>	<b>108</b>

## Pilot whales and Risso's dolphin

HR key with Swell

108 sightings, left trunc. 111 m (4%), right trunc. 1500 m (1%)



## Q-Q Plot

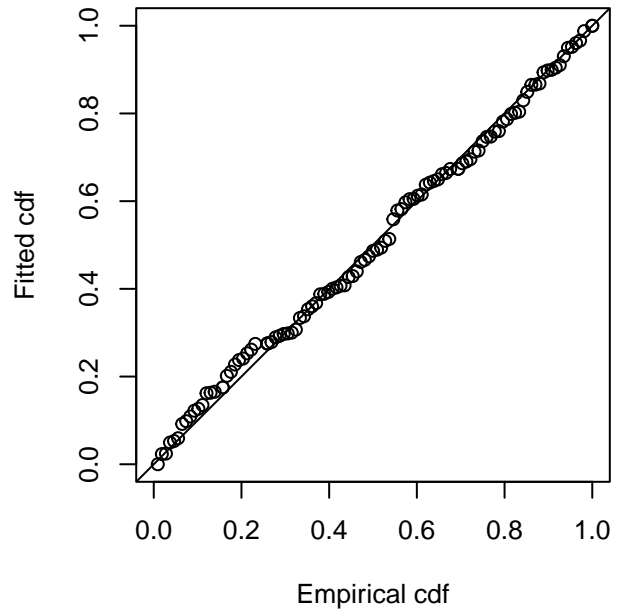


Figure 24: HDR detection function and Q-Q plot showing its goodness of fit.

Statistical output for this detection function:

Summary for ds object

Number of observations : 108  
 Distance range : 111 - 1500  
 AIC : 1479.102

Detection function:

Hazard-rate key function

Detection function parameters

Scale coefficient(s):

	estimate	se
(Intercept)	6.5207075	0.2852850
Swell	-0.1712662	0.1474231

Shape coefficient(s):

	estimate	se
(Intercept)	1.044626	0.1820091

	Estimate	SE	CV
Average p	0.3789427	0.04750114	0.1253518
N in covered region	285.0035382	41.82280744	0.1467449

Distance sampling Cramer-von Mises test (unweighted)

Test statistic = 0.045799 p = 0.901252

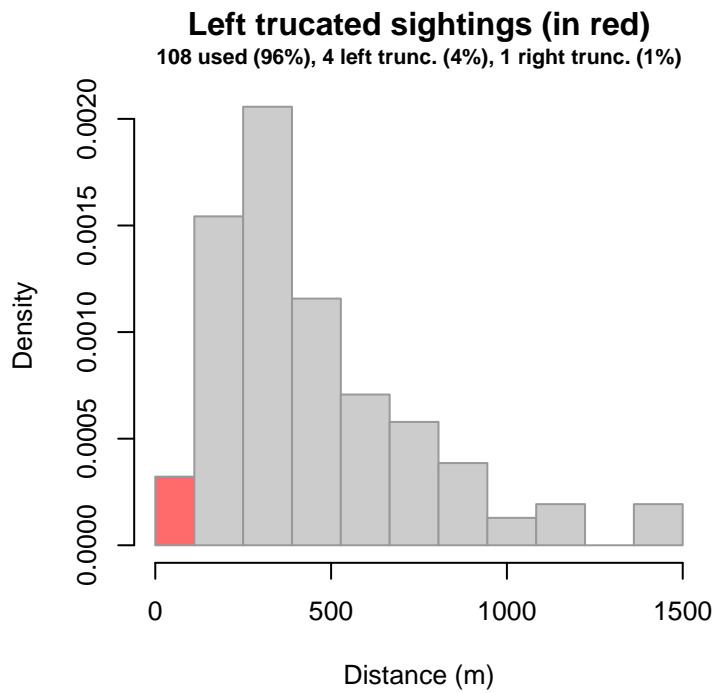


Figure 25: Density histogram of observations used to fit the HDR detection function, with the left-most bar showing observations at distances less than 111 m, which were left-truncated and excluded from the analysis [Buckland et al. (2001)]. (This bar may be very short if there were very few left-truncated sightings, or very narrow if the left truncation distance was very small; in either case it may not appear red.)

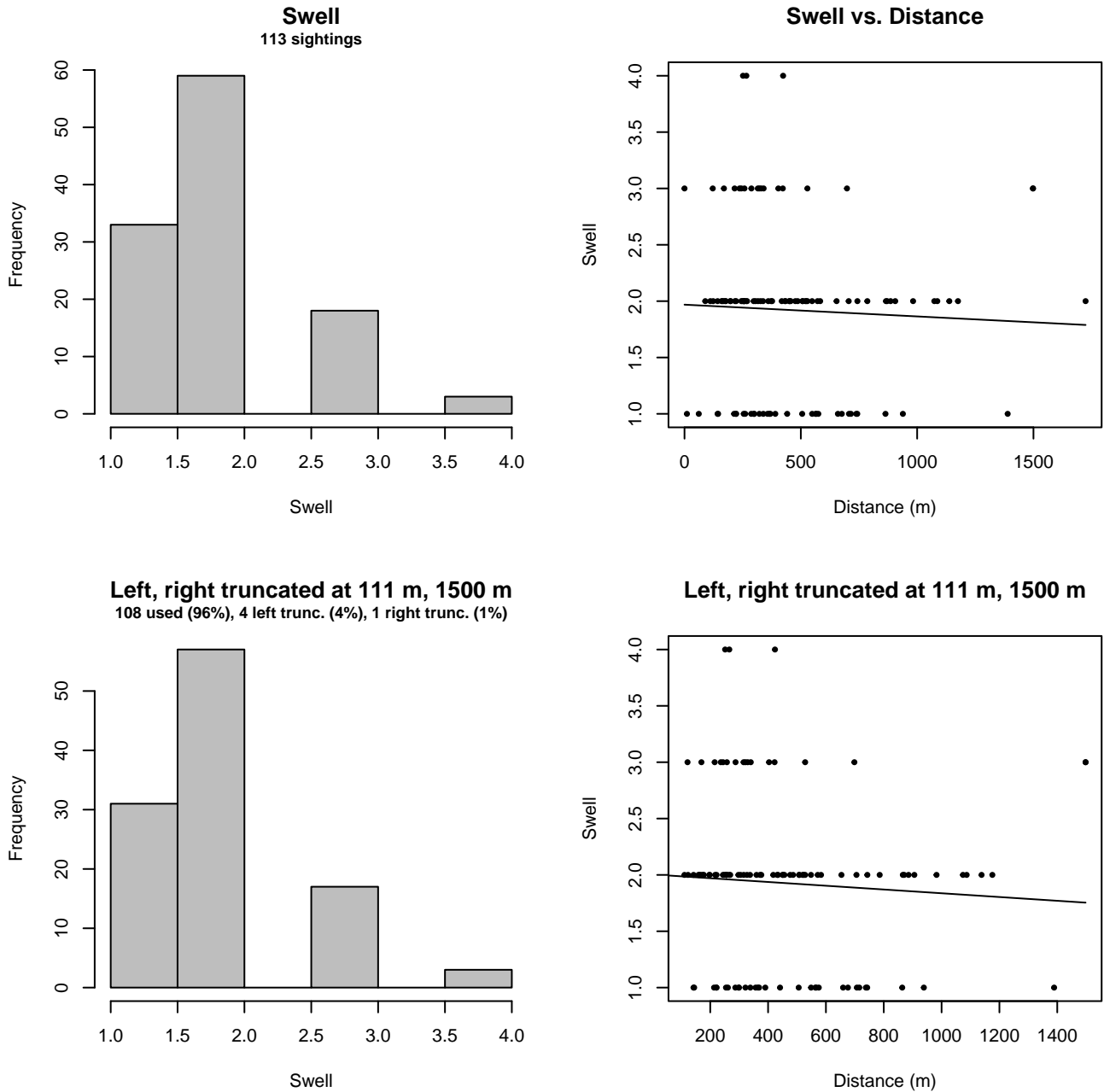


Figure 26: Distribution of the Swell covariate before (top row) and after (bottom row) observations were truncated to fit the HDR detection function.

### 3 Bias Corrections

Density surface modeling methodology uses *distance sampling* (Buckland et al. 2001) to model the probability that an observer on a line transect survey will detect an animal given the perpendicular distance to it from the transect line. Distance sampling assumes that detection probability is 1 when perpendicular distance is 0. When this assumption is not met, detection probability is biased high, leading to an underestimation of density and abundance. This is known as the  $g_0 < 1$  problem, where  $g_0$  refers to the detection probability at distance 0. Modelers often try to address this problem by estimating  $g_0$  empirically and dividing it into estimated density or abundance, thereby correcting those estimates to account for the animals that were presumed missed.

Two important sources of bias for visual surveys are known as *availability bias*, in which an animal was present on the transect line but impossible to detect, e.g. because it was under water, and *perception bias*, in which an animal was present and available but not noticed, e.g. because of its small size or cryptic coloration or behavior (Marsh and Sinclair 1989). Modelers often

estimate the influence of these two sources of bias on detection probability independently, yielding two estimates of  $g_0$ , hereafter referred to as  $g_{0A}$  and  $g_{0P}$ , and multiply them together to obtain a final, combined estimate:  $g_0 = g_{0A} \cdot g_{0P}$ .

Our overall approach was to perform this correction on a per-observation basis, to have the flexibility to account for many factors such as platform type, surveyor institution, group size, group composition (e.g. singleton, mother-calf pair, or surface active group), and geographic location (e.g. feeding grounds vs. calving grounds). The level of complexity of the corrections varied by species according to the amount of information available, with North Atlantic right whale having the most elaborate corrections, derived from a substantial set of publications documenting its behavior, and various lesser known odontocetes having corrections based only on platform type (aerial or shipboard), derived from comparatively sparse information. Here we document the corrections used for pilot whales.

### 3.1 Aerial Surveys

Palka et al. (2021) developed perception bias corrections using two team, mark recapture distance sampling (MRDS) methodology (Burt et al. 2014) for aerial surveys conducted in 2010-2017 by NOAA NEFSC and SEFSC during the AMAPPS program. These were the only extant perception bias estimates developed from aerial surveys used in our analysis, aside from estimates developed earlier by Palka and colleagues (Palka 2006; Palka et al. 2017). Those earlier efforts utilized older methods and less data than their 2021 analysis, so we applied the Palka et al. (2021) estimates to all aerial survey programs (Table 8).

We applied Palka’s estimate for NEFSC to all programs other than SEFSC, on the basis that the NEFSC estimate was made just for pilot whales without pooling other species, while the SEFSC estimate was more roughly 50/50 pilot whales and Risso’s dolphin. Also, those other programs are likely to be more similar to NEFSC than SEFSC, by virtue of scanning much farther out than SEFSC, which appeared to focus more attention directly below the plane, yielding a narrower truncation distance in the AMAPPS analysis (Palka et al. 2021). However, for all surveys, to account for the influence of large group sizes on perception bias, we followed Carretta et al. (2000) and set the perception bias correction factor for sightings of more than 25 animals to  $g_{0P} = 0.994$ .

We caution that it is possible that perception bias was different on the other aerial programs, as they often used different aircraft, flew at different altitudes, and were staffed by different personnel. Of particular concern are that many programs flew Cessna 337 Skymasters, which had flat windows, while NOAA flew de Havilland Twin Otters, which had bubble windows, which likely afforded a better view of the transect line and therefore might have required less of a correction than the Skymasters. Correcting the other programs using NOAA’s estimate as we have done is likely to yield less bias than leaving them uncorrected, but we urge all programs to undertake their own efforts to estimate perception bias, as resources allow.

We estimated availability bias corrections using the Laake et al. (1997) estimator and dive intervals reported by Palka et al. (2017) (Table 9). To estimate time in view, needed by the Laake estimator, we used results reported by Robertson et al. (2015), rescaled linearly for each survey program according to its target altitude and speed. We caution that Robertson’s analysis was done for a de Havilland Twin Otter, which may have a different field of view than that of the other aircraft used here, which mainly comprised Cessna 337 Skymasters with flat window. However, we note that McLellan et al. (2018) conducted a sensitivity analysis on the influence of the length of the “window of opportunity” to view beaked whales from a Cessna Skymaster on their final density estimates and found that they varied by only a few thousandths of an animal per kilometer when the window of opportunity more than doubled. Still, we urge additional program-specific research into estimation of availability bias.

To address the influence of group size on availability bias, we applied the group availability estimator of McLellan et al. (2018) on a per-observation basis. Following Palka et al. (2021), who also used that method, we assumed that individuals in the group dived asynchronously. The resulting  $g_{0A}$  corrections ranged from about 0.55 to 1.0 (Figure 27), with the large majority of observations having a correction of 0.98 or higher, owing to large group sizes. We caution that the assumption of asynchronous diving can lead to an underestimation of density and abundance if diving is actually synchronous; see McLellan et al. (2018) for an exploration of this effect. However, if future research finds that this species conducts synchronous dives and characterizes the degree of synchronicity, the model can be updated to account for this knowledge.

Table 8: Perception bias corrections for pilot whales applied to aerial surveys.

Surveys	Group Size	$g_{0P}$	$g_{0P}$ Source
SEFSC	$\leq 25$	0.74	Palka et al. (2021): SEFSC
All others	$\leq 25$	0.54	Palka et al. (2021): NEFSC
All	$> 25$	0.99	Caretta et al. 2000

Table 9: Surface and dive intervals for pilot whales used to estimate availability bias corrections.

Surface Interval (s)	Dive Interval (s)	Source
318	319.8	Palka et al. (2021)

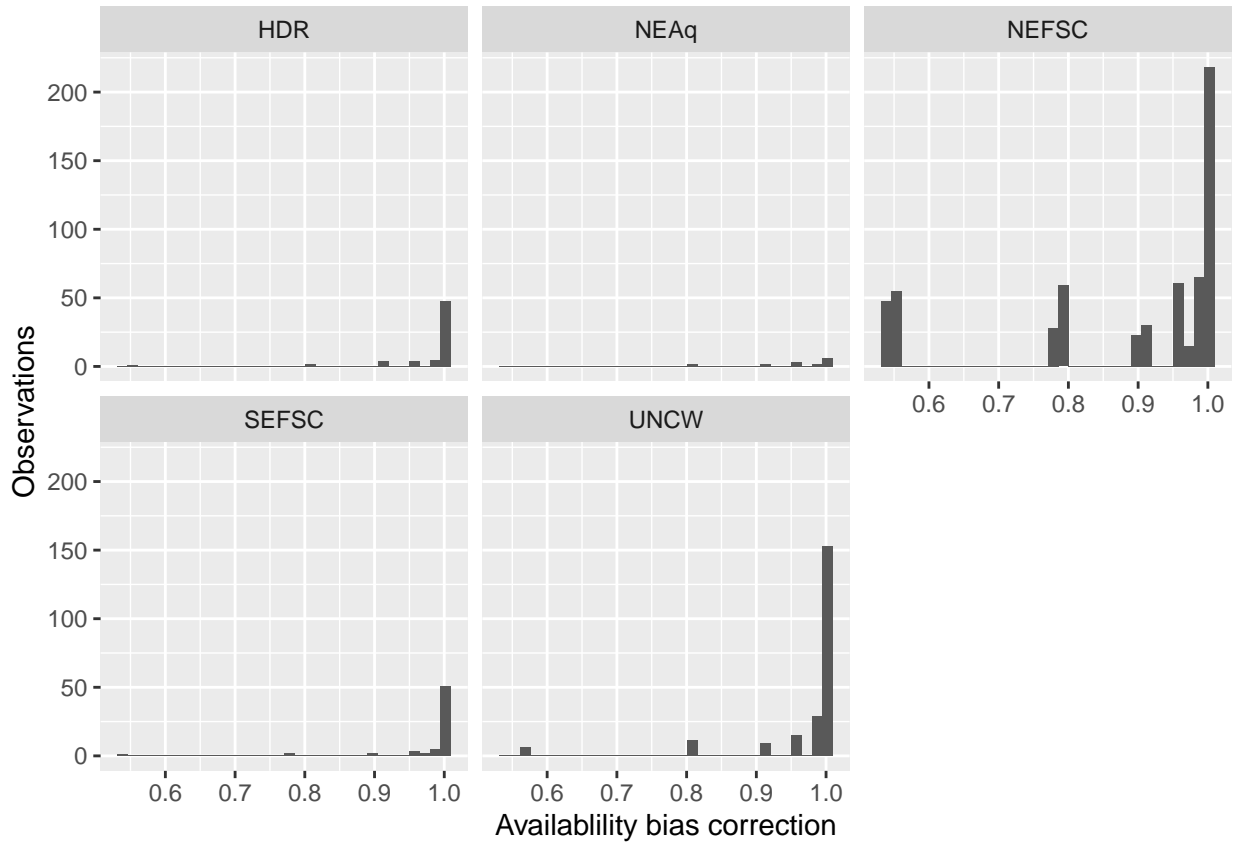


Figure 27: Availability bias corrections for pilot whales for aerial surveys, by institution.

### 3.2 Shipboard Surveys

Most of the shipboard surveys in our analysis used high-power (25x150), pedestal-mounted binoculars. Similar to aerial surveys, Palka et al. (2021) developed perception bias corrections using two team, MRDS methodology (Burt et al. 2014) for high-power binocular surveys conducted in 2010-2017 by NOAA NEFSC and SEFSC during the AMAPPS program. These were the only extant perception bias estimates developed from high-power binocular surveys used in our analysis, aside from estimates developed earlier by Palka and colleagues (Palka 2006; Palka et al. 2017). Those earlier efforts utilized older methods and less data than their 2021 analysis, so we applied the Palka et al. (2021) estimates to all shipboard surveys that searched with high-power binoculars (Table 10).

Only the MCR Song of the Whale surveys used naked eyes rather than high-power binoculars, but it did not prepare perception bias estimates for pilot whales. So as a proxy, we used the estimate for pilot whales from Cañadas et al. (2021) (Table 10).

For all surveys, to account for the influence of large group sizes on perception bias, we followed Barlow and Forney (2007) and set the perception bias correction factor for sightings of more than 20 animals to  $g_{0P} = 0.97$ . Given that the dive interval of this species (Table 9) was short relative to the amount of time a given patch of water remained in view to shipboard observers, we assumed that no availability bias correction was needed ( $g_{0A} = 1$ ), following Palka et al. (2021).

Table 10: Perception and availability bias corrections for pilot whales applied to shipboard surveys.

Surveys	Searching Method	Group Size	$g_{0P}$	$g_{0P}$ Source	$g_{0A}$	$g_{0A}$ Source
NEFSC	Binoculars	$\leq 20$	0.66	Palka et al. (2021): NEFSC	1	Assumed
SEFSC	Binoculars	$\leq 20$	0.71	Palka et al. (2021): SEFSC	1	Assumed
MCR	Naked Eye	$\leq 20$	0.74	Cañadas et al. (2021)	1	Assumed
All	All	$> 20$	0.97	Barlow and Forney (2007)	1	Assumed

## 4 Density Model

The two extant species of pilot whale, the long-finned pilot whale (*Globicephala melas*) and the short-finned pilot whale (*Globicephala macrorhynchus*) are very difficult for observers to distinguish at sea. Because the size, shape, and color pattern distinctions between the two species are so variable (including the length of the pectoral flippers), the shape of the skull is the most definitive characteristic for identifying the species (Olson 2008). Both species occur in the western North Atlantic; their ranges overlap in our east coast study area. Short-finned pilot whales, the warmer-water species, occur mainly in the southern part of the study area but range north to the southern flank of Georges Bank (Waring et al. 2014) with occasional strandings as far north as Massachusetts (Hayes et al. 2022). Long-finned pilot whales, the colder-water species, occur mainly in the northern part of the study area, but range south along the shelf break as far south as New Jersey, with occasional strandings as far south as Florida (Hayes et al. 2022). Spatial overlap in long-finned and short-finned pilot whales is known to occur along the mid-Atlantic shelf break between Delaware and the southern flank of Georges Bank (Payne and Heinemann 1993; Rone and Pace 2012).

Pilot whales feed on cephalopods and fish. Thorne et al. (2017) examined the movements and foraging behavior of short-finned pilot whales using data from 33 satellite tags deployed off Cape Hatteras, in 2014 and 2015 and found that the highest densities of pilot whale locations occurred along the shelf break from Cape Hatteras to Hudson Canyon, and distribution extended south to shelf break waters south of Cape Lookout, north into shelf break waters of Nantucket Shoals, and included Gulf Stream waters north and east of Cape Hatteras. They identified area restricted foraging behavior close to the shelf break and in submarine canyons highlighting the importance of these areas. Shearer et al. (2022) deployed digital acoustic tags (DTAGs) (Johnson and Tyack 2003) on 43 short-finned pilot whales off Cape Hatteras and found that tagged animals made deep foraging dives up to 1077 m in over half of their foraging dives and foraged almost exclusively in daytime. Additionally, the authors noted the ability of pilot whales to adapt their foraging strategies to local habitat features (Shearer et al. 2022). It has been reported that both pilot whale species forage on a variety of mesopelagic (Spitz et al. 2011; Mèndez-Fernandez et al. 2012), benthic, and epipelagic prey (Aguilar de Soto 2006).

Other work by Baird et al. (2018) has identified kernel density ranges for short-finned pilot whales tagged off of Cape Hatteras and Jacksonville between 2014 and 2017. This work demonstrates that these animals cover a significant range north and south along the continental slope, and occasionally into offshore waters. The tags revealed that an animal tagged off of Hatteras moved to Jacksonville during the tag-deployment. The authors point out that the considerable variability in movement patterns and habitat use likely reflects patterns that vary by social group and by responses to ephemeral oceanographic conditions.

As shown in Table 11, 84% of sightings reported by the surveys included in our study reported only the genus (*Globicephala*) as the taxonomic identification. Further there were only 2 observations attributed to long-finned pilot whales. According to NOAA, “the ability to separately assess the 2 species in U.S. Atlantic waters is complex and requires additional information on seasonal spatial distribution” (Waring et al. 2014). For its 2011 abundance estimates, NOAA fitted a logistic regression model to pilot whale biopsy samples collected between 1998 and 2007 from South Carolina to the southern flank of Georges Bank, using sea surface temperature and seafloor depth to classify the samples into one species or the other. NOAA then applied this model to their 2011 line-transect surveys to classify the visual sightings and produce species-specific abundance estimates. Neither the biopsy data, the 2011 regression model, nor the 2011 line transect surveys were available for our use, so we could not build upon what NOAA had done. Garrison and Rosel (2017) used a habitat-based model to predict the probability that any given sighting was a short-finned pilot whale as a function of latitude, month of the year, and sea surface temperature. They detected an area of overlap between the two species during the summer months that was primarily along the shelf break off the coast of New Jersey (between 38°N and 40°N latitude). However, Garrison expressed doubt that their classification model, which was fitted primarily to genetic samples taken in summer, would work well in colder seasons. Knowing that our objective was to model the species across all months, Garrison declined to make it available for our model. We investigated producing our own habitat-based classification model (as we had done with fin and sei whales, for example) but nearly all of the sightings reported on the surveys available to us were of not resolved to the species level, and we lacked sufficient fully-identified sightings to attempt a classification. Therefore, we modeled both species together as a guild.



Table 11: Pilot whale Observations by Species

ScientificName	n
Globicephala	1253
Globicephala macrorhynchus	230
Globicephala melas	2

In U.S. Atlantic waters, pilot whales are reportedly distributed principally along the continental shelf edge off the northeastern U.S. coast in winter and early spring (Winn 1982; Payne and Heinemann 1993; Abend and Smith 1999; Hamazaki 2002). Then in late spring, pilot whales move into more northern waters in the Gulf of Maine and Georges Bank, where they remain through late fall (Winn 1982; Payne and Heinemann 1993). Pilot whales have also been reported to occupy areas of high relief or submerged banks and have been associated with the Gulf Stream wall and thermal fronts (Waring et al. 1992; Hayes et al. 2022). The survey segments with observations used in this study occurred between 7 m to 4662 m depth, with only 30 observations occurring in waters shallower than 50 m. The sea surface salinity of segments with observations ranged from 31 to 36. The SST of segments with observations ranged from 4°C to 30°C.

Payne and Heinemann (1993) described possible seasonal movements of pilot whales from 1,033 sightings collected on surveys conducted between 1978-1988 (not used in our analysis). The authors linked some of these movements to seasonal distributions of prey species, such as squid and mackerel, but did not present evidence that pilot whales were undertaking large migrations, such as those made by baleen whales moving to and from feeding and calving grounds. Therefore, although seasonal movements were reported, there was no evidence of large-scale migratory behavior that would indicate seasonal changes in species-environment relationships large enough to warrant splitting the data into seasons and modeling them separately, as we did with several baleen whale species. Accordingly, we fitted year-round models to the entire study area.

Models fitted using contemporaneous predictors explained more deviance and had lower AIC and REML scores than models fitted to the same segments using climatological predictors, suggesting that contemporaneous predictors had more explanatory power than climatological predictors for this pilot whale guild. On this basis, we selected the models fitted with contemporaneous predictors as best for modeling pilot whale distribution and abundance.

The pilot whale model contained over 1 million km of segments with 1485 total sightings of groups. A total of 10 covariates were retained in the top model (Table 12) (Figure 31). The retained covariates included a bivariate interaction of depth and slope, sea surface temperature (SST), Fetch, epipelagic micronekton, distance to the 125m isobath, distance to canyons, sea surface salinity (SSS), Total Kinetic Energy (TKE), distance to eddy (any polarity), and distance to front. The relationship to the bivariate term Depth:Slope showed that abundance increased at high slope in all depths with another peak at depths greater than 1000 m across a wide range of slopes. The relationship to SST showed an increase in animals at temperatures above 23 degrees. The fetch covariate was retained with a positive relationship, indicating an avoidance of enclosed inshore areas. There was also a generally positive relationship to epipelagic micronekton, with abundance declining only at the highest concentrations of biomass. This is consistent with reports of pilot whales foraging in the epipelagic zone (Aguilar de Soto 2006). The relationship to the distance to the 125 m isobath showed a peak at distances close to and inshore of the isobath, as well as within 25 km offshore of the isobath. The relationship to distance to canyons indicated more animals close to canyons. This was largely consistent with Thorne et al. (2017) who identified area restricted foraging behavior close to the shelf break and in submarine canyons. There was a generally negative relationship to sea surface salinity with more animals indicated in fresher waters. This relationship elevated density in the on-shelf waters north of Cape Hatteras, where these salinities mainly occur. A positive relationship to TKE was fitted, which was not surprising given this species known association with Gulf Stream waters (Hayes et al. 2022). Finally, the relationship to distance to eddies and distance to fronts showed more animals close to both features. These relationships are largely consistent with reports that pilot whales tend to be associated with slope areas, submerged banks, the Gulf Stream wall and thermal fronts along the continental shelf edge (Hayes et al. 2022).

## 4.1 Final Model

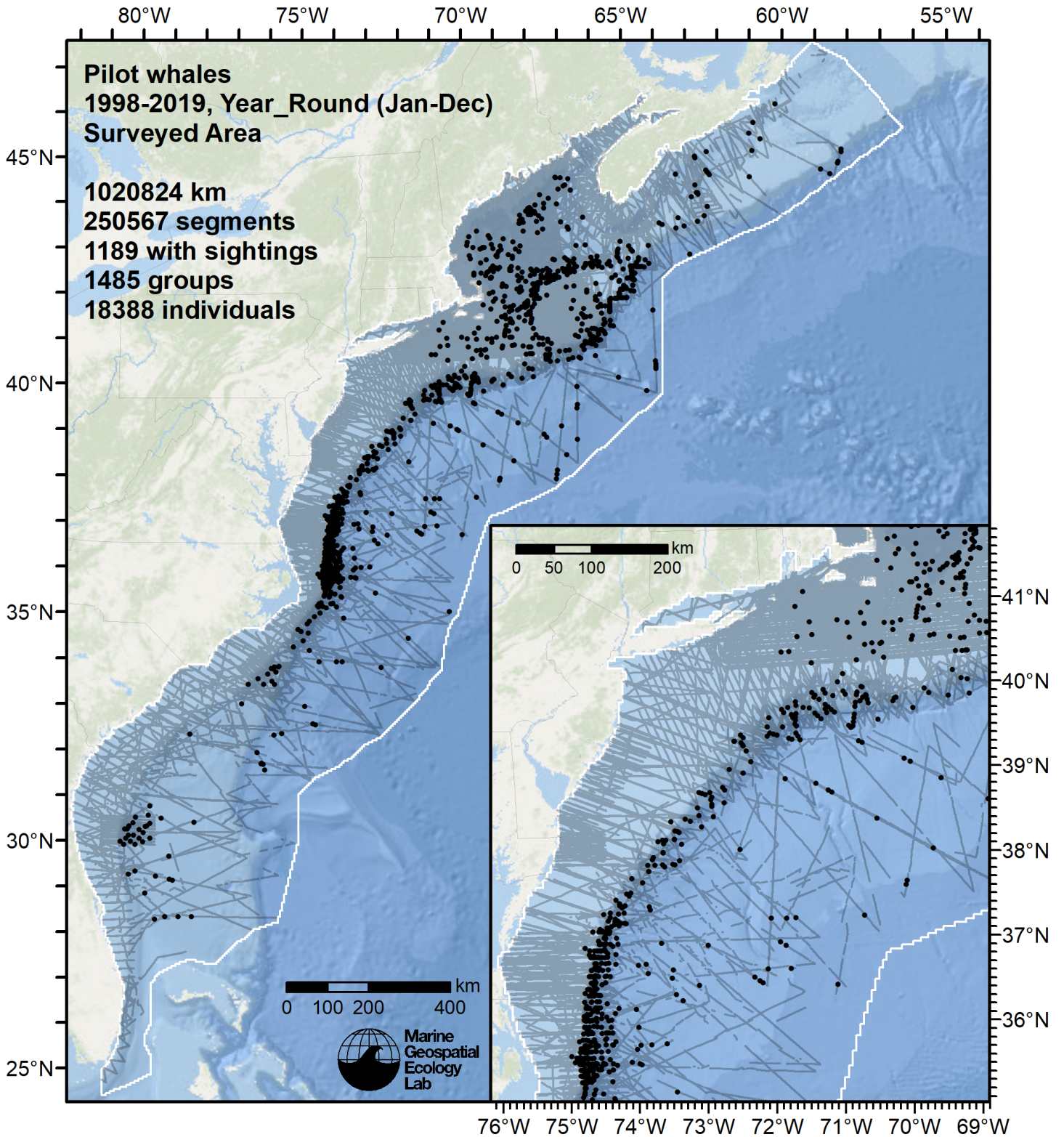


Figure 28: Survey segments used to fit the model. Black points indicate segments with observations.



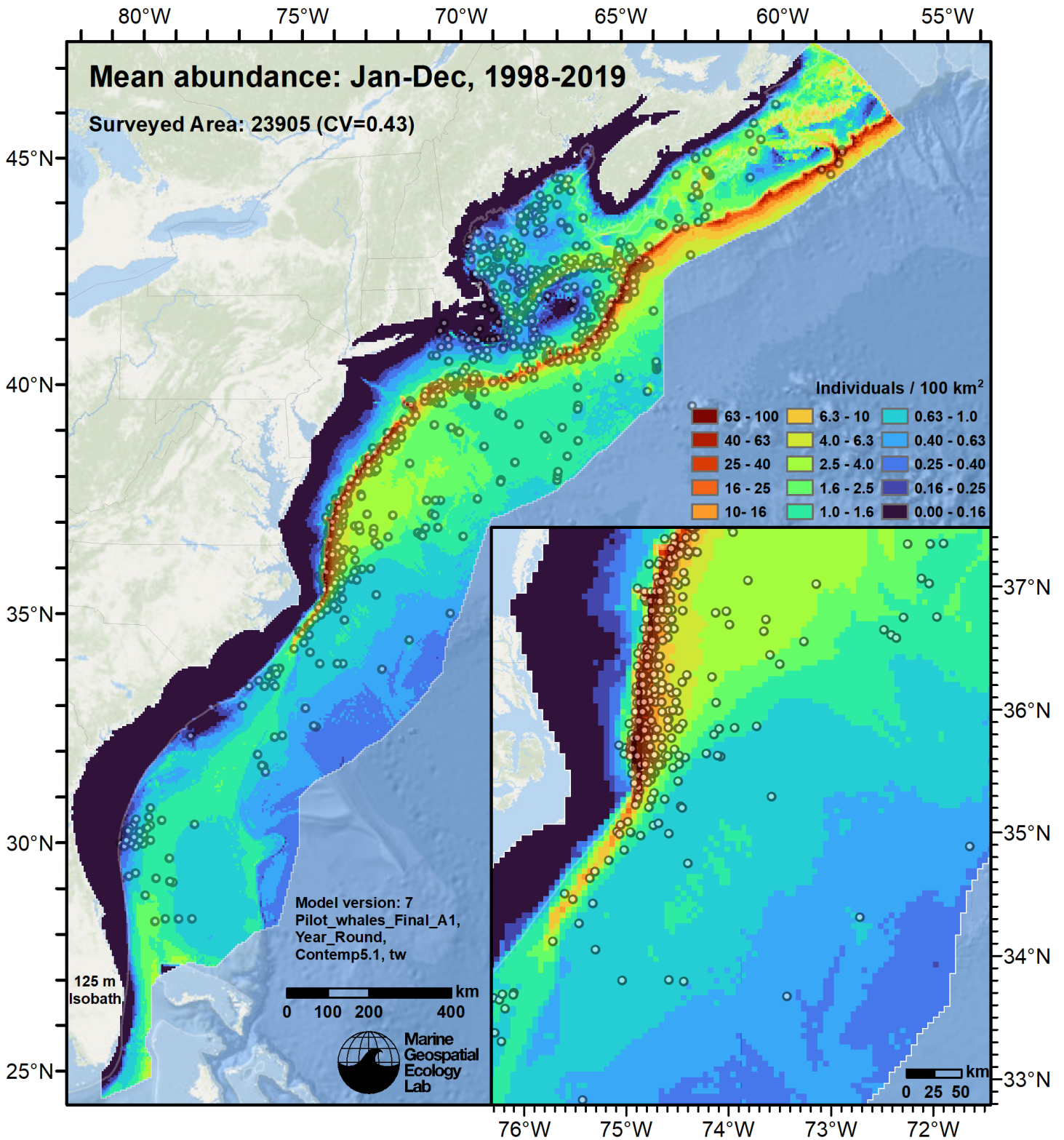


Figure 29: Pilot whales mean density for the indicated period, as predicted by the model. Open circles indicate segments with observations. Mean total abundance and its coefficient of variation (CV) are given in the subtitle. Variance was estimated with the analytic approach given by Miller et al. (2022), Appendix S1, and accounts both for uncertainty in model parameter estimates and for seasonal and interannual variability in dynamic covariates.

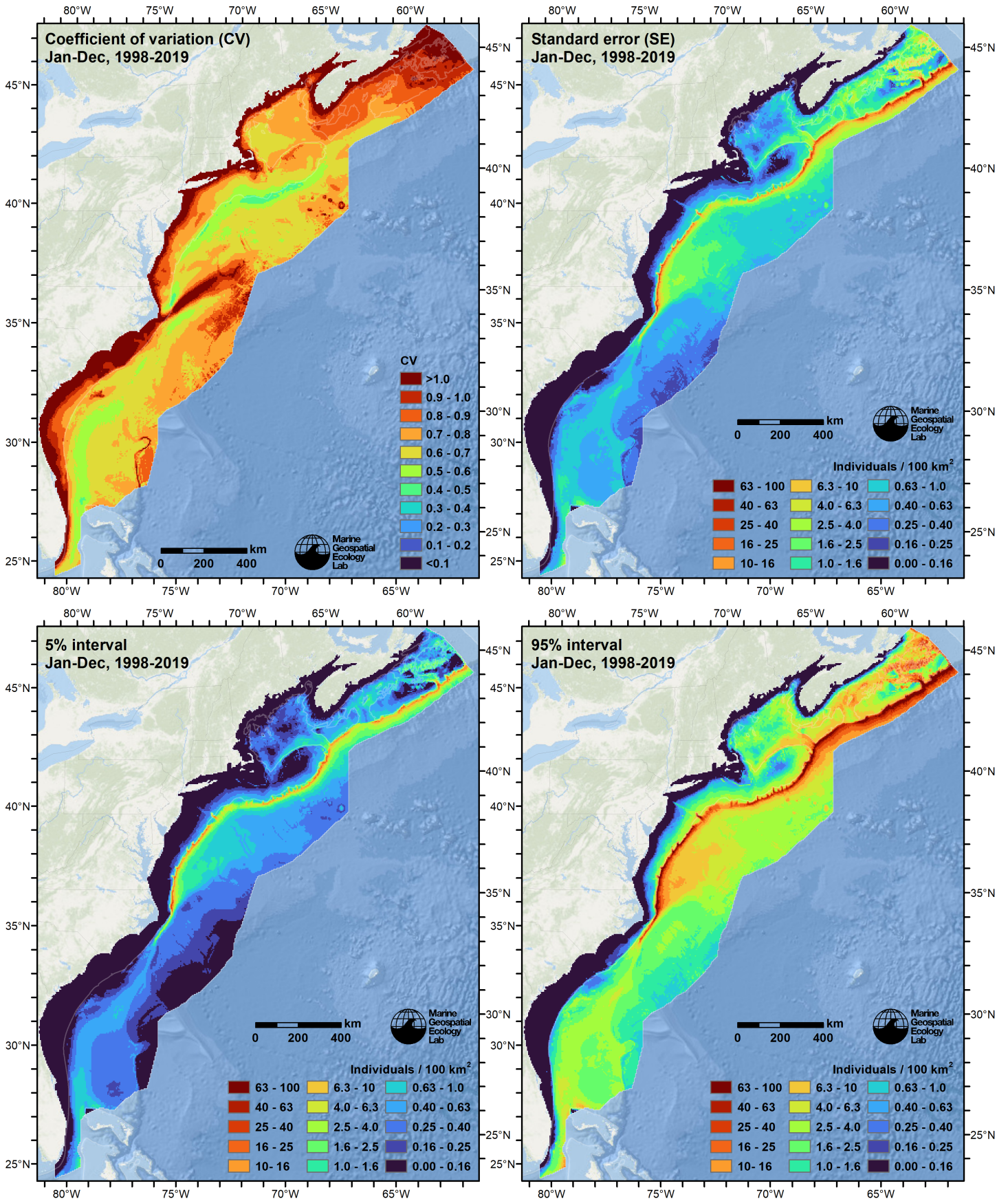


Figure 30: Uncertainty statistics for the pilot whales mean density surface (Figure 29) predicted by the model. Variance was estimated with the analytic approach given by Miller et al. (2022), Appendix S1, and accounts both for uncertainty in model parameter estimates and for seasonal and interannual variability in dynamic covariates.

Statistical output for this model:

Family: Tweedie(p=1.302)

Link function: log

Formula:

```
IndividualsCorrected ~ offset(log(SegmentArea)) + te(log10(pmax(10,
  Depth)), log10((pmax(0.3, pmin(Slope, 30))))), bs = "ts") +
  s(pmax(2.5, SST_CMC), bs = "ts") + s(Fetch_50km, bs = "ts") +
  s(log10(pmax(0.01, pmin(MnkEpi, 27))), bs = "ts") + s(pmax(-100,
  pmin(I(DistTo125m/1000), 100)), bs = "ts") + s(pmin(I(DistToCan/1000),
  350), bs = "ts") + s(pmax(31.5, SSS_HYCOM), bs = "ts") +
  s(log10(pmax(0.002, pmin(TKE, 1.2))), bs = "ts") + s(pmin(I(DistToEddy/1000),
  450), bs = "ts") + s(pmin(I(DistToFront063/1000), 70), bs = "ts")
```

Parametric coefficients:

```
      Estimate Std. Error t value Pr(>|t|)
(Intercept) -20.6340    0.1164  -177.2  <2e-16 ***
---
```

Signif. codes: 0 '\*\*\*' 0.001 '\*\*' 0.01 '\*' 0.05 '.' 0.1 ' ' 1

Approximate significance of smooth terms:

	edf	Ref.df	F	p-value
te(log10(pmax(10, Depth)),log10((pmax(0.3, pmin(Slope, 30)))))	11.8791	24	14.907	< 2e-16
s(pmax(2.5, SST_CMC))	7.8189	9	12.467	< 2e-16
s(Fetch_50km)	0.9863	9	4.405	< 2e-16
s(log10(pmax(0.01, pmin(MnkEpi, 27))))	5.1618	9	13.035	< 2e-16
s(pmax(-100, pmin(I(DistTo125m/1000), 100)))	5.3104	9	4.991	< 2e-16
s(pmin(I(DistToCan/1000), 350))	4.3128	9	5.060	< 2e-16
s(pmax(31.5, SSS_HYCOM))	3.4136	9	3.794	< 2e-16
s(log10(pmax(0.002, pmin(TKE, 1.2))))	0.9596	9	0.798	0.003985
s(pmin(I(DistToEddy/1000), 450))	1.0093	9	1.408	0.000221
s(pmin(I(DistToFront063/1000), 70))	1.0003	9	1.471	0.000131

```
te(log10(pmax(10, Depth)),log10((pmax(0.3, pmin(Slope, 30)))) ***
s(pmax(2.5, SST_CMC)) ***
s(Fetch_50km) ***
s(log10(pmax(0.01, pmin(MnkEpi, 27)))) ***
s(pmax(-100, pmin(I(DistTo125m/1000), 100))) ***
s(pmin(I(DistToCan/1000), 350)) ***
s(pmax(31.5, SSS_HYCOM)) ***
s(log10(pmax(0.002, pmin(TKE, 1.2)))) **
s(pmin(I(DistToEddy/1000), 450)) ***
s(pmin(I(DistToFront063/1000), 70)) ***
---
```

Signif. codes: 0 '\*\*\*' 0.001 '\*\*' 0.01 '\*' 0.05 '.' 0.1 ' ' 1

R-sq.(adj) = 0.0293 Deviance explained = 39.8%  
-REML = 10923 Scale est. = 40.727 n = 250567



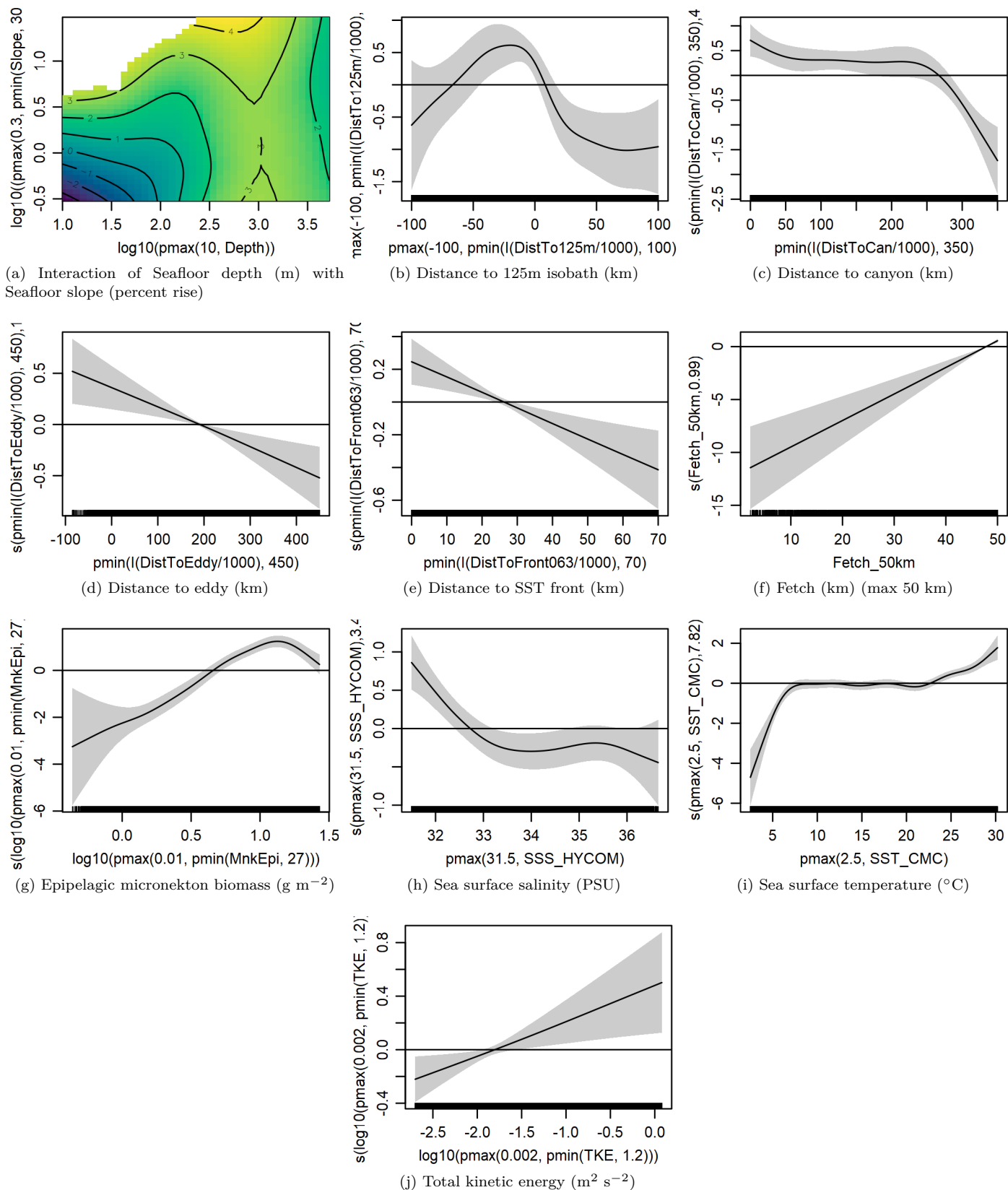


Figure 31: Functional plots for the final model. Transforms and other treatments are indicated in axis labels.  $\log_{10}$  indicates the covariate was  $\log_{10}$  transformed.  $pmax$  and  $pmin$  indicate the covariate's minimum and maximum values, respectively, were Winsorized to the values shown. Winsorization was used to prevent runaway extrapolations during prediction when covariates exceeded sampled ranges, or for ecological reasons, depending on the covariate.  $/1000$  indicates meters were transformed to kilometers for interpretation convenience.

Table 12: Covariates used in the final model.

Covariate	Description
Depth	Depth (m) of the seafloor, from SRTM30_PLUS (Becker et al. (2009))
DistTo125m	Distance (km) to the 125m isobath, derived from SRTM30_PLUS (Becker et al. (2009))
DistToCan	Distance (km) to the closest submarine canyon, derived from the Harris et al. (2014) geomorphology
DistToEddy	Monthly mean distance (km) to the edge of the closest mesoscale eddy of any polarity and age, derived with MGET (Roberts et al. (2010)) from the Aviso Mesoscale Eddy Trajectories Atlas (META2.0), produced by SSALTO/DUACS and distributed by AVISO+ ( <a href="https://aviso.altimetry.fr">https://aviso.altimetry.fr</a> ) with support from CNES, in collaboration with Oregon State University with support from NASA, using the method of Schlax and Chelton (2016), based on Chelton et al. (2011)
DistToFront063	Monthly mean distance (km) to the closest sea surface temperature front detected in daily GHRSSST Level 4 CMC0.2deg and CMC0.1deg images (Brasnett (2008); Canada Meteorological Center (2012); Meissner et al. (2016); Canada Meteorological Center (2016)) with MGET's implementation of the Canny edge detector (Roberts et al. (2010); Canny (1986))
Fetch_50km	Fetch (km): mean distance to shore averaged over 16 radial directions, limited to a maximum of 50 km
MnkEpi	Monthly mean micronekton biomass available in the epipelagic zone, expressed as wet weight ( $\text{g m}^{-2}$ ), from SEAPODYM (Lehodey et al. (2008); Lehodey et al. (2015)), provided by E.U. Copernicus Marine Service. doi: <a href="https://doi.org/10.48670/moi-00020">10.48670/moi-00020</a> . Computed as the sum of the SEAPODYM mnkc_epi, mnkc_mumeso, and mnkc_hmlmeso variables.
SSS_HYCOM	Monthly mean sea surface salinity (PSU) from the HYCOM GOFS 3.1 $1/12^\circ$ ocean model (Chassignet et al. (2009))
SST_CMC	Monthly mean sea surface temperature ( $^\circ\text{C}$ ) from GHRSSST Level 4 CMC0.2deg and CMC0.1deg (Brasnett (2008); Canada Meteorological Center (2012); Meissner et al. (2016); Canada Meteorological Center (2016))
Slope	Slope (percent rise) of the seafloor, derived from SRTM30_PLUS (Becker et al. (2009))
TKE	Monthly mean total kinetic energy ( $\text{m}^2 \text{s}^{-2}$ ) derived from Aviso Ssalto/Duacs global gridded L4 reprocessed geostrophic currents, produced and distributed by E.U. Copernicus Marine Service. doi: <a href="https://doi.org/10.48670/moi-00148">10.48670/moi-00148</a>

## 4.2 Diagnostic Plots

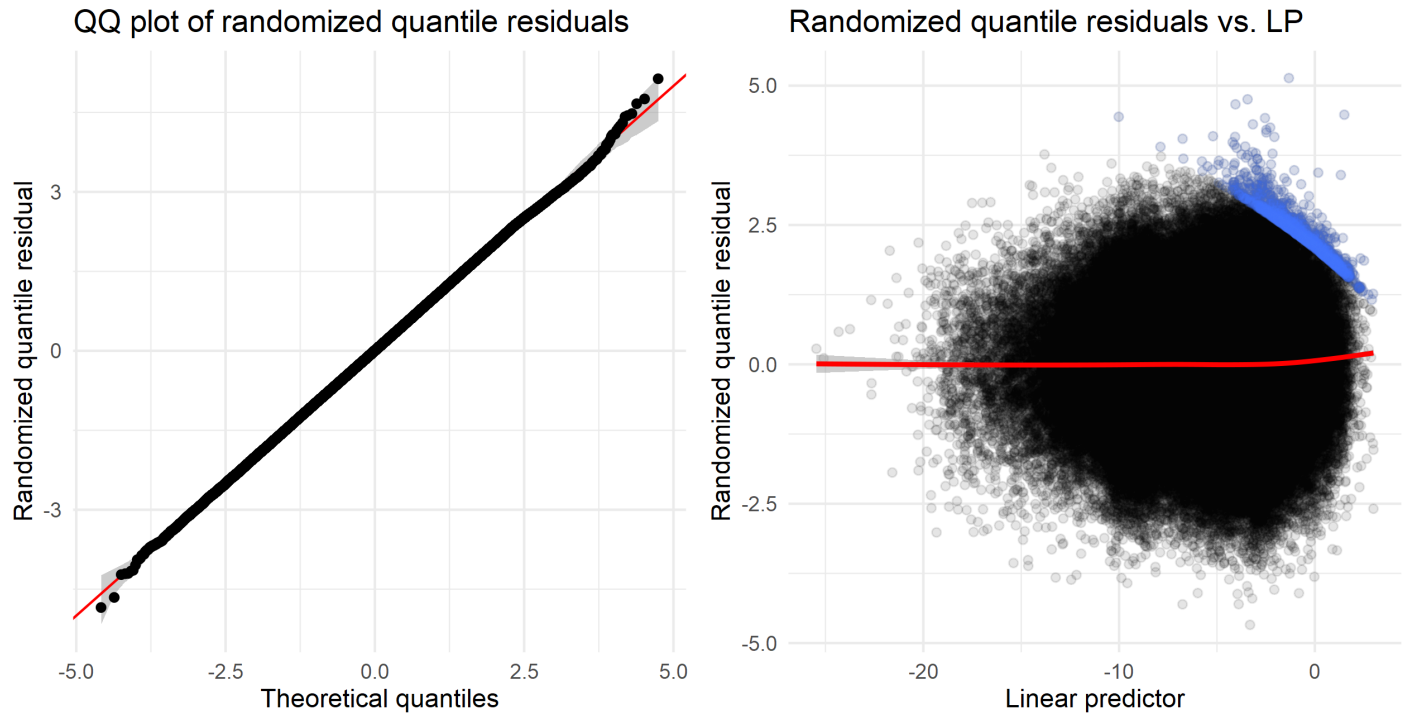


Figure 32: Residual plots for the final model.



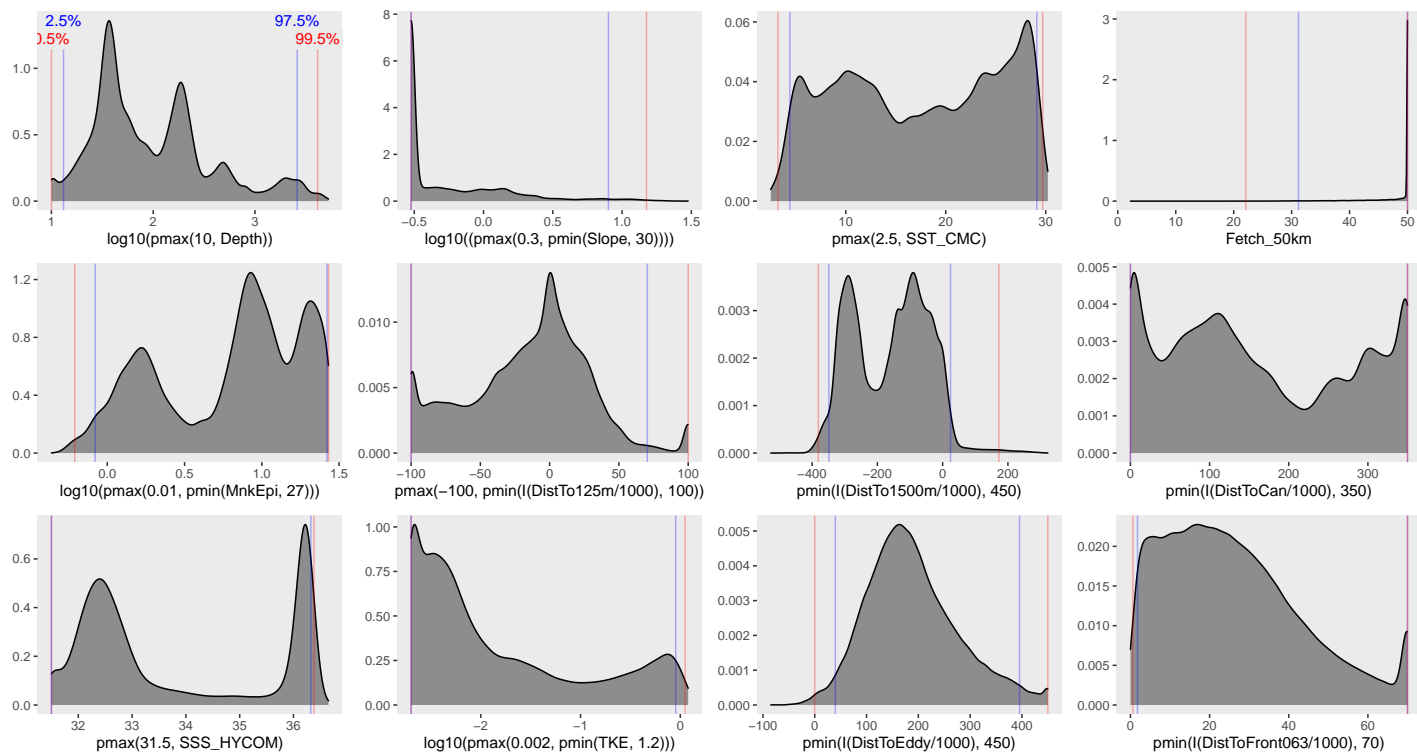


Figure 33: Density histograms showing the distributions of the covariates considered during the final model selection step. The final model may have included only a subset of the covariates shown here (see Figure 31), and additional covariates may have been considered in preceding selection steps. Red and blue lines enclose 99% and 95% of the distributions, respectively. Transforms and other treatments are indicated in axis labels.  $\log_{10}$  indicates the covariate was  $\log_{10}$  transformed.  $pmax$  and  $pmin$  indicate the covariate's minimum and maximum values, respectively, were Winsorized to the values shown. Winsorization was used to prevent runaway extrapolations during prediction when covariates exceeded sampled ranges, or for ecological reasons, depending on the covariate.  $/1000$  indicates meters were transformed to kilometers for interpretation convenience.

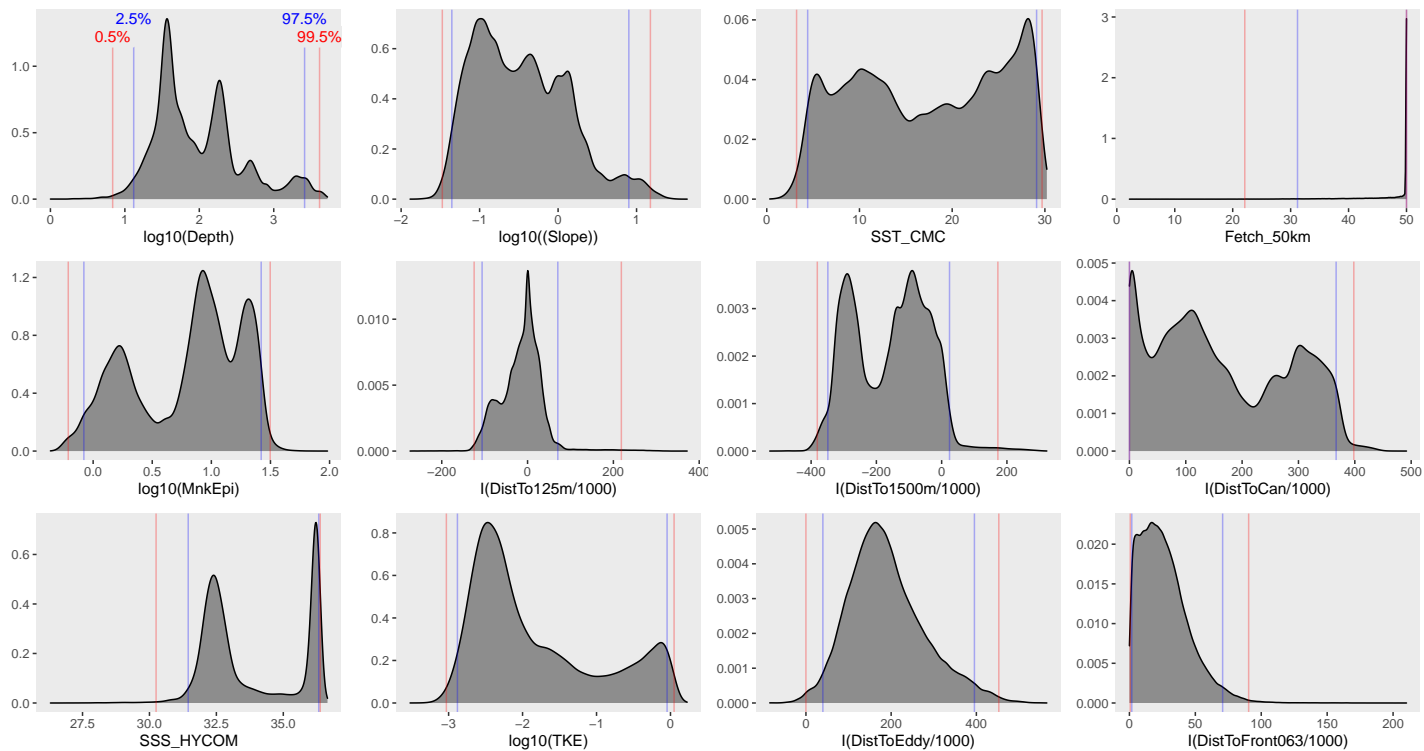


Figure 34: Density histograms shown in Figure 33 replotted without Winsorization, to show the full range of sampling represented by survey segments.

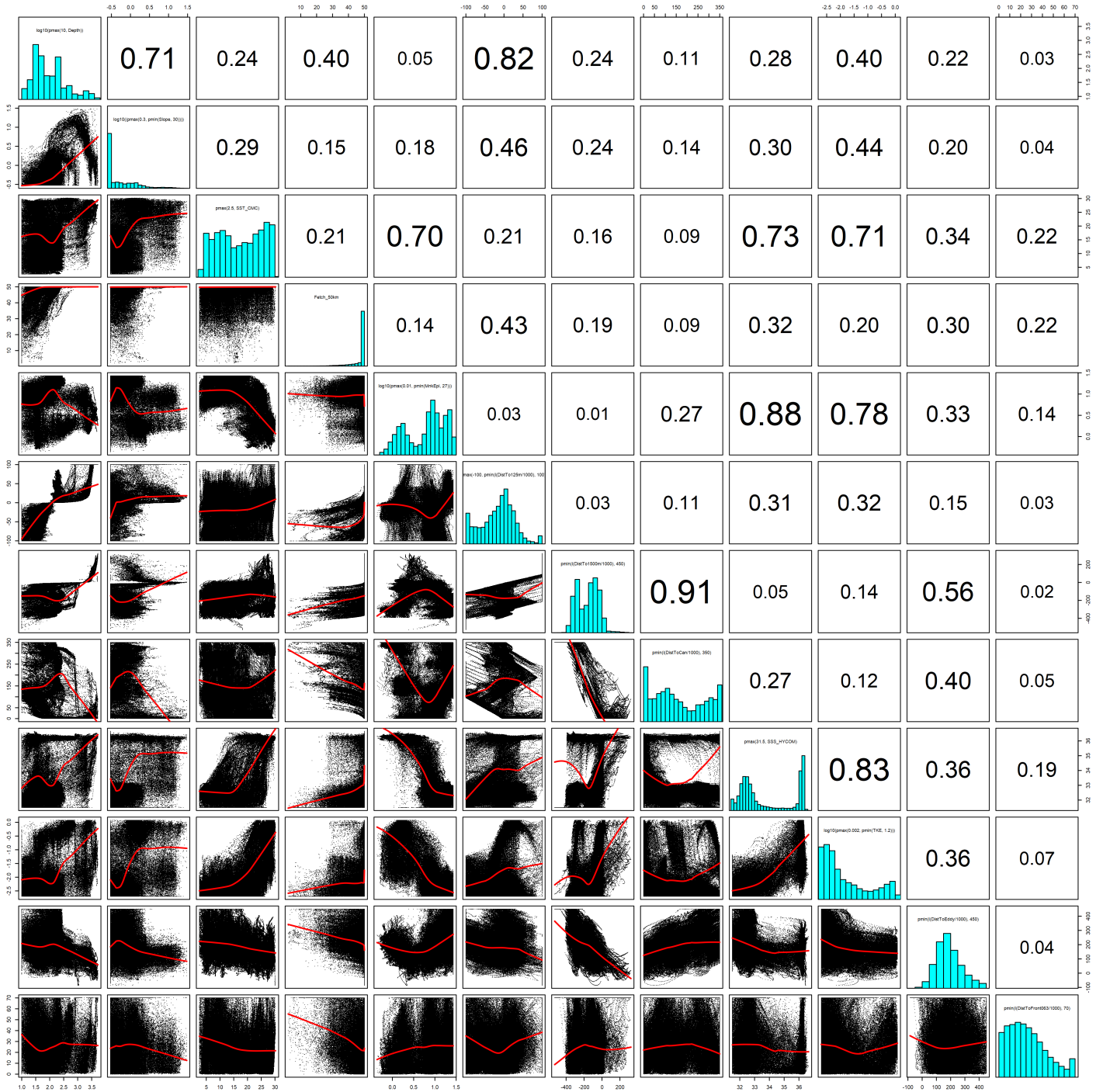


Figure 35: Scatterplot matrix of the covariates considered during the final model selection step. The final model may have included only a subset of the covariates shown here (see Figure 31), and additional covariates may have been considered in preceding selection steps. Covariates are transformed and Winsorized as shown in Figure 33. This plot is used to check simple correlations between covariates (via pairwise Pearson coefficients above the diagonal) and visually inspect for concurvity (via scatterplots and red loess curves below the diagonal).

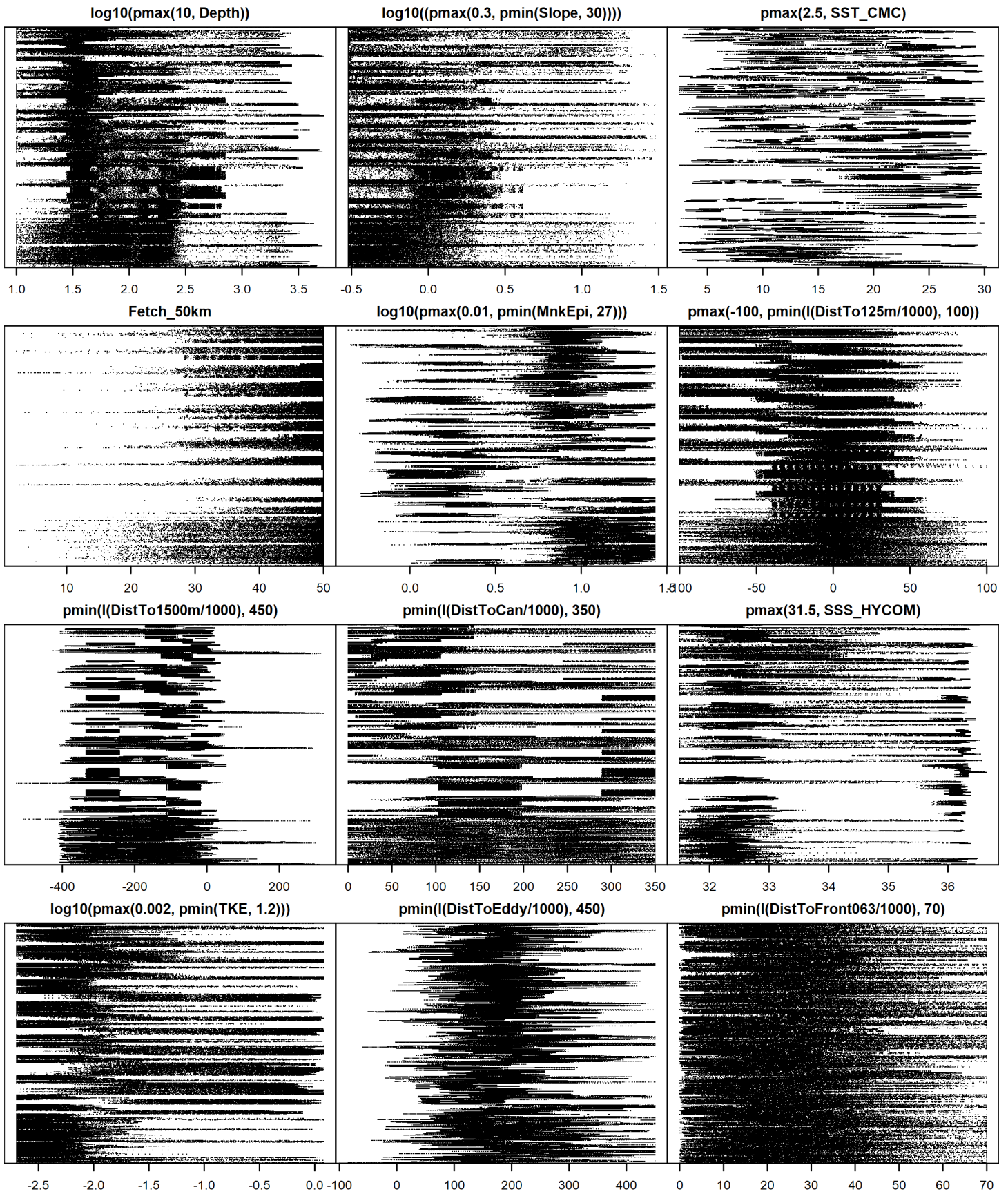


Figure 36: Dotplot of the covariates considered during the final model selection step. The final model may have included only a subset of the covariates shown here (see Figure 31), and additional covariates may have been considered in preceding selection steps. Covariates are transformed and Winsorized as shown in Figure 33. This plot is used to check for suspicious patterns and outliers in the data. Points are ordered vertically by segment ID, sequentially in time.

## 4.3 Extrapolation Diagnostics

### 4.3.1 Univariate Extrapolation

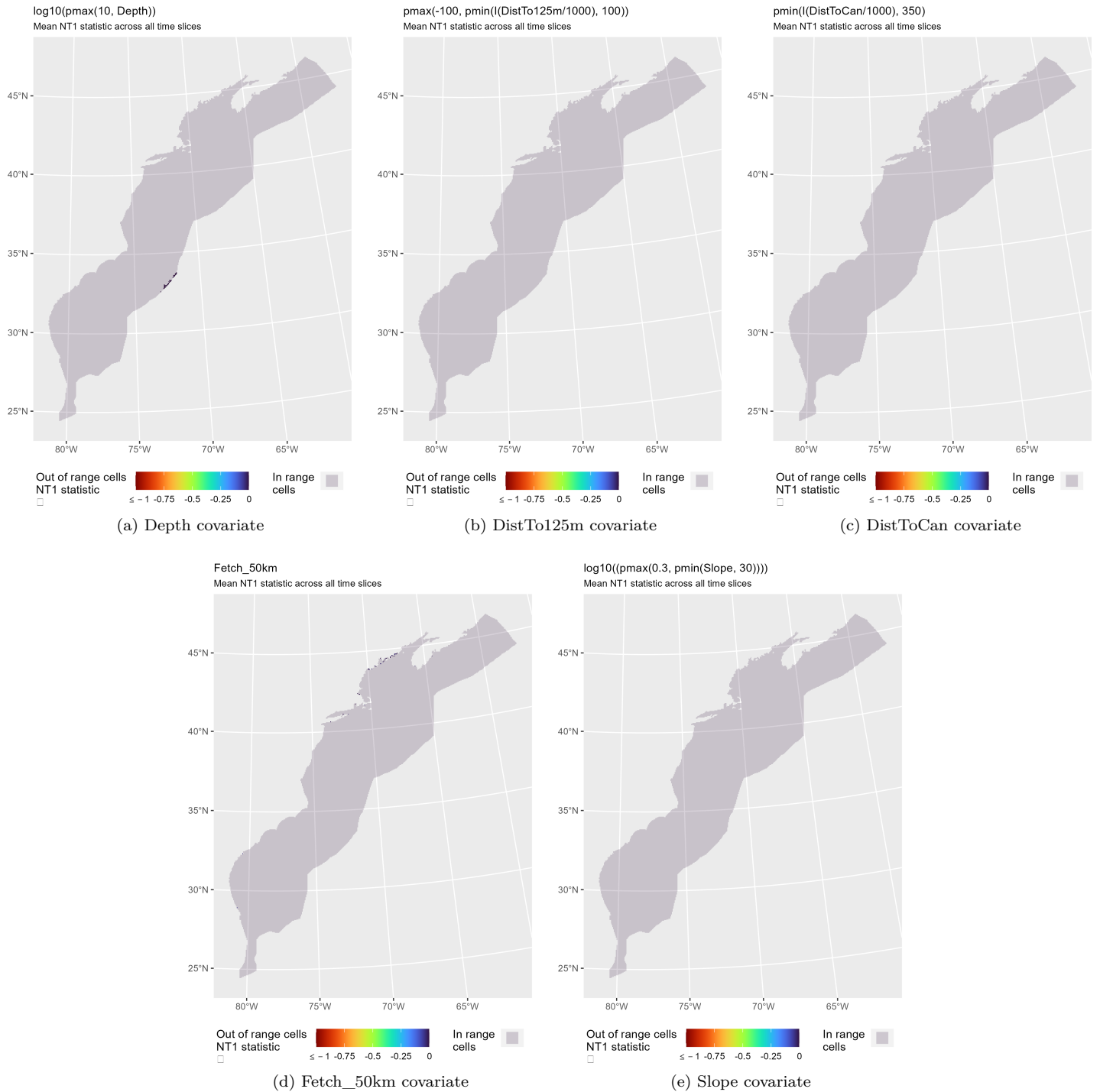


Figure 37: NT1 statistic (Mesgaran et al. (2014)) for static covariates used in the model. Areas outside the sampled range of a covariate appear in color, indicating univariate extrapolation of that covariate occurred there. Areas within the sampled range appear in gray, indicating it did not occur.

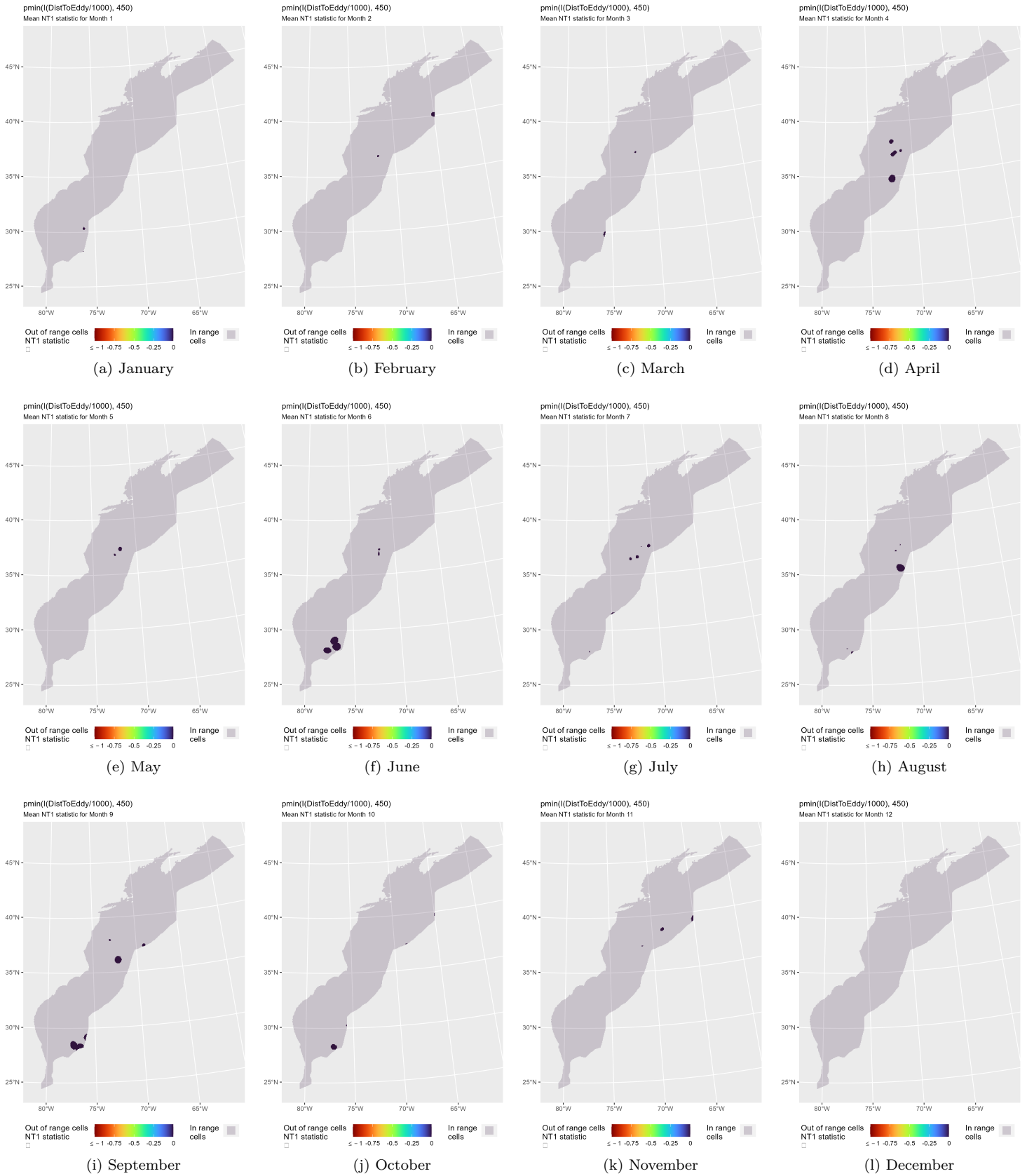


Figure 38: NT1 statistic (Mesgaran et al. (2014)) for the DistToEddy covariate in the model. Areas outside the sampled range of a covariate appear in color, indicating univariate extrapolation of that covariate occurred there during the month. Areas within the sampled range appear in gray, indicating it did not occur.

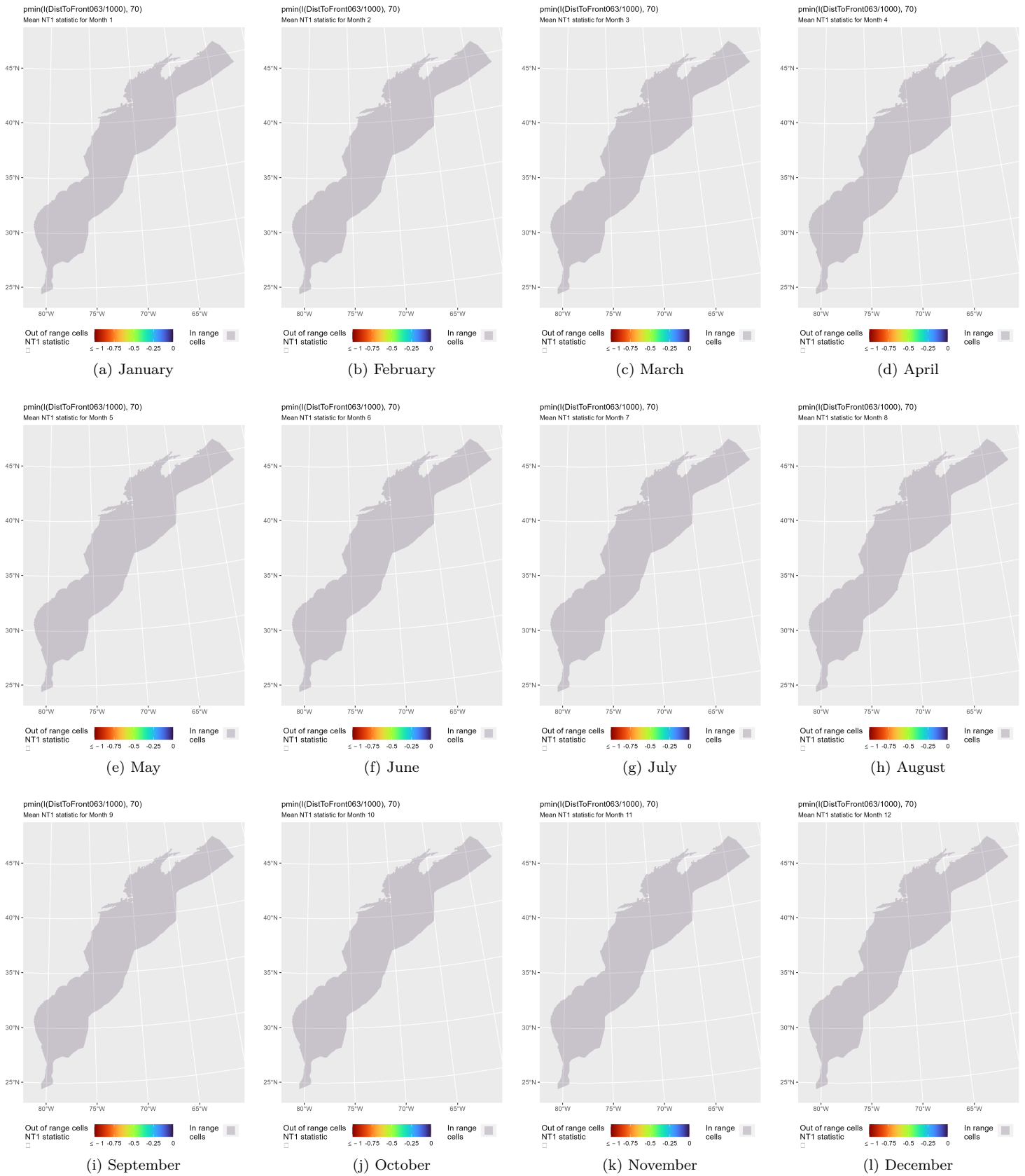


Figure 39: NT1 statistic (Mesgaran et al. (2014)) for the DistToFront063 covariate in the model. Areas outside the sampled range of a covariate appear in color, indicating univariate extrapolation of that covariate occurred there during the month. Areas within the sampled range appear in gray, indicating it did not occur.



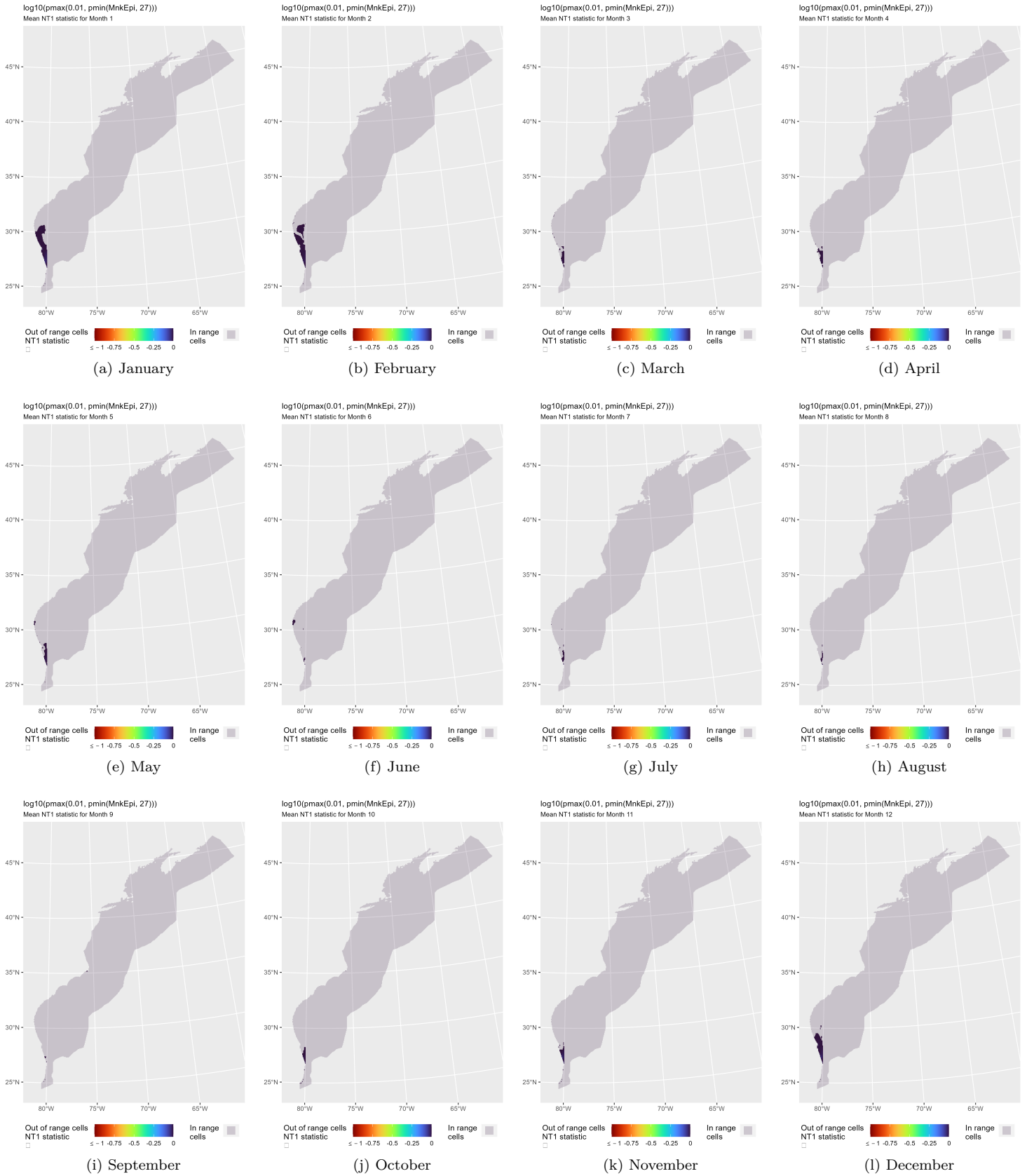


Figure 40: NT1 statistic (Mesgaran et al. (2014)) for the MnkEpi covariate in the model. Areas outside the sampled range of a covariate appear in color, indicating univariate extrapolation of that covariate occurred there during the month. Areas within the sampled range appear in gray, indicating it did not occur.



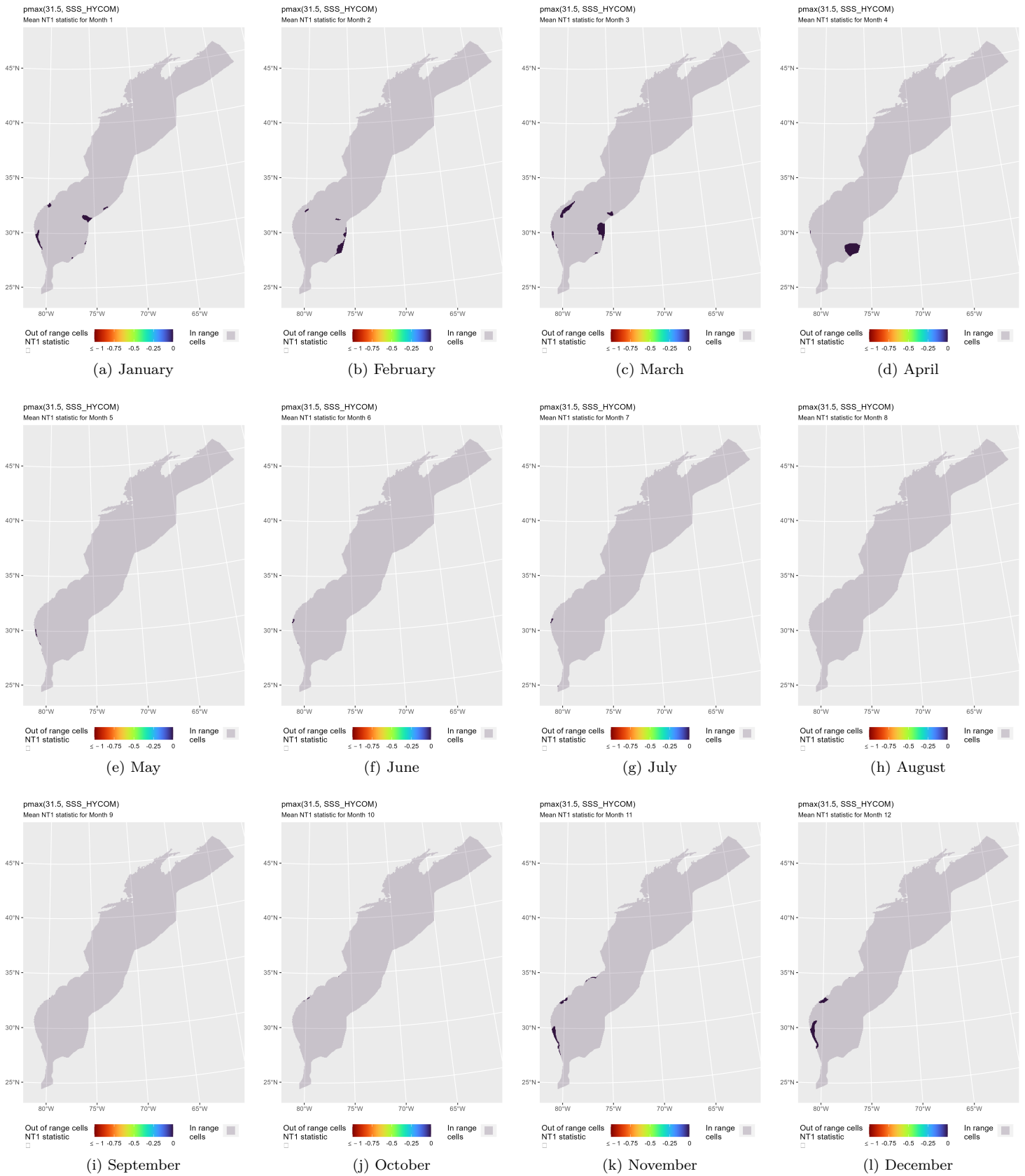


Figure 41: NT1 statistic (Mesgaran et al. (2014)) for the SSS\_HYCOM covariate in the model. Areas outside the sampled range of a covariate appear in color, indicating univariate extrapolation of that covariate occurred there during the month. Areas within the sampled range appear in gray, indicating it did not occur.

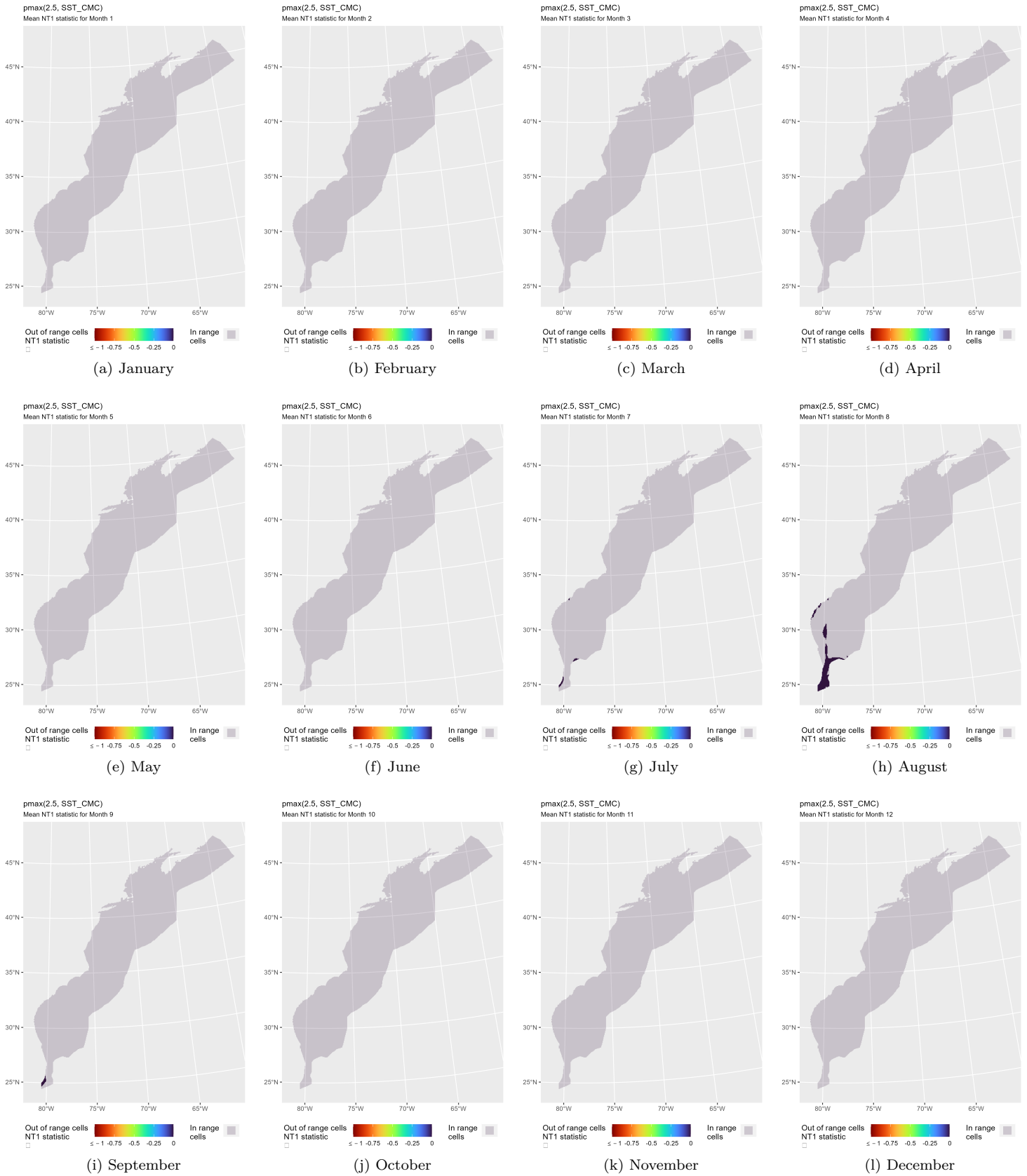


Figure 42: NT1 statistic (Mesgaran et al. (2014)) for the SST\_CMC covariate in the model. Areas outside the sampled range of a covariate appear in color, indicating univariate extrapolation of that covariate occurred there during the month. Areas within the sampled range appear in gray, indicating it did not occur.

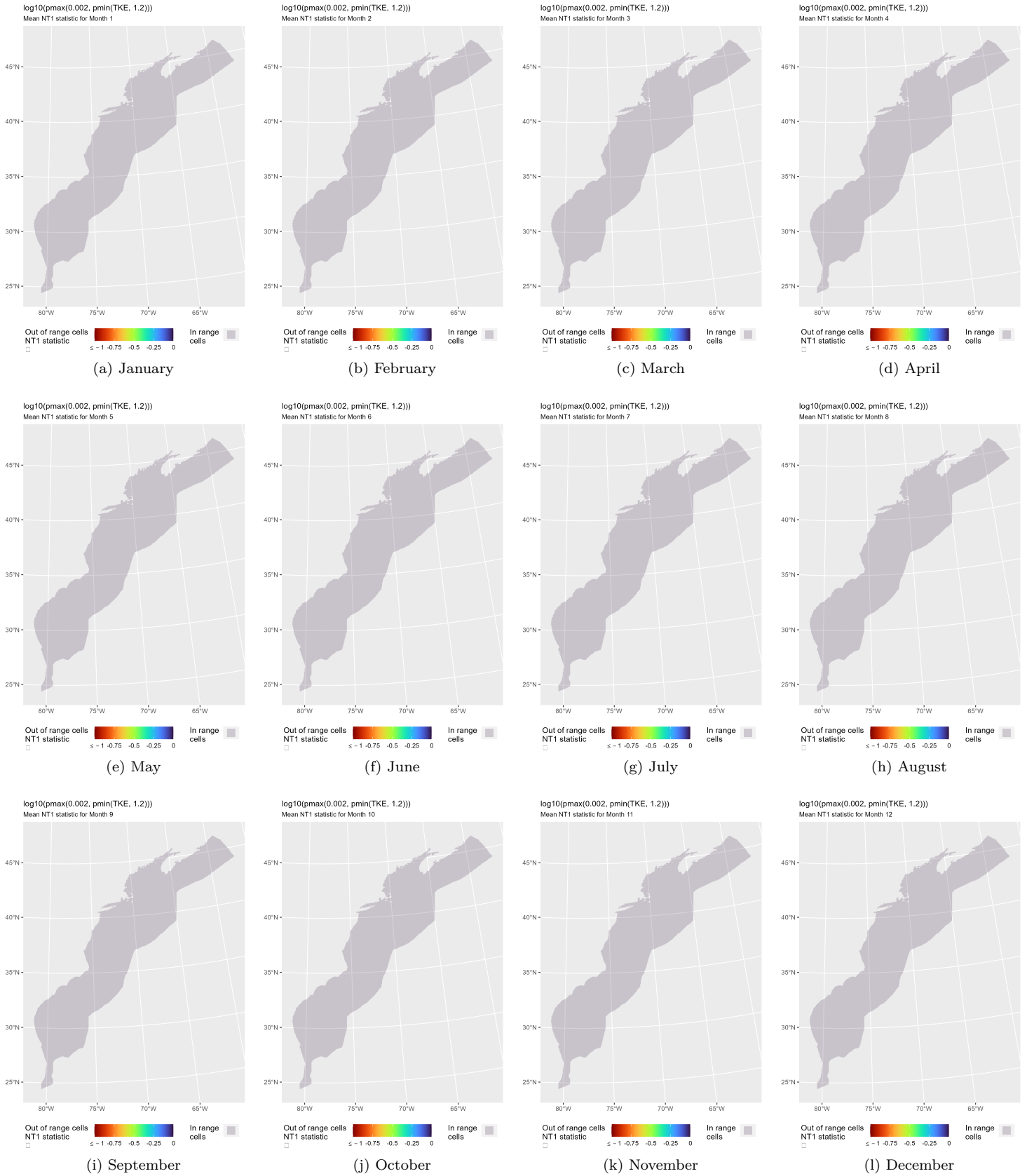


Figure 43: NT1 statistic (Mesgaran et al. (2014)) for the TKE covariate in the model. Areas outside the sampled range of a covariate appear in color, indicating univariate extrapolation of that covariate occurred there during the month. Areas within the sampled range appear in gray, indicating it did not occur.

### 4.3.2 Multivariate Extrapolation

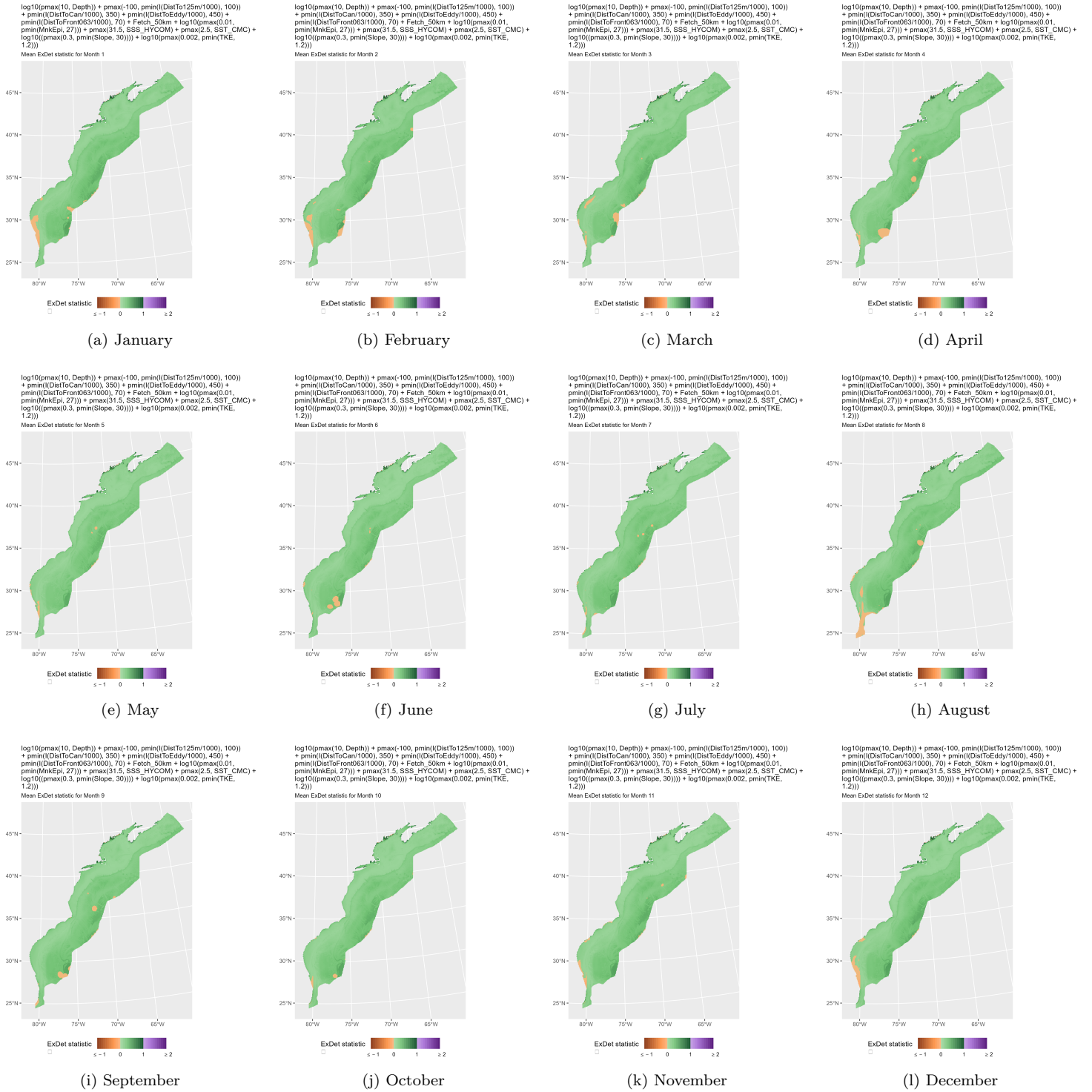


Figure 44: ExDet statistic (Mesgaran et al. (2014)) for all of the covariates used in the model. Areas in orange (ExDet < 0) required univariate extrapolation of one or more covariates (see previous section). Areas in purple (ExDet > 1), did not require univariate extrapolation but did require multivariate extrapolation, by virtue of having novel combinations of covariates not represented in the survey data, according to the NT2 statistic (Mesgaran et al. (2014)). Areas in green (0 ≤ ExDet ≤ 1) did not require either type of extrapolation.

## 5 Predictions

Based on our evaluation of this model in the context of what is known of this species (see Section 4), we summarized its predictions into single, year-round climatological density and uncertainty surfaces (Figure 46). To illustrate the seasonal dynamics that result when predictions are summarized monthly instead, we included monthly mean abundances (Figure 45, Table 13), but to avoid confusion we did not include monthly maps in this report. They are available from us on request, but we recommend the year-round map be used for decision-making purposes, as discussed in Section 6.

### 5.1 Summarized Predictions

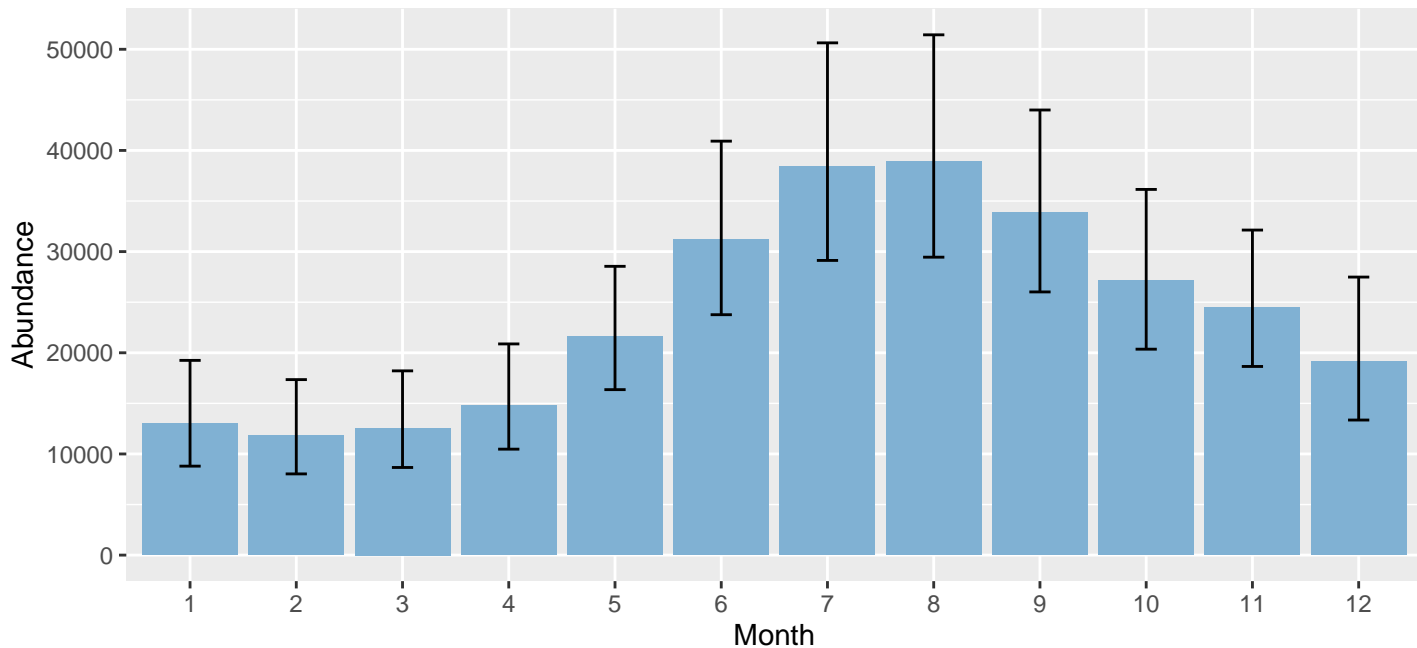


Figure 45: Mean monthly abundance for the prediction area for 1998-2019. Error bars are a 95% interval, made with a log-normal approximation using the prediction’s CV. The CV was estimated with the analytic approach given by Miller et al. (2022), Appendix S1, and accounts both for uncertainty in model parameter estimates and for temporal variability in dynamic covariates.

Table 13: Mean monthly abundance and density for the prediction area for 1998-2019. CV and intervals estimated as described for the previous figure.

Month	Abundance	CV	95% Interval	Area (km <sup>2</sup> )	Density (individuals / 100 km <sup>2</sup> )
1	13,010	0.202	8,794 - 19,247	1,272,925	1.02
2	11,800	0.198	8,027 - 17,347	1,272,925	0.93
3	12,559	0.191	8,662 - 18,211	1,272,925	0.99
4	14,787	0.177	10,475 - 20,874	1,272,925	1.16
5	21,608	0.143	16,357 - 28,545	1,272,925	1.70
6	31,182	0.139	23,763 - 40,918	1,272,925	2.45
7	38,403	0.142	29,127 - 50,635	1,272,925	3.02
8	38,917	0.143	29,450 - 51,427	1,272,925	3.06
9	33,831	0.135	26,014 - 43,996	1,272,925	2.66
10	27,126	0.147	20,355 - 36,148	1,272,925	2.13
11	24,479	0.139	18,649 - 32,131	1,272,925	1.92
12	19,156	0.186	13,352 - 27,483	1,272,925	1.50

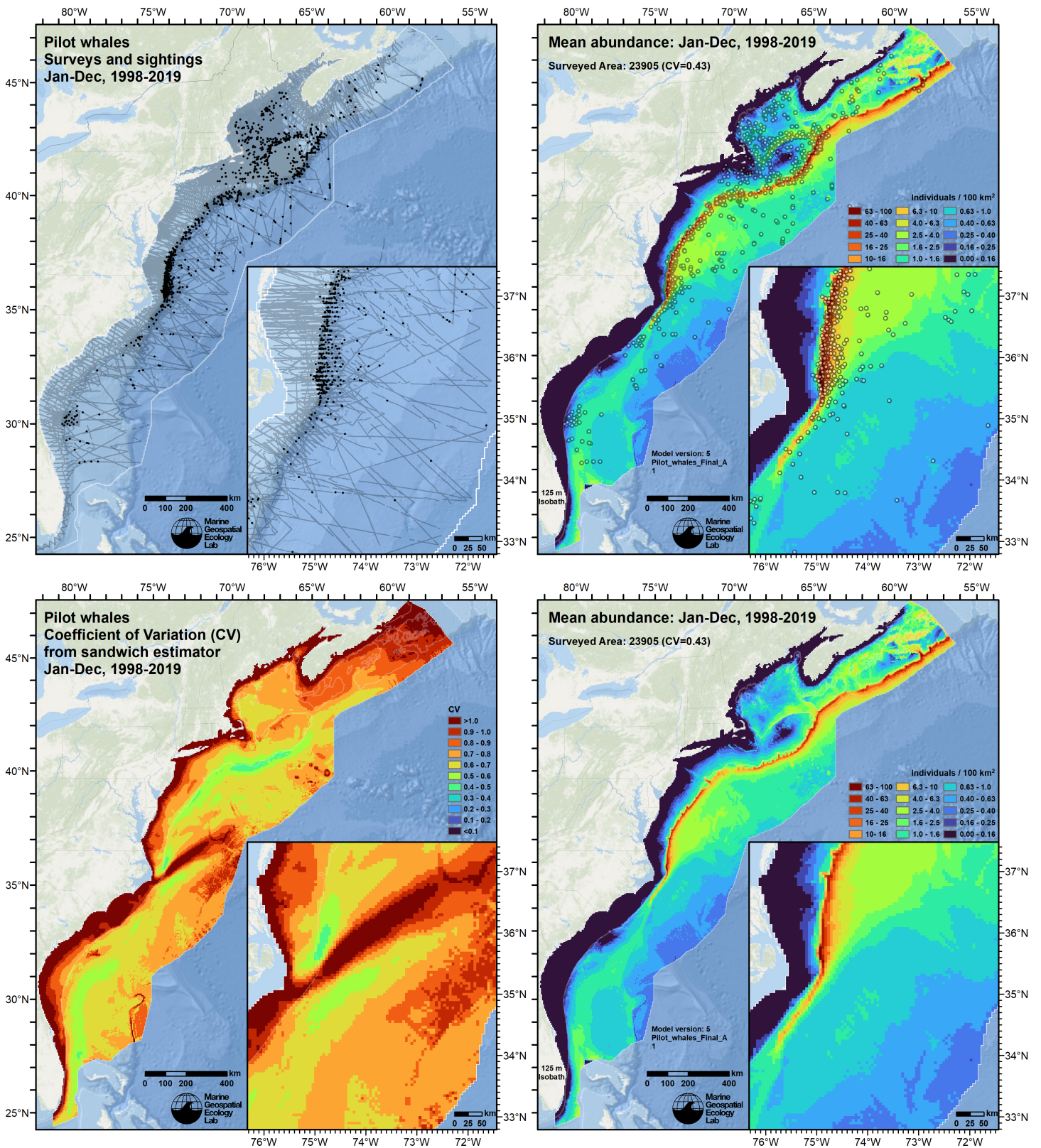


Figure 46: Survey effort and observations (top left), predicted density with observations (top right), predicted density without observations (bottom right), and coefficient of variation of predicted density (bottom left), for the given era. Variance was estimated with the analytic approach given by Miller et al. (2022), Appendix S1, and accounts both for uncertainty in model parameter estimates and for temporal variability in dynamic covariates.



## 5.2 Abundance Comparisons

### 5.2.1 NOAA Stock Assessment Report

Table 14: Comparison of regional abundance estimates from NOAA Stock Assessment Reports (SARs) to estimates from this density model extracted from roughly comparable zones (Figure 47 below). The SAR estimates were based on a single year of surveying, while the model estimates were taken from the multi-year mean density surfaces we provide to model users (Section 5.1). Lf or Sf next to SAR Area denote whether the estimates are for Short-finned (Sf) or Long-finned (Lf) pilot whales.

Stock Assessment Report				Density Model		
Month/Year	Stock Area	$N_{\text{est}}$	SAR	Period	Zone	Abundance
Jun-Aug 2011	Central Virginia to lower Bay of Fundy-Sf	4,569	2011			
Jun-Aug 2011	Central Virginia to lower Bay of Fundy-Lf	5,636	2011			
Jun-Aug 2011	Total: Central Virginia to lower Bay of Fundy	10,205	2011	1998-2019	NEFSC	8,384
Jun-Aug 2011	Central Florida to Central Virginia-Sf	16,946	2011	1998-2019	SEFSC	5,988
Jun-Aug 2011	Total	27,151	2011	1998-2019	NEFSC+SEFSC	14,372
Jul-Aug 2007	N.Labrador to Scotian Shelf-Lf <sup>a</sup>	16,058	2007	1998-2019	Canada	9,492
Jun-Aug 2016	New Jersey to lower Bay of Fundy-Sf <sup>b</sup>	3,810	2021			
Jun-Aug 2016	Central Virginia to lower Bay of Fundy-Lf <sup>b</sup>	10,997	2021			
Jun-Aug 2016	Total: Central Virginia to lower Bay of Fundy <sup>c</sup>	14,807	2021	1998-2019	NEFSC	8,384
Jun-Aug 2016	Central Florida to New Jersey-Sf <sup>d</sup>	25,114	2021	1998-2019	SEFSC	5,988
Jun-Aug 2016	Total	39,921	2021	1998-2019	NEFSC+SEFSC	14,372

<sup>a</sup> Our Canada zone is roughly comparable to the SAR's Bay of Fundy/Scotian Shelf area (excluding the Gulf of St. Lawrence) and may not be directly comparable to the N. Labrador to Scotian Shelf region estimate provided by the SAR Lawson and Gosselin (2011).

<sup>b</sup> Estimate originally from Palka (2020).

<sup>c</sup> Estimates combined for Long and Short-finned pilot whales from Palka (2020) for a region that roughly compares to the NEFSC region but may not be directly comparable given that the short finned pilot whale area reported by the SAR is using a polygon that cuts the north and south at New Jersey rather than central Virginia.

<sup>d</sup> Estimate originally from Garrison (2020).

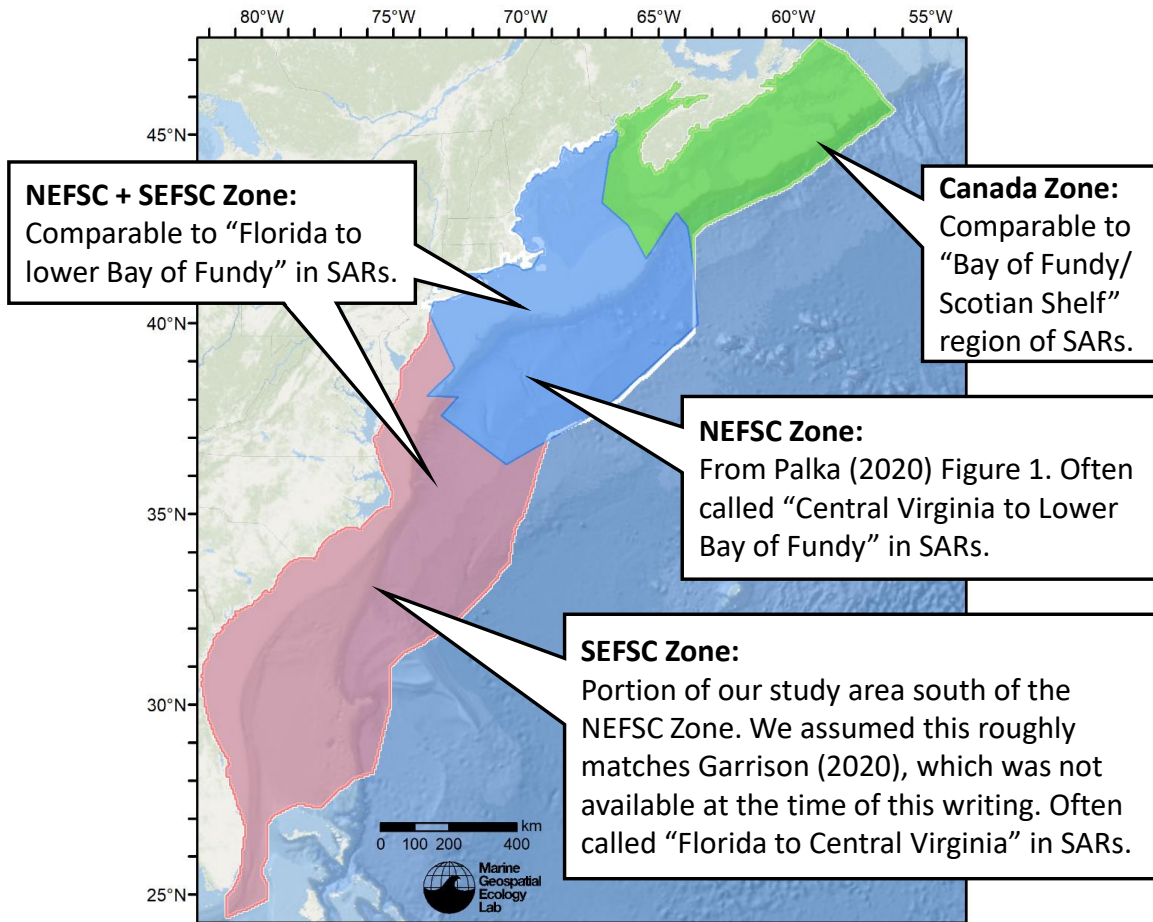


Figure 47: Zones for which we extracted abundance estimates from the density model for comparison to estimates from the NOAA Stock Assessment Report.



## 5.2.2 Previous Density Model

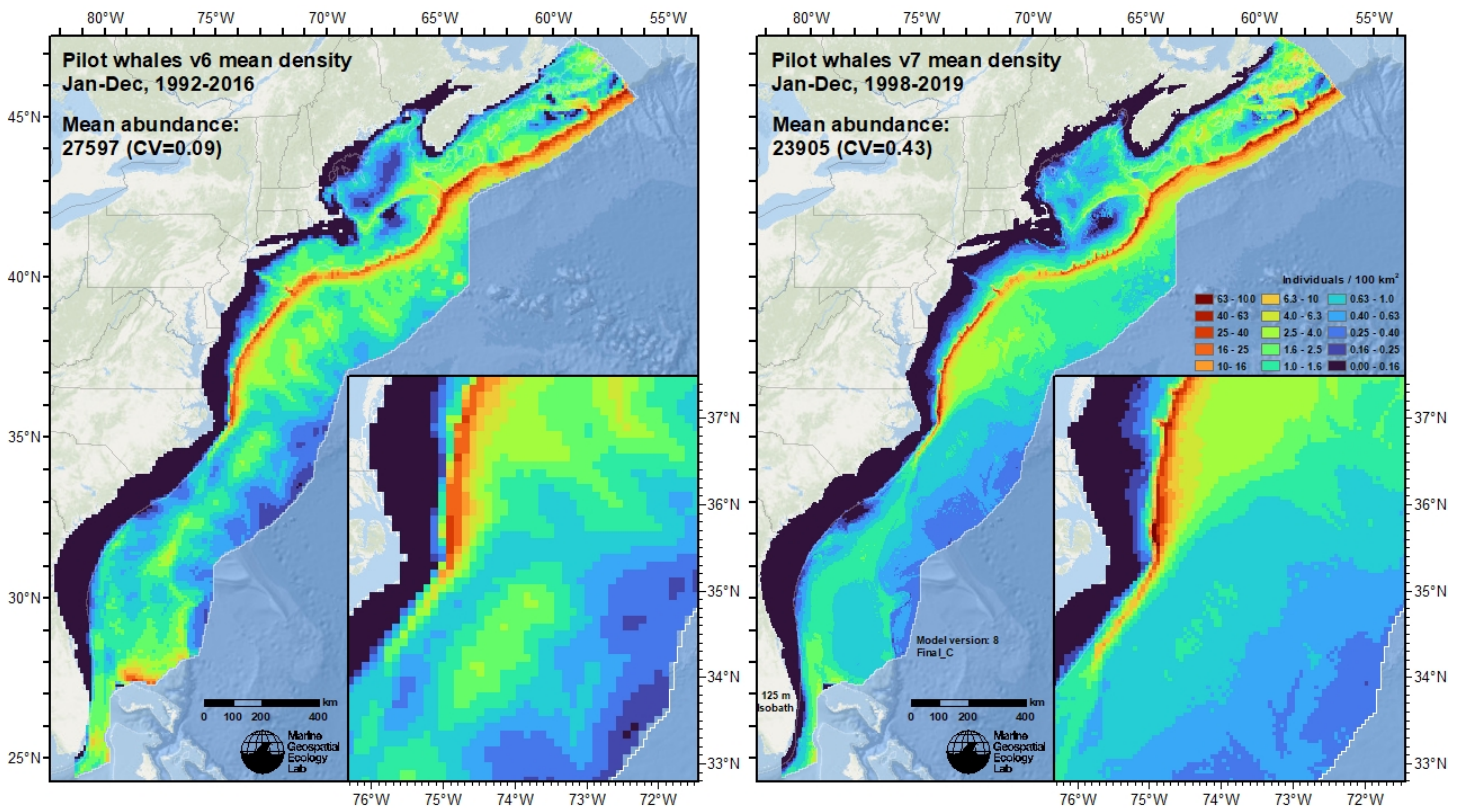


Figure 48: Comparison of the mean density predictions from the previous model (left) released by Roberts et al. (2017) to those from this model (right).

## 6 Discussion

The model predicted a year-round mean abundance of 23,905 pilot whales, with the highest abundances predicted along the slope. The abundance in the southern portion of the study area, presumably short-finned pilot whale habitat, was predicted to be highest along the slope of the shelf on the Blake Plateau. Strong seasonal variability was evident in the model predictions with the lowest abundance of 11,800 pilot whales predicted in February and the highest abundance of 38,917 pilot whales predicted in August (Figure 45). The model showed that as winter progresses abundance decreased in the Gulf of Maine and on the Scotian shelf and then increased moving into summer with more animals distributed throughout the Gulf of Maine again and then abundance in both regions waned throughout fall. This is in rough accordance with the Payne and Heinemann (1993) description of a seasonal clockwise progression around the Gulf of Maine. However, given the lack of evidence for such strong seasonal movement of pilot whales we provided year-round mean abundance estimates for this species.

The extrapolation statistics show some extrapolation in univariate space. Depth showed a few cells of extrapolated values at the eastern mid-Atlantic edge of the study area (Figure 37). The distance to eddy covariate showed some univariate extrapolation in all months (Figure 38). In this case distances “inside” the eddy ring are negative values, and the extrapolation cells indicate very large eddies, with large cores that are far from the ring in the negative direction. This is unlikely to be a major issue, as large eddies needed to trigger the extrapolation were infrequent and as such, unlikely to have yielded a big effect in the final model. A few out of range cells of epipelagic micronekton occur in the western edge of the southeastern study area near West Palm Beach, FL., where no animals were observed or predicted, thereby there were no expected effects in the final model (Figure 40). Sea surface salinity showed small swaths of out of range cells in the southwestern and southeastern edges of the study area in all months except August and September (Figure 41). Finally, SST showed some out of range swaths of cells in the western and southern most portions of the southern study area in August (Figure 42).

In comparison to the 2021 SAR (Hayes et al. 2021) this model estimated 43% fewer animals in the NEFSC region and 76% fewer animals in the SEFSC region. This resulted in a total of 64% (25,549) fewer pilot whales in the NEFSC and SEFSC regions combined. The SAR report estimates a total of 39,921 pilot whales in the central Florida to Lower Bay of Fundy region during summer months (Jun- Aug) (10,997 long-finned and 28,924 short-finned) whereas this model predicts a year-round mean of 14,372 pilot whales and a summer abundance (Jun-Aug) of 20,345 pilot whales (note: summer estimates

from this model are presented herein for discussion purposes but not shown in the Abundance Comparison table above). However, these numbers are not directly comparable given the short-finned pilot whale area from which this abundance is reported uses a polygon that cuts the north and south at New Jersey rather than central Virginia. The N. Labrador to Scotian Shelf abundance reported in the 2016 SAR (16,058) is likely most comparable to our Canada region although our region did not extend as far north. Our model year-round mean estimate was 9,492 animals which may be a reasonable fraction of the estimated number of animals in the N. Labrador to Scotian Shelf region. There are a few possible reasons that may contribute to the observed difference between the modeled abundance and the SARs estimates. First, many surveys were used in our model from multiple years and seasons, whereas the SAR estimate is from one year (2016) and season (summer). For example, comparisons to previous SAR estimates (Waring et al. 2016) from 2011 surveys are closer to this model's estimates. The total 2016 SAR abundance, made from surveys in 2011, for the NEFSC region (10,205) is only 18% higher than the year-round mean estimate from this model (8,384). However, the estimate for the SEFSC region from the 2016 SAR (16,946), made from surveys in 2011, is still 65% higher than the year-round mean estimate from this model (5,988). Inter-annual variation and especially seasonal variation in abundance likely explain some differences between the model estimate herein and the SAR estimates. For example, the low winter abundances predicted from this model result in lower year-round mean abundances when compared to the SAR summer estimates. Additionally, different  $g(0)$  estimates applied to non-NOAA surveys in our model may contribute to differences in reported abundances. And finally, it may be possible that pilot whale populations are increasing in the East Coast study area. If so, the use of older surveys in our models may be driving down the overall mean abundance estimate. In future models, restricting the model to more recent survey years may be necessary. It should also be noted, that as mentioned above, the regions that our comparative estimates were extracted from are not directly comparable to the short-finned pilot whale region, which may have also contributed to differences in these comparisons.

In comparison to the Roberts et al. (2017) pilot whale model (27,597), year-round mean abundance was lower by 13% (3,692 animals) in the new model. However, it is important to note that the old model was climatological whereas this was a contemporaneous model. As such, this model predicted lower abundance in winter months which drove down the overall mean abundance.

We emphasize that the provided density surface represents mean year-round density, which is likely to be lower than typical summer density. It may be higher than typical winter density, but this is less certain. With more data, it may be possible to offer predictions confidently at monthly temporal resolution. Until then, model users should be mindful that density may be higher in summer months (June- August) and lower in winter than indicated by our year-round density surface.

Finally, we note high pilot whale density was predicted throughout the year at an area of the shelf break and continental slope north of where the Gulf Stream separates from the shelf at Cape Hatteras. Sightings were reported in this vicinity in nearly every month of the year. Marine spatial planners seeking to site activities that are potentially harmful to pilot whales would be well advised to avoid this area at all times.

## References

- Abend A, Smith TD (1999) [Review of the distribution of the long-finned pilot whale \(\*Globicephala melas\*\) in the North Atlantic and Mediterranean](#). U.S. Department of Commerce, Woods Hole, MA
- Aguilar de Soto N (2006) Acoustic and diving behaviour of the short finned pilot whales (*Globicephala macrorhynchus*) and Blainville's beaked whale (*Mesoplodon densirostris*) in the Canary Islands. Implications on the effects of man-made noise and boat collisions.
- Baird RW, Webster DL, Swaim ZT, Aschettino JM, Foley HJ, Cioffi WR, Anderson DB, Read AJ (2018) Spatial Use by Cuvier's Beaked Whales and Short-finned Pilot Whales Satellite Tagged off North Carolina in 2017. 68.
- Barco SG, Burt L, DePerte A, Digiovanni R Jr. (2015) Marine Mammal and Sea Turtle Sightings in the Vicinity of the Maryland Wind Energy Area July 2013-June 2015, VAQF Scientific Report #2015-06. Virginia Aquarium & Marine Science Center Foundation, Virginia Beach, VA
- Barlow J, Forney KA (2007) [Abundance and population density of cetaceans in the California Current ecosystem](#). Fishery Bulletin 105:509–526.
- Becker JJ, Sandwell DT, Smith WHF, Braud J, Binder B, Depner J, Fabre D, Factor J, Ingalls S, Kim S-H, Ladner R, Marks K, Nelson S, Pharaoh A, Trimmer R, Von Rosenberg J, Wallace G, Weatherall P (2009) Global Bathymetry and Elevation Data at 30 Arc Seconds Resolution: SRTM30\_PLUS. Marine Geodesy 32:355–371. doi: [10.1080/01490410903297766](https://doi.org/10.1080/01490410903297766)
- Brasnett B (2008) The impact of satellite retrievals in a global sea-surface-temperature analysis. Quarterly Journal of the Royal Meteorological Society 134:1745–1760. doi: [10.1002/qj.319](https://doi.org/10.1002/qj.319)

- Buckland ST, Anderson DR, Burnham KP, Laake JL, Borchers DL, Thomas L (2001) Introduction to Distance Sampling: Estimating Abundance of Biological Populations. Oxford University Press, Oxford, UK
- Burt ML, Borchers DL, Jenkins KJ, Marques TA (2014) Using mark-recapture distance sampling methods on line transect surveys. *Methods in Ecology and Evolution* 5:1180–1191. doi: [10.1111/2041-210X.12294](https://doi.org/10.1111/2041-210X.12294)
- Canada Meteorological Center (2012) GHRSSST Level 4 CMC0.2deg Global Foundation Sea Surface Temperature Analysis Version 2.0. PODAAC, CA, USA. doi: [10.5067/GHCMC-4FM02](https://doi.org/10.5067/GHCMC-4FM02)
- Canada Meteorological Center (2016) GHRSSST Level 4 CMC0.1deg Global Foundation Sea Surface Temperature Analysis Version 3.0. PODAAC, CA, USA. doi: [10.5067/GHCMC-4FM03](https://doi.org/10.5067/GHCMC-4FM03)
- Cañadas A, Roberts JJ, Yack TM, Halpin PN (2021) Development of Exploratory Marine Species Density Models in the NAVEUR/C6F Study Area. Report prepared for Naval Facilities Engineering Command, Atlantic under Contract No. N62470-15-D-8006, Task Order 18F4048. Duke University Marine Geospatial Ecology Lab, Durham, NC
- Canny JF (1986) A computational approach to edge detection. *IEEE Transactions on Pattern Analysis and Machine Intelligence* 8:679–698. doi: [10.1016/B978-0-08-051581-6.50024-6](https://doi.org/10.1016/B978-0-08-051581-6.50024-6)
- Carretta JV, Lowry MS, Stinchcomb CE, Lynn MS, E. CR (2000) Distribution and abundance of marine mammals at San Clemente Island and surrounding offshore waters: Results from aerial and ground surveys in 1998 and 1999. NOAA Administrative Report LJ-00-02. NOAA National Marine Fisheries Service, Southwest Fisheries Center, La Jolla, CA
- Chassignet E, Hurlburt H, Metzger EJ, Smedstad O, Cummings J, Halliwell G, Bleck R, Baraille R, Wallcraft A, Lozano C, Tolman H, Srinivasan A, Hankin S, Cornillon P, Weisberg R, Barth A, He R, Werner F, Wilkin J (2009) US GODAE: Global Ocean Prediction with the HYbrid Coordinate Ocean Model (HYCOM). *Oceanog* 22:64–75. doi: [10.5670/oceanog.2009.39](https://doi.org/10.5670/oceanog.2009.39)
- Chelton DB, Schlax MG, Samelson RM (2011) Global observations of nonlinear mesoscale eddies. *Progress in Oceanography* 91:167–216. doi: [10.1016/j.pocean.2011.01.002](https://doi.org/10.1016/j.pocean.2011.01.002)
- Cole T, Gerrior P, Merrick RL (2007) [Methodologies of the NOAA National Marine Fisheries Service Aerial Survey Program for Right Whales \(\*Eubalaena glacialis\*\) in the Northeast U.S., 1998-2006](#). U.S. Department of Commerce, Woods Hole, MA
- Cotter MP (2019) Aerial Surveys for Protected Marine Species in the Norfolk Canyon Region: 2018–2019 Final Report. HDR, Inc., Virginia Beach, VA
- Foley HJ, Paxton CGM, McAlarney RJ, Pabst DA, Read AJ (2019) Occurrence, Distribution, and Density of Protected Species in the Jacksonville, Florida, Atlantic Fleet Training and Testing (AFTT) Study Area. Duke University Marine Lab, Beaufort, NC
- Garrison LP (2020) [Abundance of cetaceans along the southeast U.S. East coast from a summer 2016 vessel survey](#). PRD Contribution # PRD-2020-04. NOAA National Marine Fisheries Service, Southeast Fisheries Science Center, Miami, FL
- Garrison LP, Rosel PE (2017) Partitioning short-finned and long-finned pilot whale bycatch estimates using habitat and genetic information.
- Garrison LP, Martinez A, Maze-Foley K (2010) [Habitat and abundance of cetaceans in Atlantic Ocean continental slope waters off the eastern USA](#). *Journal of Cetacean Research and Management* 11:267–277.
- Hamazaki T (2002) [Spatiotemporal prediction models of cetacean habitats in the mid-western North Atlantic ocean \(from Cape Hatteras, North Carolina, USA to Nova Scotia, Canada\)](#). *Marine Mammal Science* 18:920–939.
- Harris PT, Macmillan-Lawler M, Rupp J, Baker EK (2014) Geomorphology of the oceans. *Marine Geology* 352:4–24. doi: [10.1016/j.margeo.2014.01.011](https://doi.org/10.1016/j.margeo.2014.01.011)
- Hayes SA, Josephson EA, Maze-Foley K, Rosel PE, Turek J, Byrd B, Chavez-Rosales S, Cole TVN, Garrison LP, Hatch J, Henry A, Horstman SC, Litz J, Lyssikatos MC, Mullin KD, Orphanides C, Ortega-Ortiz J, Pace RM, Palka DL, Powell J, Rappucci G, Wenzel FW (2021) [US Atlantic and Gulf of Mexico Marine Mammal Stock Assessments 2020](#). NOAA National Marine Fisheries Service, Northeast Fisheries Science Center, Woods Hole, MA
- Hayes SA, Josephson E, Maze-Foley K, Rosel PE, Wallace J, Brossard A, Chavez-Rosales S, Cole TVN, Garrison LP, Hatch J, Henry A, Horstman SC, Litz J, Lyssikatos MC, Mullin KD, Murray K, Orphanides C, Ortega-Ortiz J, Pace RM, Palka DL, Powell J, Rappucci G, Soldevilla M, Wenzel FW (2022) [US Atlantic and Gulf of Mexico Marine Mammal Stock Assessments 2021](#). NOAA National Marine Fisheries Service, Northeast Fisheries Science Center, Woods Hole, MA
- Johnson MP, Tyack PL (2003) A digital acoustic recording tag for measuring the response of wild marine mammals to sound. *IEEE J Oceanic Eng* 28:3–12. doi: [10.1109/JOE.2002.808212](https://doi.org/10.1109/JOE.2002.808212)



- Laake JL, Calambokidis J, Osmek SD, Rugh DJ (1997) Probability of Detecting Harbor Porpoise From Aerial Surveys: Estimating  $g(0)$ . *Journal of Wildlife Management* 61:63–75. doi: [10.2307/3802415](https://doi.org/10.2307/3802415)
- Lawson JW, Gosselin J-F (2011) Fully-corrected cetacean abundance estimates from the Canadian TNASS survey. National Marine Mammal Peer Review Meeting, Ottawa, Canada,
- Lehodey P, Senina I, Murtugudde R (2008) A spatial ecosystem and populations dynamics model (SEAPODYM)–Modeling of tuna and tuna-like populations. *Progress in Oceanography* 78:304–318. doi: [10.1016/j.pocean.2008.06.004](https://doi.org/10.1016/j.pocean.2008.06.004)
- Lehodey P, Conchon A, Senina I, Domokos R, Calmettes B, Jouanno J, Hernandez O, Kloser R (2015) Optimization of a micronekton model with acoustic data. *ICES Journal of Marine Science* 72:1399–1412. doi: [10.1093/icesjms/fsu233](https://doi.org/10.1093/icesjms/fsu233)
- Leiter S, Stone K, Thompson J, Accardo C, Wikgren B, Zani M, Cole T, Kenney R, Mayo C, Kraus S (2017) North Atlantic right whale *Eubalaena glacialis* occurrence in offshore wind energy areas near Massachusetts and Rhode Island, USA. *Endang Species Res* 34:45–59. doi: [10.3354/esr00827](https://doi.org/10.3354/esr00827)
- Mallette SD, Lockhart GG, McAlarney RJ, Cummings EW, McLellan WA, Pabst DA, Barco SG (2014) Documenting Whale Migration off Virginia’s Coast for Use in Marine Spatial Planning: Aerial and Vessel Surveys in the Proximity of the Virginia Wind Energy Area (VA WEA), VAQF Scientific Report 2014-08. Virginia Aquarium & Marine Science Center Foundation, Virginia Beach, VA
- Mallette SD, Lockhart GG, McAlarney RJ, Cummings EW, McLellan WA, Pabst DA, Barco SG (2015) Documenting Whale Migration off Virginia’s Coast for Use in Marine Spatial Planning: Aerial Surveys in the Proximity of the Virginia Wind Energy Area (VA WEA) Survey/Reporting Period: May 2014 - December 2014, VAQF Scientific Report 2015-02. Virginia Aquarium & Marine Science Center Foundation, Virginia Beach, VA
- Mallette SD, McAlarney RJ, Lockhart GG, Cummings EW, Pabst DA, McLellan WA, Barco SG (2017) [Aerial Survey Baseline Monitoring in the Continental Shelf Region of the VACAPES OPAREA: 2016 Annual Progress Report](#). Virginia Aquarium & Marine Science Center Foundation, Virginia Beach, VA
- Marsh H, Sinclair DF (1989) Correcting for Visibility Bias in Strip Transect Aerial Surveys of Aquatic Fauna. *The Journal of Wildlife Management* 53:1017. doi: [10.2307/3809604](https://doi.org/10.2307/3809604)
- McAlarney R, Cummings E, McLellan W, Pabst A (2018) Aerial Surveys for Protected Marine Species in the Norfolk Canyon Region: 2017 Annual Progress Report. University of North Carolina Wilmington, Wilmington, NC
- McLellan WA, McAlarney RJ, Cummings EW, Read AJ, Paxton CGM, Bell JT, Pabst DA (2018) Distribution and abundance of beaked whales (Family Ziphiidae) Off Cape Hatteras, North Carolina, U.S.A. *Marine Mammal Science*. doi: [10.1111/mms.12500](https://doi.org/10.1111/mms.12500)
- Meissner T, Wentz FJ, Scott J, Vazquez-Cuervo J (2016) Sensitivity of Ocean Surface Salinity Measurements From Spaceborne L-Band Radiometers to Ancillary Sea Surface Temperature. *IEEE Trans Geosci Remote Sensing* 54:7105–7111. doi: [10.1109/TGRS.2016.2596100](https://doi.org/10.1109/TGRS.2016.2596100)
- Méndez-Fernandez P, Bustamante P, Bode A, Chouvelon T, Ferreira M, López A, Pierce GJ, Santos MB, Spitz J, Vinagada JV, Caurant F (2012) Foraging ecology of five toothed whale species in the Northwest Iberian Peninsula, inferred using carbon and nitrogen isotope ratios. *Journal of Experimental Marine Biology and Ecology* 413:150–158. doi: [10.1016/j.jembe.2011.12.007](https://doi.org/10.1016/j.jembe.2011.12.007)
- Mesgaran MB, Cousens RD, Webber BL (2014) Here be dragons: A tool for quantifying novelty due to covariate range and correlation change when projecting species distribution models. *Diversity Distrib* 20:1147–1159. doi: [10.1111/ddi.12209](https://doi.org/10.1111/ddi.12209)
- Miller DL, Becker EA, Forney KA, Roberts JJ, Cañadas A, Schick RS (2022) Estimating uncertainty in density surface models. *PeerJ* 10:e13950. doi: [10.7717/peerj.13950](https://doi.org/10.7717/peerj.13950)
- Mullin KD, Fulling GL (2003) [Abundance of cetaceans in the southern U.S. North Atlantic Ocean during summer 1998](#). *Fishery Bulletin* 101:603–613.
- O’Brien O, Pendleton DE, Ganley LC, McKenna KR, Kenney RD, Quintana-Rizzo E, Mayo CA, Kraus SD, Redfern JV (2022) Repatriation of a historical North Atlantic right whale habitat during an era of rapid climate change. *Sci Rep* 12:12407. doi: [10.1038/s41598-022-16200-8](https://doi.org/10.1038/s41598-022-16200-8)
- Olson P (2008) Pilot whales: *Globicephala melas* and *G. muerorhynchus*. In: Perrin WF TJ Wursig B (ed) *Encyclopedia of Marine Mammals*, 2nd ed, 2nd edn. Academic Press, San Diego, CA, pp 847–852
- Palka D (2020) [Cetacean Abundance in the US Northwestern Atlantic Ocean Summer 2016](#). *Northeast Fish Sci Cent Ref Doc. 20-05*. NOAA National Marine Fisheries Service, Northeast Fisheries Science Center, Woods Hole, MA
- Palka D, Aichinger Dias L, Broughton E, Chavez-Rosales S, Cholewiak D, Davis G, DeAngelis A, Garrison L, Haas H, Hatch J, Hyde K, Jech M, Josephson E, Mueller-Brennan L, Orphanides C, Pegg N, Sasso C, Sigourney D, Soldevilla M, Walsh

- H (2021) [Atlantic Marine Assessment Program for Protected Species: FY15 – FY19 \(OCS Study BOEM 2021-051\)](#). U.S. Department of the Interior, Bureau of Ocean Energy Management, Washington, DC
- Palka DL (2006) [Summer abundance estimates of cetaceans in US North Atlantic navy operating areas \(NEFSC Reference Document 06-03\)](#). U.S. Department of Commerce, Northeast Fisheries Science Center, Woods Hole, MA
- Palka DL, Chavez-Rosales S, Josephson E, Cholewiak D, Haas HL, Garrison L, Jones M, Sigourney D, Waring G, Jech M, Broughton E, Soldevilla M, Davis G, DeAngelis A, Sasso CR, Winton MV, Smolowitz RJ, Fay G, LaBrecque E, Leiness JB, Dettloff K, Warden M, Murray K, Orphanides C (2017) [Atlantic Marine Assessment Program for Protected Species: 2010-2014 \(OCS Study BOEM 2017-071\)](#). U.S. Department of the Interior, Bureau of Ocean Energy Management, Washington, DC
- Payne PM, Heinemann DW (1993) The distribution of pilot whales in shelf/shelf edge and slope waters of the northeastern United States, 1978-1988. Report of the International Whaling Commission (Special Issue 14) 51–68.
- Quintana-Rizzo E, Leiter S, Cole T, Hagbloom M, Knowlton A, Nagelkirk P, O'Brien O, Khan C, Henry A, Duley P, Crowe L, Mayo C, Kraus S (2021) Residency, demographics, and movement patterns of North Atlantic right whales *Eubalaena glacialis* in an offshore wind energy development area in southern New England, USA. *Endang Species Res* 45:251–268. doi: [10.3354/esr01137](#)
- Read AJ, Barco S, Bell J, Borchers DL, Burt ML, Cummings EW, Dunn J, Fougères EM, Hazen L, Hodge LEW, Laura A-M, McAlarney RJ, Peter N, Pabst DA, Paxton CGM, Schneider SZ, Urian KW, Waples DM, McLellan WA (2014) [Occurrence, distribution and abundance of cetaceans in Onslow Bay, North Carolina, USA](#). *Journal of Cetacean Research and Management* 14:23–35.
- Redfern JV, Kryc KA, Weiss L, Hodge BC, O'Brien O, Kraus SD, Quintana-Rizzo E, Auster PJ (2021) Opening a Marine Monument to Commercial Fishing Compromises Species Protections. *Front Mar Sci* 8:645314. doi: [10.3389/fmars.2021.645314](#)
- Roberts JJ, Best BD, Dunn DC, Treml EA, Halpin PN (2010) Marine Geospatial Ecology Tools: An integrated framework for ecological geoprocessing with ArcGIS, Python, R, MATLAB, and C++. *Environmental Modelling & Software* 25:1197–1207. doi: [10.1016/j.envsoft.2010.03.029](#)
- Roberts JJ, Best BD, Mannocci L, Fujioka E, Halpin PN, Palka DL, Garrison LP, Mullin KD, Cole TVN, Khan CB, McLellan WA, Pabst DA, Lockhart GG (2016) Habitat-based cetacean density models for the U.S. Atlantic and Gulf of Mexico. *Scientific Reports* 6:22615. doi: [10.1038/srep22615](#)
- Roberts JJ, Mannocci L, Halpin PN (2017) Final Project Report: Marine Species Density Data Gap Assessments and Update for the AFTT Study Area, 2016-2017 (Opt. Year 1), Document Version 1.4. Duke University Marine Geospatial Ecology Lab, Durham, NC
- Roberts JJ, Yack TM, Halpin PN (2023) Marine mammal density models for the U.S. Navy Atlantic Fleet Training and Testing (AFTT) study area for the Phase IV Navy Marine Species Density Database (NMSDD), Document Version 1.3. Duke University Marine Geospatial Ecology Lab, Durham, NC
- Robertson FC, Koski WR, Brandon JR, Thomas TA, Trites AW (2015) [Correction factors account for the availability of bowhead whales exposed to seismic operations in the Beaufort Sea](#). *Journal of Cetacean Research and Management* 15:35–44.
- Rone BK, Pace RM (2012) A simple photograph-based approach for discriminating between free-ranging long-finned (*Globicephala melas*) and short-finned (*G. macrorhynchus*) pilot whales off the east coast of the United States. *Marine Mammal Science* 28:254–275. doi: [10.1111/j.1748-7692.2011.00488.x](#)
- Ryan C, Boisseau O, Cucknell A, Romagosa M, Moscrop A, McLanaghan R (2013) [Final report for trans-Atlantic research passages between the UK and USA via the Azores and Iceland, conducted from R/V Song of the Whale 26 March to 28 September 2012](#). Marine Conservation Research International, Essex, UK
- Schlx MG, Chelton DB (2016) [The "Growing Method" of Eddy Identification and Tracking in Two and Three Dimensions](#). College of Earth, Ocean and Atmospheric Sciences, Oregon State University, Corvallis, OR
- Shearer J, Jensen F, Quick N, Friedlaender A, Southall B, Nowacek D, Bowers M, Foley H, Swaim Z, Waples D, Read A (2022) Short-finned pilot whales exhibit behavioral plasticity in foraging strategies mediated by their environment. *Mar Ecol Prog Ser* 695:1–14. doi: [10.3354/meps14132](#)
- Spitz J, Chérel Y, Bertin S, Kiszka J, Dewez A, Ridoux V (2011) Prey preferences among the community of deep-diving odontocetes from the Bay of Biscay, Northeast Atlantic. *Deep Sea Research Part I: Oceanographic Research Papers* 58:273–282. doi: [10.1016/j.dsr.2010.12.009](#)
- Stone KM, Leiter SM, Kenney RD, Wikgren BC, Thompson JL, Taylor JKD, Kraus SD (2017) Distribution and abundance of cetaceans in a wind energy development area offshore of Massachusetts and Rhode Island. *J Coast Conserv* 21:527–543. doi: [10.1007/s11852-017-0526-4](#)

- Thorne L, Foley H, Baird R, Webster D, Swain Z, Read A (2017) Movement and foraging behavior of short-finned pilot whales in the Mid-Atlantic Bight: Importance of bathymetric features and implications for management. *Mar Ecol Prog Ser* 584:245–257. doi: [10.3354/meps12371](https://doi.org/10.3354/meps12371)
- Waring GT, Fairfield CP, Ruhsam CM, Sano M (1992) Cetaceans associated with Gulf Stream features off the northeastern USA shelf. *ICES Marine Mammals Comm* CM 29.
- Waring GT, Josephson E, Maze-Foley K, Rosel PE, Cole TVN, Engleby L, Garrison LP, Henry A, Mullin KD, Orphanides C, Pace RM, Palka DL, Lyssikatos M, Wenzel FW (2014) [US Atlantic and Gulf of Mexico Marine Mammal Stock Assessments - 2013](#). National Marine Fisheries Service, Woods Hole, MA
- Waring GT, Josephson E, Maze-Foley K, Rosel PE, Byrd B, Cole TVN, Engleby L, Garrison LP, Hatch J, Henry A, Horstman SC, Litz J, Lyssikatos MC, Mullin KD, Orphanides C, Pace RM, Palka DL, Soldevilla M, Wenzel FW (2016) [US Atlantic and Gulf of Mexico Marine Mammal Stock Assessments - 2015](#). NOAA National Marine Fisheries Service, Northeast Fisheries Science Center, Woods Hole, MA
- Winn HE (1982) CeTAP: A Characterization of Marine Mammals and Turtles in the Mid- and North Atlantic Areas of the U.S. Outer Continental Shelf: Final Report. University of Rhode Island Graduate School of Oceanography, Kingston, RI